SCATTERING BY IMPERFECTLY CONDUCTING BODIES

A Dissertation

Presented to

the Faculty of Graduate Studies

University of Manitoba

In Partial Fulfillment

of the Requirements for the Degree

Doctor of Philosophy

---

by

Prakash Bhartia

March 1971

ABSTRACT

The ray optical method is employed to derive an asymptotic solution for the far field scattering by an imperfectly conducting sphere. The procedure makes use of the exact solution and is tested for perfectly conducting spheres where considerable improvement in Senior's solution is introduced. Apart from leading to good agreement with the exact solution for spheres of radii as small as one wavelength, the method provides better physical insight into the scattering mechanism and considerable saving in computational effort. Two specific ranges of impedance, one below and the other above the free space intrinsic impedance, are identified. Numerical results are presented for various sphere sizes and surface impedances while the behaviour of the imperfectly conducting sphere and its departure from the perfectly conducting sphere are demonstrated and explained for the forward, bistatic and monostatic cross sections.

To extend the technique to cylindrical geometries for which no exact solutions are available, it is shown that available numerical solutions may be used to replace the need for exact solutions provided that they are extended to imperfectly conducting bodies using the Leontovich impedance boundary conditions. Results based on these numerical techniques are presented for the imperfectly conducting circular and square cylinders as well as the circular cylinder coated with a radially inhomogeneous dielectric. Finally, results for the imperfectly conducting rectangular and spherical cavities are also presented and analyzed on the basis of the perturbation and boundary value techniques, respectively.

ACKNOWLEDGMENTS

The author wishes to express his sincere appreciation of the interest and encouragement given him by Dr. M.A.K. Hamid. He is indebted particularly to Dr. L. Shafai and Dr. W.M. Boerner for their interest and cooperation. Thanks are due to friends and colleagues for their comments and discussions and to Mrs. L. McAlinden for the expertly typed manuscript.

The financial assistance of the University of Manitoba in the form of University Fellowships is highly appreciated.

TABLE OF CONTENTS

LIST OF TABLES

LIST OF FIGURES

FIGURE PAGE

CHAPTER I

INTRODUCTION

Though the Leontovich boundary conditions have been known for the past few decades, solutions for problems incorporating this condition have only been possible for a few geometries. Besides the mathematical difficulties encountered, even in the cases when exact solutions obtained by using these conditions are known (e.g. the sphere and the circular cylinder), the effect of the impedance is not fully understood. These condtions relate the tangential components of the electric and magnetic fields through an impedance factor which is a function of the properties of the surface and polarization of the incident field. Though the surface impedance concept is not new, the idea of incorporating it into the initial formulation of the boundary value problem dates to the early 1940's. The electromagnetic properties of the material are specified in terms of an effective surface impedance, thereby simplifying the formulation considerably and making solutions tractable.

An exposition of the impedance boundary conditions for a flat or curved surface or at an interface where the properties of the medium vary from point to point is given by Senior [1,2], who also gives the proof of the conditions as well as their degree of generality and restrictions. For a curved surface, the conditions are a valid approximation to the true conditions, if the radii of curvature are everywhere large compared with the wavelength and the refractive index of the coating is large compared to unity. They are also justified when the impedance varies from point to point, provided that the variation is slow. The conditions

are appropriate for a number of problems involving imperfectly conducting scatterers, rough surfaces and absorber and dielectric coated bodies, and perform in one operation a perturbational solution about the perfectly conducting case without explicitly considering the surface conditions. Thus, the wide range of surface conditions, that are taken into account in a single formulation incorporating the impedance boundary condition, makes the study of such problems most interesting and important. However, in doing so, a suitable method of solution which is conceptually simple and at the same time gives good physical insight into the electromagnetic wave propagation phenomena over bodies which satisfy the impedance boundary conditions, is required.

Impedance boundary conditions have been used mainly in guided wave propagation [3-18] with particular emphasis on the rectangular waveguide with lossy walls [3-10]. The solutions in this case have been restricted mainly to the case when only one wall is imperfectly conducting. This is because of the difficulty experienced in applying the impedance boundary conditions for other cases, and the non-existence of normal waveguide modes, thereby making the analysis considerably involved. In scattering and diffraction theory, the condition has been applied to the wedge [19-25] and cone [19] with little success, the only tractable results for the wedge being obtained when only one face satisfies the impedance condition [22-25]. The main difficulty in this case is the choice of a suitable mathematical representation for the scattered field. With the use of Hankel functions, as in the case of the perfectly conducting wedge or cone, it has not been possible to satisfy the impedance boundary conditions. The imperfectly conducting half-plane is one of

the few cases for which solutions have been obtained [26-29] and extended to linear and anisotropic variations of the surface impedance [30-33].

In the case of the imperfectly conducting sphere and cylinder, which are the principal scatterers considered here, only a limited amount of information exists. In the case of the sphere, the exact solution is known [34-37] and Wait and Jackson [34] have computed the solution to investigate the scattering behaviour. However, this gives little physical insight into the scattering mechanism. The ray optical analyses of others [38-40] are restricted to the monostatic case and do not lead to numerical results, due to the lack of creeping wave propagation coefficients which require finding the complex roots of transcendental equations. This restriction, together with the mathematical complexities of contour integration and the considerable amount of labour involved in obtaining results for the bistatic and forward regions, have restricted the solution to the monostatic case. In the case of imperfectly conducting cylinders, the exact solution is available for the circular cylinder [41-43] and an integral equation formulation for other cross sections [44]. However, the latter method requires considerable computation time. Furthermore, no results describing the physical effects of surface impedance on the scattering properties of cylinders are available in the literature.

The basic analytical approach in this thesis is based on the ray-optical method by Keller [45-46]. The method is an extension of geometrical optics to include a class of rays, called diffracted rays, which account for the shadow region fields. The total field at any point in space is given by the sum of the fields on all rays passing

through that point, while the amplitude of the field on individual rays is assumed to behave according to the principle of conservation of energy and the phase is directly proportional to the optical length of the ray. The method provides excellent physical understanding of the scattering mechanism and offers considerable computational advantage due to the simplicity of the asymptotic expressions obtained for the fields.

The motivation for research in this area has been to obtain better physical understanding of the behaviour of imperfectly conducting bodies, with particular emphasis on the sphere. Results for other imperfectly conducting bodies like the circular and square cylinders, and the interior problems of the rectangular and spherical cavities are also obtained and analyzed, primarily to obtain numerical results for the "ray-numerical" method proposed and secondly to support or add to the available information on the characteristics of imperfectly conducting bodies, derived from the sphere solution.

In Chapter II the ray optical solution for the perfectly conducting sphere is analyzed for accuracy and the range of applicability in the bistatic range extended. Furthermore, the solution is extended to the scattering by multiple spheres and the results are shown to provide better agreement with the experimental results of Mevel [47], than has been possible by the multipole expansion method [48].

The ray optical solution for the perfectly conducting sphere is extended to the scattering by an imperfectly conducting sphere in Chapter III. An asymptotic solution for a sphere of large electrical radius ka is derived by the application of Watson's transformation to the exact series solution. The scattered field is reduced to the sum

contribution from rays associated with a geometrical optics term and a series of creeping waves. Using the method of Striefer [49], decay coefficients which are the complex roots of a transcendental equation are obtained in a series form and field expressions for the monostatic, bistatic and forward scattering are derived and analyzed. The results show favourable agreement with the exact solution. Two specific ranges are identified where the surface impedance is below or above the free space intrinsic impedance and it is shown that the scattering cross section in either range, determine the complete behaviour for the reciprocal impedance in the other. The departure from the perfectly conducting sphere is also demonstrated for the forward, backward and bistatic cross sections for various resistive, reactive and complex impedance coatings. The solution is shown to lead to easier analysis and physical insight into the scattering behaviour.

To extend the ray method to other geometries, the ray-numerical method is proposed in Chapter IV. This defines ray diffraction and propagation coefficients in place of mode diffraction and decay coefficients and is demonstrated for the case of the perfectly conducting cylinder. To employ the technique for imperfectly conducting cylindrical bodies, the transmission matrix method and the phase shift method previously employed for perfectly conducting cylinders are extended and results for the circular, square and circular cylinder with an inhomogeneous dielectric coating are presented and analyzed. The rectangular and spherical cavities are also investigated using the perturbation and boundary value techniques respectively.

In Chapter V some applications using the results obtained are

suggested. The discussion of the results and conclusions are finally presented in Chapter VI.

Most of the material in this thesis has been published or accepted for publication [50-54].

CHAPTER II

THE RAY OPTICAL SOLUTION FOR CONDUCTING SPHERES

2.1 Background of the Method

Although various methods have been employed for solving scattering problems, the ray optical method or the geometrical theory of diffraction is perhaps the simplest conceptually and leads to satisfactory results when the characteristic dimension (ka) of the body is much larger than unity. Since very few problems have exact solutions, such approximate techniques are of basic importance in applied electromagnetic theory. In addition to its mathematical simplicity, the ray method gives a physical insight into the mechanisms responsible for scattering or diffraction.

The geometrical theory of diffraction is an extension of the classical geometrical optics theory. Both theories assume that energy is propagated along ray paths obeying Fermat's principle [45], such that the optical path length is stationary. The classical geometrical optics theory is inadequate to deal with scattering and diffraction problems, since it neglects phase and polarization information and fails to account for the fields in the shadow region. The phase and polarization information is often added artificially when the approximation becomes identical to the first term of an asymptotic solution to Maxwell's equations as introduced by Luneberg [55] and Kline [56,57]. In spite of this, the diffracted field due to edges, vertices, corners and shadow boundaries were still unaccounted for and this led to the development of the geometrical theory of diffraction.

Keller's geometrical theory of diffraction [45,46] overcomes the defects of the geometrical optics theory, by introducing new rays called diffracted rays. Here diffracted energy is still assumed to propagate along ray paths obeying Fermat's principle. The total field at an observation point is the sum of fields on all the rays passing through that point. The phase of the field on a ray is assumed to be proportional to the optical length of the ray relative to some reference point where the phase is known. The amplitude is assumed to behave according to the principle of conservation of energy and is formulated as the product of the incident field at the point of diffraction times the diffraction coefficient. Diffraction coefficients are determined by comparison with the leading term in the asymptotic expansion of the exact solution of canonical problems and have been found for various bodies, e.g. the wedge [58], half plane [59], cone [60], and have been employed for the scattering by multiple [59] and smooth bodies [61,62]. Alternatively, approximate values may be obtained from experimental measurements.

Although the ray technique provides excellent physical understanding of scattering and diffraction processes and offers considerable computational advantages, it, nevertheless, suffers from a number of drawbacks. The incident and reflected fields are discontinuous across the shadow lines and the diffracted field becomes infinite at shadow boundaries, edges and caustics and certain corrections must be made [63, 64]. However, for an arbitrary body, no general method of correction is available and caustic correction terms must be determined in the same way as for diffraction coefficients [64-66]. Furthermore, the general validity of Keller's theory has not been established.

In spite of these shortcomings, the geometrical theory of diffraction has been applied successfully to treat a wide variety of interior and exterior electromagnetic problems [67-70]. The range of problems already solved indicates that the method is one of the most promising approximate methods for computational purposes. The scattering of plane waves by a perfectly conducting sphere and multiple spheres is developed in this chapter using this technique.

2.2 Ray Scattering by a Perfectly Conducting Sphere

The solution for the scattering of a plane wave by a perfectly conducting sphere using the ray optical approach was formulated by Senior and Goodrich [71] in a form convenient for computational purposes. The accuracy of this solution is examined in this section and certain corrections in the results are presented.

Assuming a plane wave polarized in the x direction and incident along the negative z axis on a perfectly conducting sphere of radius a, as shown in Fig. 2.1, we have for the incident electric and magnetic fields

$$E^i = \hat{x}\, e^{-jkz}$$

and (2.1)

$$H^i = \hat{y}\, Y_o e^{-jkz}$$

where Y_o is the intrinsic admittance of free space and the $e^{j\omega t}$ time dependence has been suppressed. Using the standard Mie Series as given by Stratton [72] and the spherical coordinates (r,θ,ϕ), the exact expressions for the far field components are

$$E_r = 0 \qquad (2.2a)$$

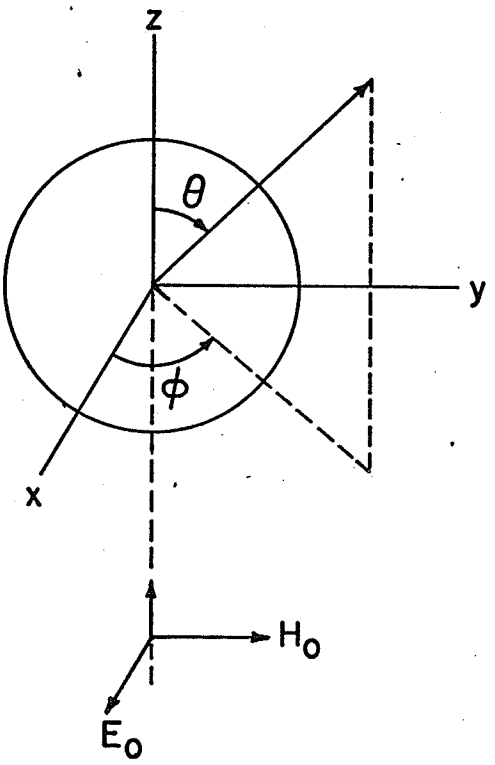

INCIDENT PLANE WAVE

FIG. 2.1 SCATTERING GEOMETRY OF A SPHERE

$$E_\theta = j \cos\phi \frac{e^{-jkr}}{kr} \sum_{\ell=1}^{\infty} (-1)^\ell \frac{2\ell + 1}{\ell(\ell + 1)} \left[\frac{\psi_\ell'(ka)}{\xi_\ell^{(1)'}(ka)} \frac{\partial}{\partial\theta} P_\ell^1(\cos\theta) \right.$$

$$\left. - \frac{\psi_\ell(ka)}{\xi_\ell^{(1)}(ka)} \frac{P_\ell^1(\cos\theta)}{\sin\theta} \right] \tag{2.2b}$$

$$E_\phi = - j \sin\phi \frac{e^{-jkr}}{kr} \sum_{\ell=1}^{\infty} (-1)^\ell \frac{2\ell + 1}{\ell(\ell + 1)} \left[\frac{\psi_\ell'(ka)}{\xi_\ell^{(1)'}(ka)} \frac{P_\ell^1(\cos\theta)}{\sin\theta} \right.$$

$$\left. - \frac{\psi_\ell(ka)}{\xi_\ell^{(1)}(ka)} \frac{\partial}{\partial\theta} P_\ell^1(\cos\theta) \right] \tag{2.2c}$$

where $\psi_\ell(ka) = ka\, j_\ell(ka)$ and $\xi_\ell^{(1)}(ka) = ka\, h_\ell^{(1)}(ka)$, $j_\ell(ka)$ and $h_\ell^{(1)}(ka)$ are spherical Bessel and Hankel functions, the prime notation denotes differentiation with respect to the total argument and $P_\ell^1(\cos\theta)$ are the Legendre functions of degree one and order ℓ.

Denoting the summations in (2.2b) and (2.2c) by $S_1(\theta)$ and $S_2(\theta)$,

$$S_1(\theta) = \sum_{\ell=1}^{\infty} (-1)^\ell \frac{2\ell + 1}{\ell(\ell + 1)} \left[\frac{\psi_\ell'(ka)}{\xi_\ell^{(1)'}(ka)} \frac{\partial}{\partial\theta} P_\ell^1(\cos\theta) \right.$$

$$\left. - \frac{\psi_\ell(ka)}{\xi_\ell^{(1)}(ka)} \frac{P_\ell^1(\cos\theta)}{\sin\theta} \right] \tag{2.3a}$$

and

$$S_2(\theta) = \sum_{\ell=1}^{\infty} (-1)^\ell \frac{2\ell + 1}{\ell(\ell + 1)} \left[\frac{\psi_\ell'(ka)}{\xi_\ell^{(1)'}(ka)} \frac{P_\ell^1(\cos\theta)}{\sin\theta} \right.$$

$$\left. - \frac{\psi_\ell(ka)}{\xi_\ell^{(1)}(ka)} \frac{\partial}{\partial\theta} P_\ell^1(\cos\theta) \right] \tag{2.3b}$$

Further, using Watson's transformation and writing $S_1(\theta)$ as the sum of

a geometric optics term, $S_1^o(\theta)$, and a creeping wave solution, $S_1^c(\theta)$, we obtain the following expressions for the backscattered field [71]:

$$S_1^o(0) = \frac{j}{2}\, ka\, e^{2jka}\left[1 + \frac{j}{2ka} + 0\left(\frac{1}{ka^3}\right)\right] \tag{2.4a}$$

and

$$\begin{aligned} S_1^c(0) = &- \tau^4 e^{-j\pi ka + j\,\pi/6}\left\{\sum_{\ell=1}^{\infty} \frac{1}{\beta_\ell [A_i(-\beta_\ell)]^2}\left[1 + \frac{e^{-j\,\pi/3} 8\beta_n}{15\tau^2}\right.\right. \\ &\left. \cdot \left(1 + \frac{9}{32\beta_\ell^2}\right) + 0(\tau^{-4})\right] \\ &\times \exp\left[-e^{j\,\pi/6}\beta_\ell \tau\pi - \frac{e^{-j\,\pi/6}\beta_\ell^2 \pi}{60\tau}\left(1 - \frac{9}{\beta_\ell^3}\right) + 0(\tau^{-3})\right] \\ &- \sum_{m=1}^{\infty} \frac{1}{[A_i'(-\alpha_m)]^2}\left[1 + e^{-j\,\pi/3}\,\frac{8\alpha_m}{15\tau^2} + 0(\tau^{-4})\right] \\ &\left.\left. \times \exp\left[-e^{j\,\pi/6}\alpha_m \pi\tau - \frac{e^{-j\,\pi/6}\alpha_m^2 \pi}{60\tau} + 0(\tau^{-3})\right]\right\} \end{aligned} \tag{2.4b}$$

where $\tau = \left(\frac{ka}{2}\right)^{1/3}$, α_m are the zeros of the Airy functions $A_i(-\alpha)$ and β_ℓ are the zeros of $A_i'(-\beta)$ as defined in [71].

Similarly in the bistatic case the expressions for the E plane polarization for the range of bistatic angles $\delta < \theta < \pi - \delta$, where $\delta = 0\left(\frac{1}{ka}\right)$, we obtain for the geometric optics term

$$S_1^o(\theta) = \frac{j}{2}\, ka\, e^{2j\, ka\, \cos\theta/2}\left[1 + \frac{j}{2ka\, \cos^3\theta/2} - \frac{7\sin^2\theta/2}{4(ka)^2\cos^6\theta/2} + \ldots\right] \tag{2.5a}$$

while the creeping wave contribution is given by

$$S_1^c(\theta) = -\sqrt{\left(\frac{ka}{2\pi\sin\theta}\right)}\,\tau e^{-j\,\pi/12}\sum_{\ell=1}^{\infty}\frac{1}{\beta_\ell[A_i(-\beta_\ell)]^2}$$

$$\cdot\left[1+\frac{e^{-j\,\pi/3}}{60\tau^2}\left(17\beta_\ell+\frac{9}{\beta_\ell^2}\right)+0(\tau^{-3})\right]$$

$$\times\left\{\left[1+\frac{7j}{16\tau^3}\cot\theta+0(\tau^{-5})\right]\exp\left[(\pi-\theta)(-jka-e^{j\,\pi/6}\beta_\ell\tau\right.\right.$$

$$\left.-\frac{e^{-j\,\pi/6}\beta_\ell^2}{60\tau}\left(1-\frac{9}{\beta_\ell^3}\right)+0(\tau^{-3})\right]-j\left[1-\frac{7j}{16\tau^3}\cot\theta+0(\tau^{-5})\right]$$

$$\left.\cdot\exp\left[(\pi+\theta)(-jka-e^{j\,\pi/6}\beta_\ell\tau-\frac{e^{-j\,\pi/6}\beta_\ell^2}{60\tau}\left(1-\frac{9}{\beta_\ell^3}\right)+0(\tau^{-3})\right]\right\}$$

$$-j\sqrt{\left(\frac{ka}{2\pi\sin\theta}\right)}\frac{e^{-j\,\pi/12}}{2\tau^2\sin\theta}\sum_{m=1}^{\infty}\frac{1}{[A_i'(-\alpha_m)]^2}\left[1+0(\tau^{-2})\right]$$

$$\left\{\times\exp\left[(\pi-\theta)(-jka-e^{j\,\pi/6}\alpha_m\tau-\frac{e^{-j\,\pi/6}\alpha_m^2}{60\tau}+0(\tau^{-3}))\right]\right.$$

$$\left.+j\exp\left[(\pi+\theta)(-jka-e^{j\,\pi/6}\alpha_m\tau-\frac{e^{-j\,\pi/6}\alpha_m^2}{60\tau}+0(\tau^{-3}))\right]\right\}$$

(2.5b)

The corresponding expressions for $S_2^o(\theta)$ and $S_2^c(\theta)$ for the H plane polarization are evaluated in an identical manner and given by

$$S_2^o(\theta) = \frac{j}{2}\,ka\,e^{2jka\,\cos\theta/2}\left[1+\frac{j\cos\theta}{2ka\cos^3\theta/2}+\frac{1}{4(ka)^2}\right.$$

$$\left.\cdot\frac{(6+\cos\theta)\sin^2\theta/2}{\cos^6\theta/2}+0\left(\frac{1}{ka^3}\right)\right] \qquad (2.6a)$$

$$S_2^c(\theta) = j\sqrt{\left(\frac{ka}{2\pi\sin\theta}\right)}\,\frac{e^{-j\,\pi/12}}{2\tau^2\sin\theta}\sum_{n=1}^{\infty}\frac{1}{\beta_n[A_i(-\beta_n)]^2}\left[1 + O(\tau^{-2})\right]$$

$$\times\left\{\exp\left[(\pi-\theta)(-jka - e^{j\,\pi/6}\beta_n\tau - e^{-j\,\pi/6}\frac{\beta_n^2}{60\tau}\left(1 - \frac{9}{\beta_n^3}\right.\right.\right.$$

$$\left.\left.\left. + O(\tau^{-3})\right)\right] + j\exp\left[(\pi+\theta)(-jka - e^{j\,\pi/6}\beta_n\tau\right.\right.$$

$$\left.\left. - e^{-j\,\pi/6}\frac{\beta_n^2}{60\tau}\left(1 - \frac{9}{\beta_n^2}\right) + O(\tau^{-3})\right)\right]\right\}$$

$$+\sqrt{\left(\frac{ka}{2\pi\sin\theta}\right)}\,\tau e^{-j\,\pi/12}\sum_{m=1}^{\infty}\frac{1}{[A_i'(-\alpha_m)]^2}$$

$$\cdot\left[1 + e^{-j\,\pi/3}\frac{17\alpha_m}{60\tau^2} + O(\tau^{-4})\right]\times\left\{\left[1 + \frac{7j}{16\tau^3}\cot\theta + O(\tau^{-5})\right]\right.$$

$$\cdot\exp\left[(\pi-\theta)(-jka - e^{j\,\pi/6}\alpha_m\tau - \frac{e^{-j\,\pi/6}\alpha_m^2}{60\tau} + O(\tau^{-3}))\right]$$

$$-j\left[1 - \frac{7j}{16\tau^3}\cot\theta + O(\tau^{-5})\right]\exp\left[(\pi+\theta)(-jka - e^{j\,\pi/6}\alpha_m\tau\right.$$

$$\left.\left. - \frac{e^{-j\,\pi/6}\alpha_m^2}{60\tau} + O(\tau^{-3}))\right]\right\} \qquad (2.6b)$$

Finally due to the fact that the forward scattering direction corresponds to a caustic, the expressions for the geometric optics and creeping wave terms must be evaluated independently and the results for the two

polarizations are related by

$$S_2(\pi) = - S_1(\pi) \tag{2.7}$$

The expressions for the forward field result in the following solutions for the geometric optics term

$$S_1^o(\pi) = \frac{1}{2}\left[(ka)^2 - \frac{11}{12}\right] \tag{2.8a}$$

and

$$S_1^c(\pi) = \tau^4\left[.082972 - j \cdot 144019 + \frac{1}{\tau^2}(.385229 + j \cdot 667169)\right.$$

$$\left. - \frac{1}{\tau^4}(.069342) + O(\tau^{-6})\right] + \tau^4 e^{-j\pi/3} \sum_{\ell=1}^{\infty} \frac{1}{\beta_\ell [A_i(-\beta_\ell)]^2}$$

$$\left[1 + \frac{e^{-j\pi/3}}{60\tau}(32\beta_\ell + \frac{9}{\beta_\ell^2}) + O(\tau^{-4})\right] \sum_{m=0}^{\infty} (-1)^m \exp\left\{-2j\pi(m+1)\right.$$

$$\left.\left[ka + \tau\beta_\ell e^{-j\pi/3} + \frac{e^{-2j\pi/3}}{60\tau}(\beta_\ell^2 - \frac{9}{\beta_\ell}) + O(\tau^{-3})\right]\right\}$$

$$+ \tau^4 e^{-j\pi/3} \sum_{n=1}^{\infty} \frac{1}{[A_i'(-\alpha_n)]^2}\left[1 + \frac{8\alpha_n}{15\tau^2} e^{-j\pi/3} + O(\tau^{-4})\right]$$

$$\sum_{m=0}^{\infty} (-1)^m \exp\left\{-2j\pi(m+1)\left[ka + \tau\alpha_n e^{-j\pi/3} + \frac{\alpha_n^2 e^{-2j\pi/3}}{60\tau}\right.\right.$$

$$\left.\left. + O(\tau^{-3})\right]\right\} \tag{2.8b}$$

for the creeping wave term.

Equations (2.4b) and (2.5b) describe the dominant contribution from the creeping waves corresponding to a travelling distance of half a

sphere circumference. However, the improvement in the accuracy resulting from the higher order creeping waves, e.g. m = 1,2, in (2.8b) is numerically insignificant and therefore neglected in the computations.

To verify the solution, it is first necessary to check the accuracy of the predicted fields. Table 2.1 compares the monostatic phase (ρ_s) and normalized E plane cross-sections ($\sigma_s/\pi a^2$) computed from the exact results and from our expressions for ka of 4.19 (chosen because of the available data in the two sphere scattering problem, to be discussed in the next section), 5.0 and 10.0.

TABLE 2.1

EXACT AND APPROXIMATE VALUES OF MONOSTATIC CROSS-SECTIONS AND PHASES

	$\sigma_s/\pi a^2$		Phase ρ_s	
ka	Exact	Approx.	Exact	Approx.
4.19	0.638626	0.635060	-51.51°	-51.95°
5	1.16884	1.17615	30.197°	30.35°
10	0.92923	0.93015	-114.768°	-114.797°

To check the validity of (2.5), we compare the approximate and exact cross-sections for the above values of ka in Figs. 2.2a-2.2c. For the case ka = 10.0, it is seen that beyond the bistatic angle of 120° the asymptotic expression fails to reproduce the correct results since the product $ka\cos^3\theta$ is 1.25 at $\theta = 120°$ which is not much larger than unity, as required for the validity of the geometric optics term. In particular, for scattering from two spheres in the broadside configuration, the accuracy of the approximate bistatic results at

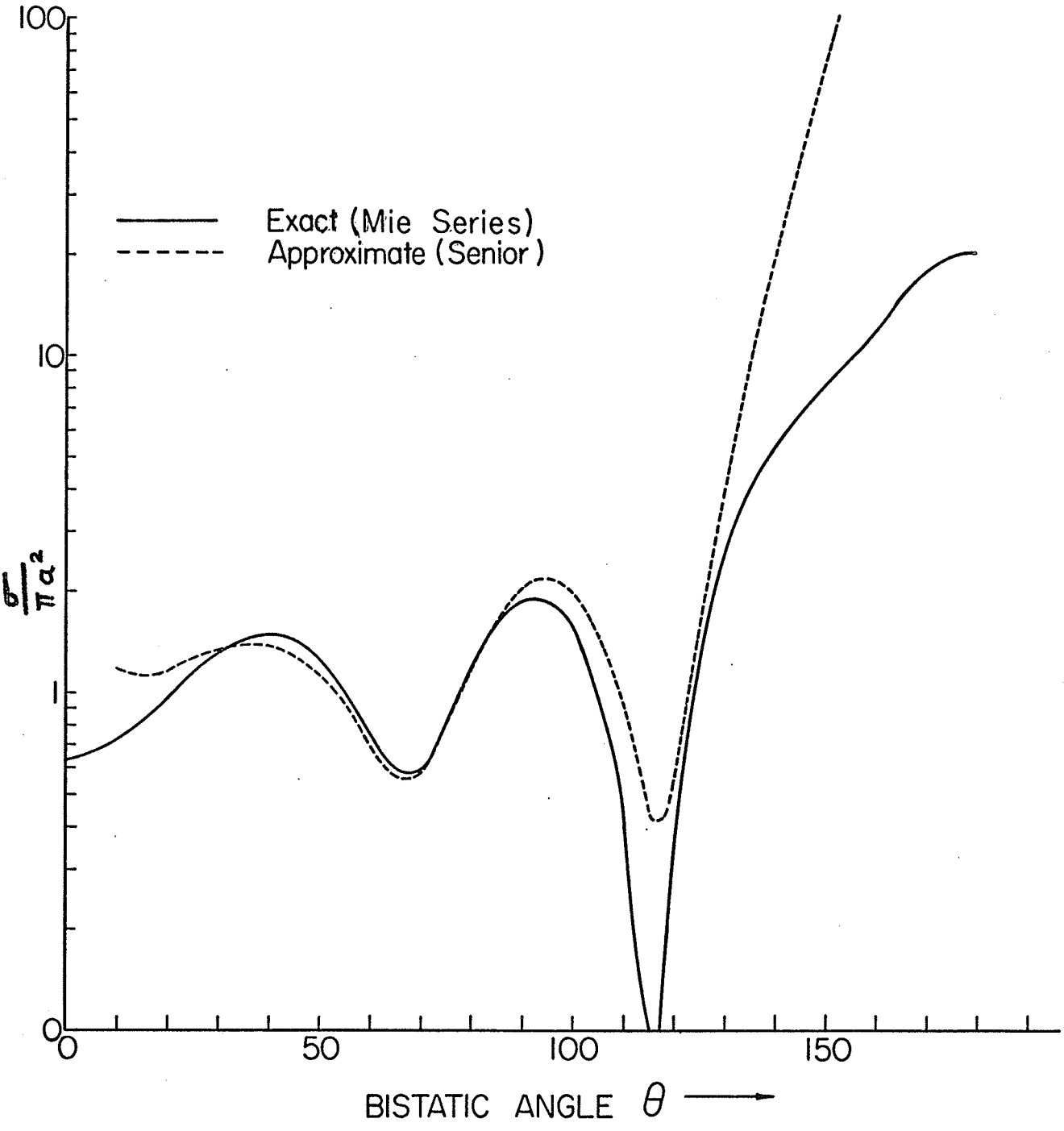

Scattering cross-section vs bistatic angle

(E-Plane, Ka = 4.19)

FIG. 2.2a

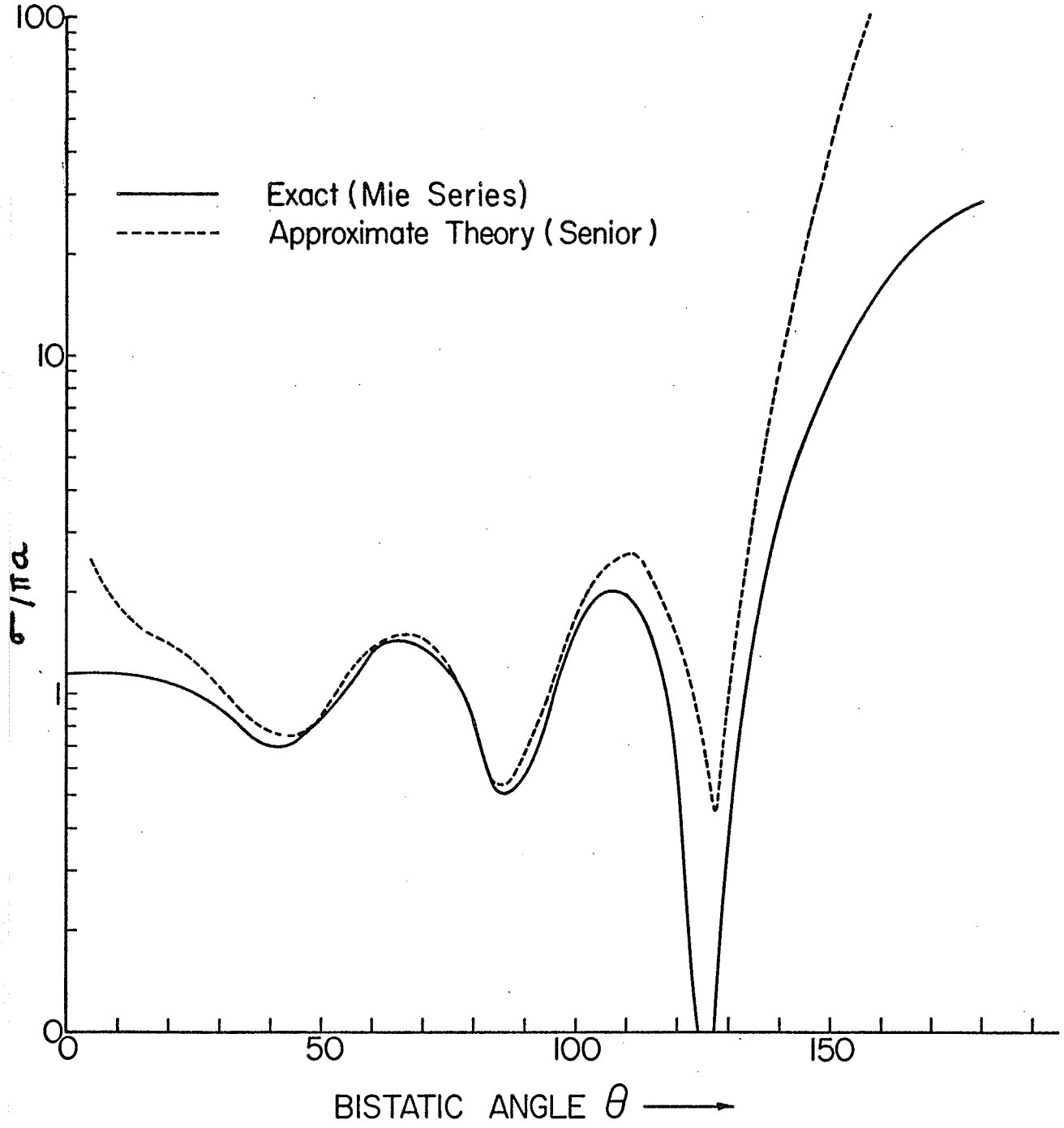

Scattering cross-section vs bistatic angle
(E Plane, Ka = 5.0)

FIG. 2.2b

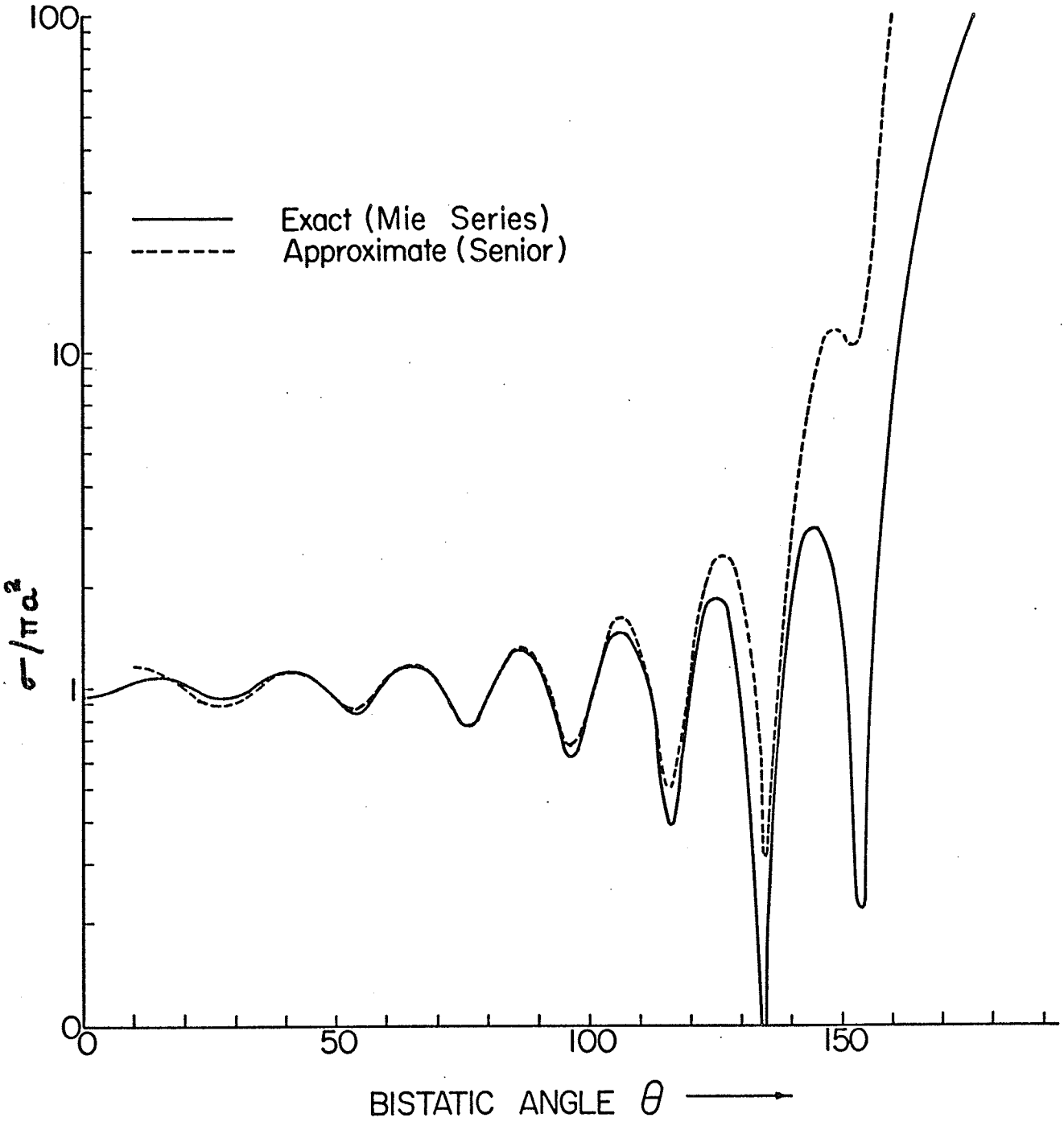

Scattering cross-section vs bistatic angle
(E Plane, Ka = 10.0)

FIG. 2.2c

$\theta = 90°$ are of importance and it is seen that, here too, the asymptotic theory is not in sufficiently good agreement. For lower values of ka, the same discrepancy is observed as is evident from Fig. 2.1a. Hence we conclude that the bistatic approximate results require considerable improvement since besides the above constraint on the geometric optics term, the solution is further restricted to the range of bistatic angles $\delta < \theta < \pi - \delta$, where $\delta = 0(1/ka)$, which would prevent a solution for arbitrary angles of incidence and observation.

Table 2.2 compares the exact and approximate results for forward scattering cross-section and phase for the above three values of ka.

TABLE 2.2

EXACT AND APPROXIMATE VALUES OF FORWARD SCATTERING CROSS-SECTIONS AND PHASES

	$\sigma_s/\pi a^2$		Phase ρ_s	
ka	Exact	Approx.	Exact	Approx.
4.19	20.095	19.047	94.179°	94.3°
5	28.073	27.032	93.178°	93.3°
10	106.358	105.33	90.79°	90.8°

This indicates that the expressions for scattering in the forward direction are reasonably accurate. It remains to show how the approximate theory could be used if the bistatic results are improved.

In order to improve the approximate theory, we investigate the functional nature of the geometric optics terms (on the assumption that the creeping wave formulation is reasonably accurate), by examining the exact results and comparing these graphically with the approximate

geometric optics solution, as shown in Fig. 2.3 for ka = 4.19. From this we observe that the geometric optics term in (2.5a) is a monotonically increasing function, while that obtained using (2.5b) and the exact solution has an oscillatory nature. However, the Kirchhoff-Huygens formulation for the plane wave scattering from a sphere, as formulated by Yerukhimovich and Pimenov [73] and later put into a suitable form for computation purposes by Erukhimovich [74], leads to better results. Here use is made of Federov's expressions for fields obtained in quadratures, by the vector potential method, in terms of currents induced on the surface of a perfectly conducting sphere due to an incident plane wave [75]. Separate solutions for the bistatic range of angles $0 \leq \theta \leq \theta_{lim}$ and $\theta_{lim} \leq \theta \leq \pi$ were obtained, where θ_{lim} is given by the relationship

$$\cos\left(\frac{\theta_{lim}}{2}\right) \simeq 1.81\, b_1/2ka \simeq 1/\tau^2 \tag{2.9}$$

and $b_1 = 2.335\tau$.

This formulation leads to an alternative geometric optics term [74] involving the zero order Bessel function of the first kind

$$S_1^o(\theta) = j\,\frac{ka}{2}\left(1 + \frac{j}{2ka\cos\theta/2}\right) e^{j\,2ka\cos\theta/2} + \frac{J_o(ka\sin\theta)}{2ka\cos\theta/2} \tag{2.10}$$

The first term in (2.10) is identical to the first two terms in (2.5a), while the second term involves a Bessel function rather than the higher order diverging terms in (2.5a). Equation (2.10) is plotted in Fig. 2.3 and is shown to be quite suitable for our purposes. Fig. 2.4 shows the results of combining the creeping wave term in (2.5b) and the geometric

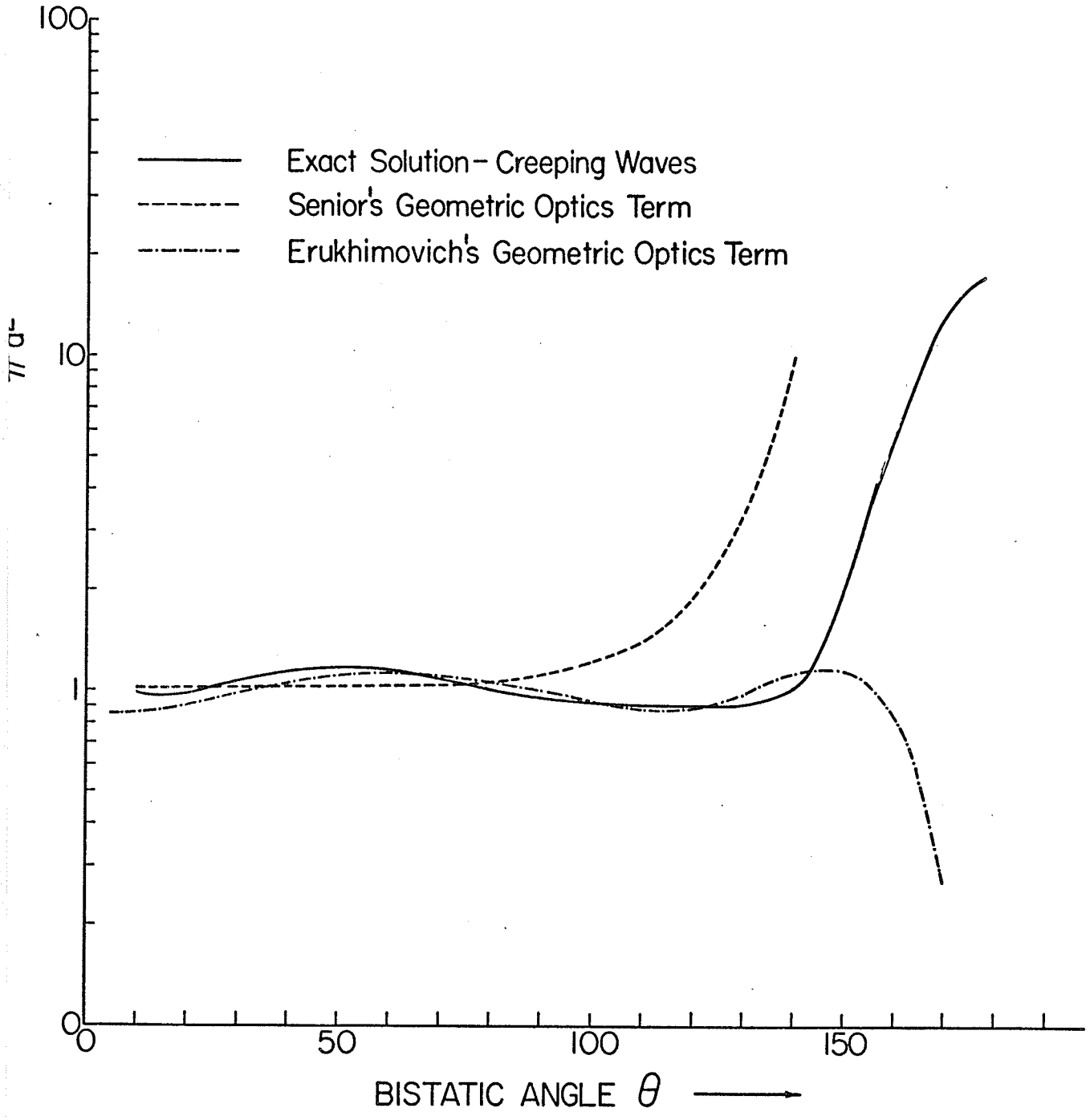

Geometric optics term vs bistatic angle (Ka = 4.19)

FIG. 2.3

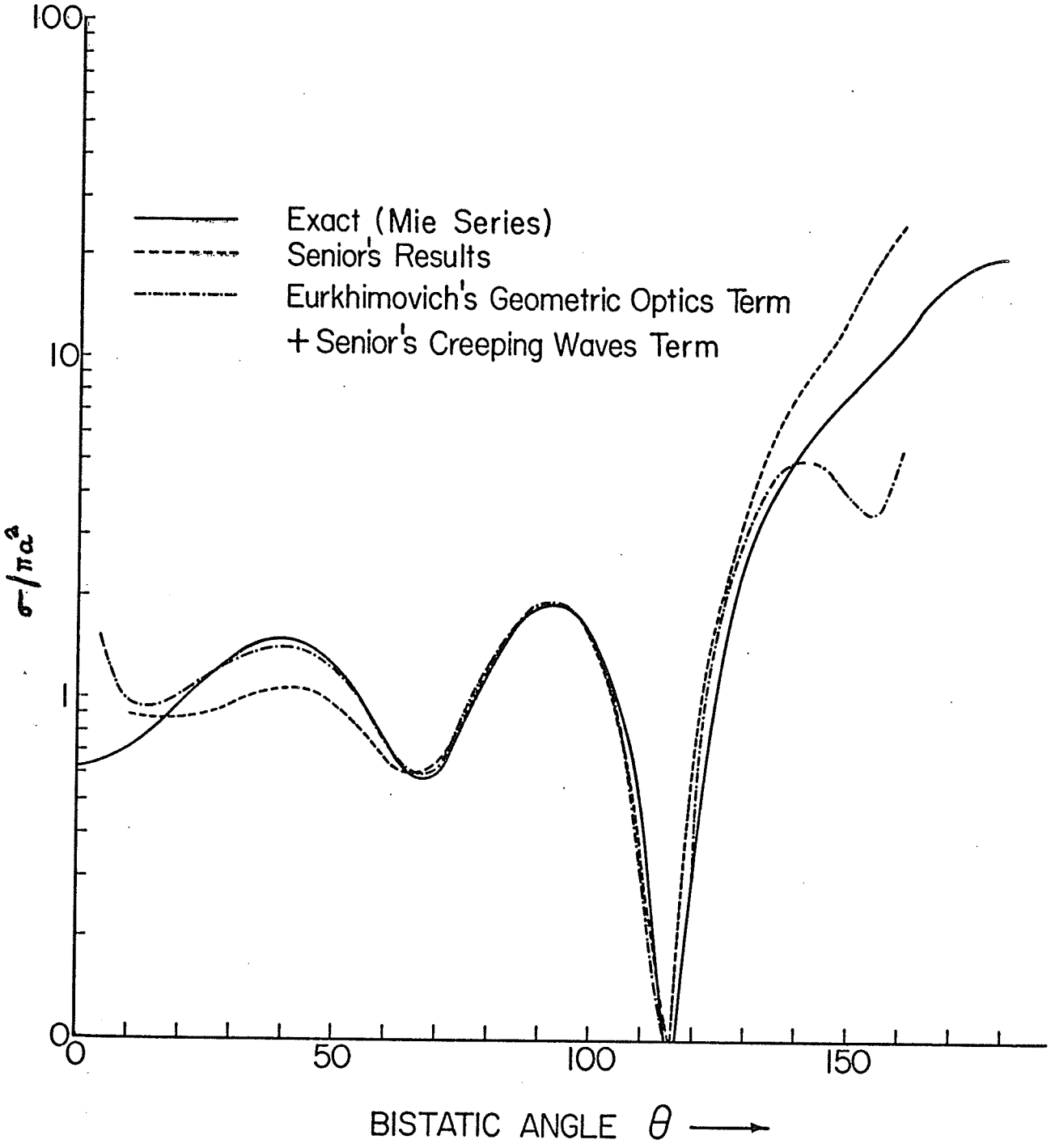

Comparison of scattering cross-section solutions
(E Plane, Ka = 4.19)

FIG. 2.4

optics term in (2.10) for ka = 4.19. The curve agrees very well with the exact results over a much larger angular range than possible using the optics term (2.5a). Further as the value of ka is increased, we can expect better agreement and over a larger range of the bistatic angle, since θ_{lim} will increase. In particular, we note the agreement for $\theta = 90°$ which is important for broadside scattering by two spheres, to be discussed in the next section. Since these results are reasonably accurate, the combined expression for the approximate solution for the single sphere may be extended with confidence to the two sphere problem.

2.3 The Scattering by Two Perfectly Conducting Spheres

The problem of electromagnetic scattering of plane waves by two spheres is a fundamental one in the theory of many body scattering. This is especially so, since the sphere is one of the few bodies for which an exact solution is available. The problem has been treated by Trinks [76] for broadside incidence and small identical spheres, and by Germogenova [77] for very small spheres and arbitrary angles of incidence. Bonkowski et al [78] also investigated the backscattering for the broadside configuration. Zitron and Karp [79,80] have analyzed the two and three dimensional scattering for bodies of arbitrary shape and more recently Twersky [81] has employed a vector dyadic formalism to study the same problem, but the results do not lend themselves easily to computation. Of considerable interest is the paper by Angelakos and Kumagai [82] who have presented experimental results for the two and three sphere scattering and used theoretical extensions of [78] for comparison purposes. Liang and Lo [48] have utilized the method of multipole

expansions, together with the translational addition theorem for vector spherical wave functions developed by Cruzan [83] to derive the solution for the scattering by two spheres of different sizes and for an arbitrary angle of incidence. Results, which take into account first and second order scattering, were presented and compared with the experimental results of Mevel [47] for the broadside case and with those of Angelakos and Kumagai for the endfire case. As observed by these authors, the calculations are complicated and tedious and errors due to slow convergence are likely. Furthermore, for large spheres (i.e. ka greater than one wavelength) these expressions are not suited for numerical calculations. Recently Bruning and Lo [84] have used conventional geometric optics and modified geometric theory of diffraction to obtain results which agree well with those computed by Liang and Lo [48] but are still in discrepancy when compared with experimental results.

To alleviate the above difficulties, the aim of this section is to obtain a simple relation in a form more convenient and suited for calculation purposes, using geometrical diffraction theory. Knowing the solution for the scattered field from a single sphere the solution for the multiple sphere case is easily obtained. The single sphere results have been analyzed in the last section for accuracy and will be used here to obtain results for the two sphere case.

Furthermore, the approach is shown to be more readily adaptable for scattering from multiple spheres than previous formulations, as considered in the next section, and scattering cross-sections for arbitrary angles of incidence and observation are easily calculated using this method.

The solution for the scattering of plane waves by two spheres will be developed for an arbitrary angle of incidence and an arbitrary angle of observation for two non-identical spheres. We assume that the spacing of the spheres is large compared to their dimensions and to the wavelength.

Consider a plane wave incident on two spheres whose centers are at a distance kd apart on the z axis as shown in Fig. 2.5. Let sphere 1 have a radius 'a' and sphere 2 radius 'b'. Further assume that the angles of incidence and observation are θ_i and θ_o measured with respect to the x axis, as shown. Using the ray technique, the field at any point may be obtained as the sum of the field scattered by each sphere individually plus fields re-scattered by one sphere due to fields scattered by the other.

At a sufficiently large distance from the sphere, the scattered field resembles a plane wave. This in turn is scattered by the second sphere perturbing its scattered field, which response in turn is scattered by the first sphere perturbing the scattered field of the first sphere. This successive process is repeated to obtain higher order terms and the perturbed patterns are superimposed to obtain the total solution.

If $E_a(\theta)$ represents the unperturbed bistatic scattered field at an angle θ of the sphere of radius a and, similarly $E_b(\theta)$ is that of sphere of radius b, then the total scattered electric field at any arbitrary angle of observation θ_o is given by

$$E_T = E_1 + E_2 \tag{2.11}$$

where E_1 and E_2 are due to the rays scattered by spheres 1 and 2 respectively. Hence

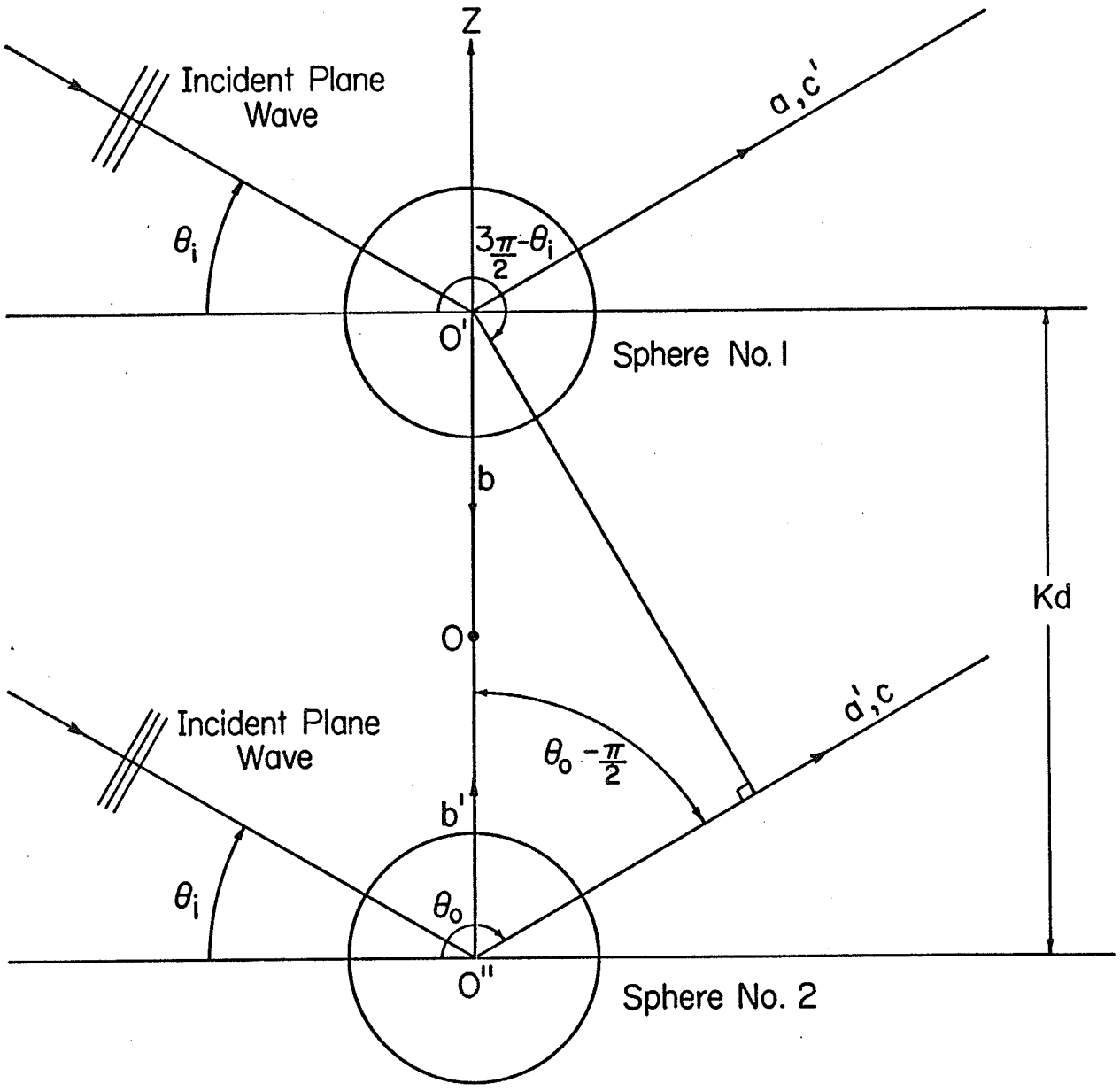

The two sphere scattering configuration

FIG. 2.5

$$E_T = E_a(\theta_o - \theta_i) + E_b(\theta_o - \theta_i)e^{-jkd[\sin\theta_i+\sin(\pi-\theta_o)]}$$

$$+ \frac{E_a(3\pi/2) - \theta_i)E_b(\theta_o - \pi/2)}{kd} e^{-jkd[1+\sin(\pi-\theta_o)]}$$

$$+ \frac{E_a(3\pi/2 - \theta_i)E_b(0)E_a(3\pi/2 - \theta_o)}{kd^2} e^{-2jkd}$$

$$+ \frac{E_a(3\pi/2 - \theta_i)E_b(0)E_a(0)E_b(\theta_o - \pi/2)}{kd^3} e^{-jkd[3+\sin(\pi-\theta_o)]}$$

$$+ \frac{E_a(3\pi/2 - \theta_i)E_b^2(0)E_a(0)E_a(3\pi/2 - \theta_o)}{kd^4} e^{-j4kd} + \ldots$$

$$+ \frac{E_b(\pi/2 - \theta_i)}{kd} E_a(3\pi/2 - \theta_o)e^{-jkd(1+\sin\theta_i)}$$

$$+ \frac{E_b(\pi/2 - \theta_i)E_a(0)E_b(\theta_o - \pi/2)}{kd^2}$$

$$\cdot \exp\left[- jkd(2 + \sin\theta_i + \sin(\pi - \theta_o)\right]$$

$$+ \frac{E_b(\pi/2 - \theta_i)E_a(0)E_b(0)E_a(3\pi/2 - \theta_o)}{kd^3} e^{-jkd(3+\sin\theta_i)}$$

$$+ \frac{E_b(\pi/2 - \theta_i)E_a^2(0)E_b(\theta_o - \pi/2)E_b(0)}{kd^4} e^{-jkd[4+\sin\theta_i+\sin(\pi-\theta_o)]} + \ldots$$

(2.12)

Combining terms and summing over all possible interactions, we obtain

$$E_T = E_a(\theta_o - \theta_i) + E_b(\theta_o - \theta_i)e^{-jkd[\sin\theta_i+\sin(\pi-\theta_o)]}$$

$$+ \frac{E_a(3\pi/2 - \theta_i)}{kd\cdot A} E_b(\theta_o - \pi/2)e^{-jkd[1+\sin(\pi-\theta_o)]}$$

$$+ \frac{E_a(3\pi/2 - \theta_o)}{kd} E_b(0) e^{-2jkd}$$

$$+ \frac{E_b(\pi/2 - \theta_i)}{kd \cdot A} E_a(3\pi/2 - \theta_o) e^{-jkd(1+\sin\theta_i)}$$

$$+ \frac{E_a(0) E_b(\theta_o - \pi/2)}{kd} e^{-jkd(2+\sin\theta_i+\sin(\pi-\theta_o)} \qquad (2.13)$$

where

$$A = 1 - \frac{E_a(0) E_b(0) e^{-2jkd}}{kd^2} \qquad (2.14)$$

Evaluation of E_T leads to the evaluation of scattering cross-sections for two spheres.

2.4 Extension to the Multiple Sphere Problem

The extension of the procedure in order to deal with the scattering by a number of spheres arbitrarily distributed, can be demonstrated by formulating the three sphere problem. Let the spheres A, B and C of radii a, b and c respectively, lie at the corners of a triangle with sides kd_1, kd_2 and kd_3 and angles θ_1, θ_2, θ_3 as shown in Fig. 2.6. For plane wave incidence, we denote the angles of incidence and observation by θ_i and θ_o and we let $E_a(\theta)$, $E_b(\theta)$ and $E_c(\theta)$ represent the unperturbed scattered fields, at the bistatic angle θ, due to the spheres A, B and C respectively. With the center of sphere A as the origin of the system of coordinates, the total far field, on basis of the previous section, is obtained as a superposition of the fields scattered by the three spheres and is given by

$$E_T = E_a(\theta_o - \theta_i) + E_b(\theta_o - \theta_i) e^{-jkd_i[\sin\theta_i+\sin(\pi-\theta_o)]}$$

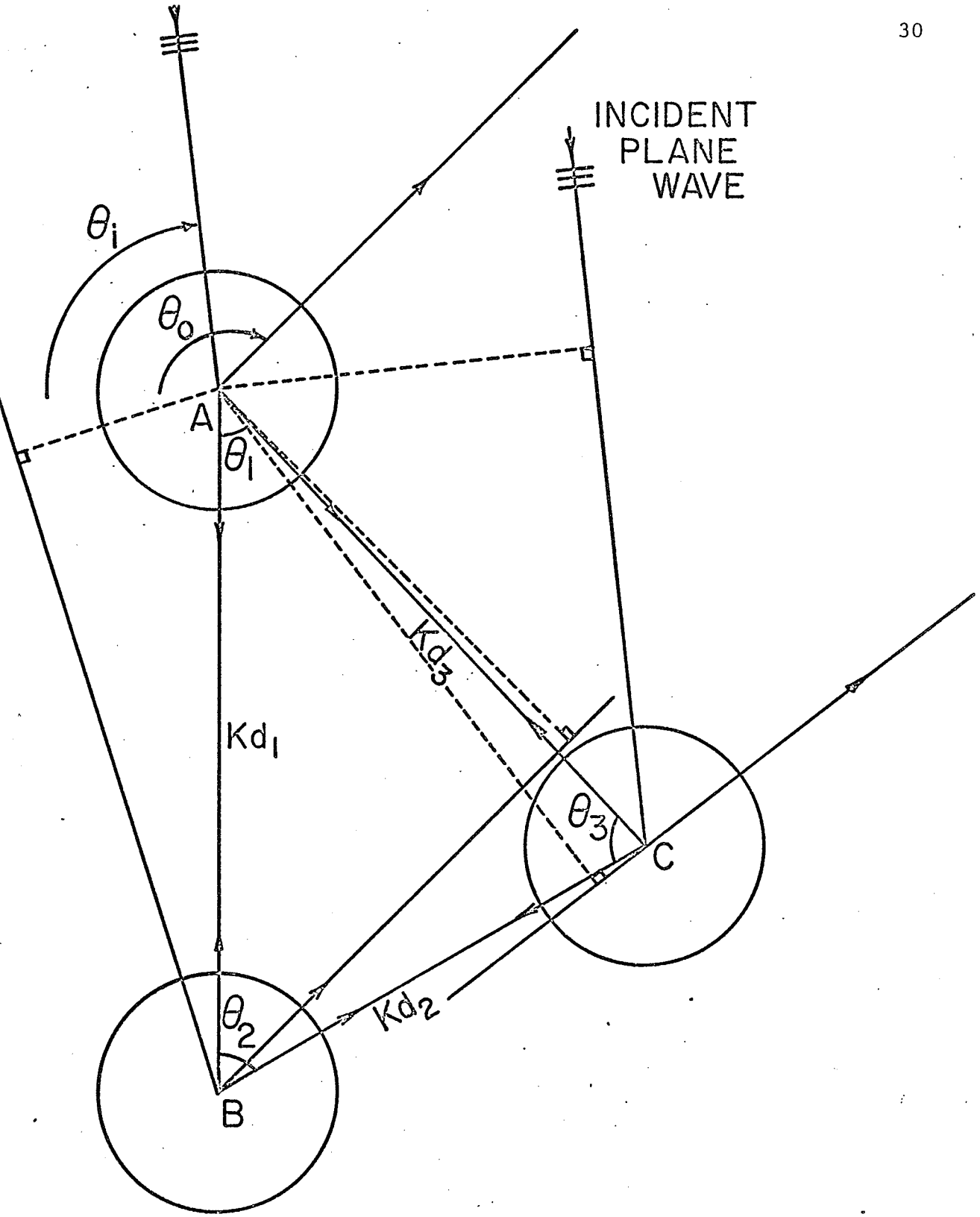

FIG. 2.6 Three sphere scattering geometry

$$+ E_c(\theta_o - \theta_i)e^{-jkd_3[\sin(3\pi/2-\theta_o-\theta_1)-\sin(\theta_o+\theta_1-\pi)}$$

$$+ \frac{E_a(3\pi/2 - \theta_i)E_b(\theta_o - \pi/2)}{kd_1} e^{-jkd_1[1+\sin(\pi-\theta_o)]}$$

$$+ \frac{E_a(3\pi/2 - \theta_i - \theta_1)E_c(\theta_o - \pi/2 - \theta_1)}{kd_3} e^{-jkd_3[1-\sin(\theta_o+\theta_1-\pi)]}$$

$$+ \frac{E_b(\pi/2 - \theta_i)E_a(3\pi/2 - \theta_o)}{kd_1} e^{-jkd_1(1+\sin\theta_i)}$$

$$+ \frac{E_b(\pi/2 - \theta_i + \theta_2)E_c(\pi/2 + \theta_o - \theta_2)}{kd_2} \cdot e^{[-jkd_1\sin\theta_i-jkd_2+\sin(\theta_o+\theta_1-\pi)]}$$

$$+ \frac{E_c(\theta_i - \pi/2 - \theta_3)E_a(3\pi/2 - \theta_1 - \theta_o)}{kd_3} e^{-jkd_3} e^{-jkd_3\sin(\pi-\theta_i-\theta_1)}$$

$$+ \frac{E_c(\theta_o - \theta_2)E_b(\theta_2 - \theta_o + \pi/2)}{kd_2} e^{-jkd_3-jkd_3\sin(\pi-\theta_i-\theta_1)-jkd_1\sin(\pi-\theta_o)}$$

$$+ \ldots. \qquad (2.15)$$

Equation (2.15) contains interaction terms taking into account up to the first order only. Similarly, the higher order interaction terms are easily formulated. A matrix formulation for the scattering by a randomly distributed set of spheres can be drawn up in close analogy to the radiation by an array of antennas, as is evident from the nature of the terms in (2.13) and (2.15). The above equations hold only when the separation distance between any two spheres is much greater than the wavelength and the diameters of the spheres. However, taking an asymptotic expansion of the various terms in the Mie series solution [85] for the scattering of a plane wave by a sphere, the scattered field due to one

sphere can be expressed in terms of incident plane waves and their derivatives evaluated in the neighbourhood of the adjacent sphere. Carrying out this process of successive scattering, we will obtain a solution which will predict accurately the scattered field from a random distribution of spheres. Calculations of this nature have been carried out by Twersky [86] for an arbitrary planar configuration of parallel cylinders and, in particular, for two identical cylinders. It is evident that for an arbitrary configuration, the computations would be more tedious than for the two sphere case. However, using the fact that the fields scattered by the various spheres are "consistent" with one another simplifies the calculations. Further, the problem would perhaps be simplified if considered as a problem of caustic-caustic interactions which will considerably reduce the computations, particularly if the scattering matrix approach is used.

2.5 Numerical Results

Using the bistatic data compiled by Ross and Bhartia [87] from the exact solution for various ka values, and equation (2.13), we can generate polar plots for a particular set of spheres at various distances of separation. Bistatic results may also be generated for two spheres. However, to verify the expressions, we consider the endfire and broadside cases for which experimental data is available. Fig. 2.7 shows a plot of normalized backscattering cross section with various sphere separations for two identical spheres of ka = 4.19 in the broadside set up. Curves taking into account only the first order interaction and a single curve taking account all interactions are presented. Thus we

see that even taking into account first order interactions and using the exact solutions for a single sphere, we obtain better agreement with the experimental results of Mevel [47] than has been possible with previous formulations. A curve using the approximate theory of Section 2.2 is also plotted and once again we find better agreement than obtained previously. Also, though equation (2.13) is for large sphere separations, it, nevertheless, gives agreement with experiment even in the region where the sphere separation is not large compared to the sphere size. With increasing sphere size, the approximate theory results are more accurate and so a better agreement with experiments will be obtained.

Fig. 2.8 shows the backscattered section for spheres in the endfire position having a ka of 7.41. Here again the above remarks about the accuracy apply. Fig. 2.9 is a plot for the backscattered cross-section when two identical spheres at a fixed distance apart are rotated. In this figure $\theta = 0$ corresponds to the broadside position of the spheres and $\theta = 90°$ to the endfire position. No comparison with experiment is possible here due to lack of such data.

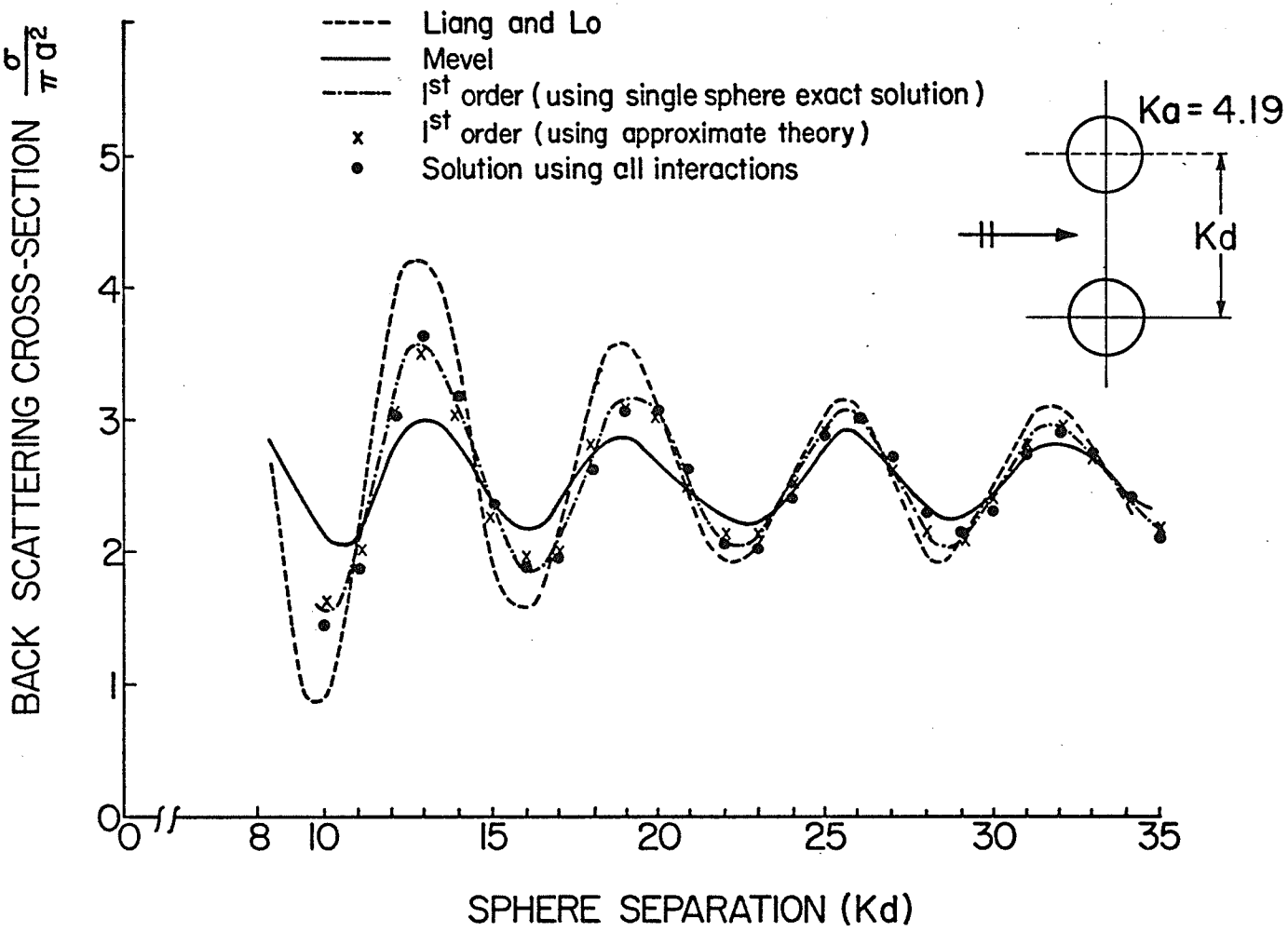

FIG. 2.7 Broadside backscattering cross-section vs sphere separation (Ka = 4.19)

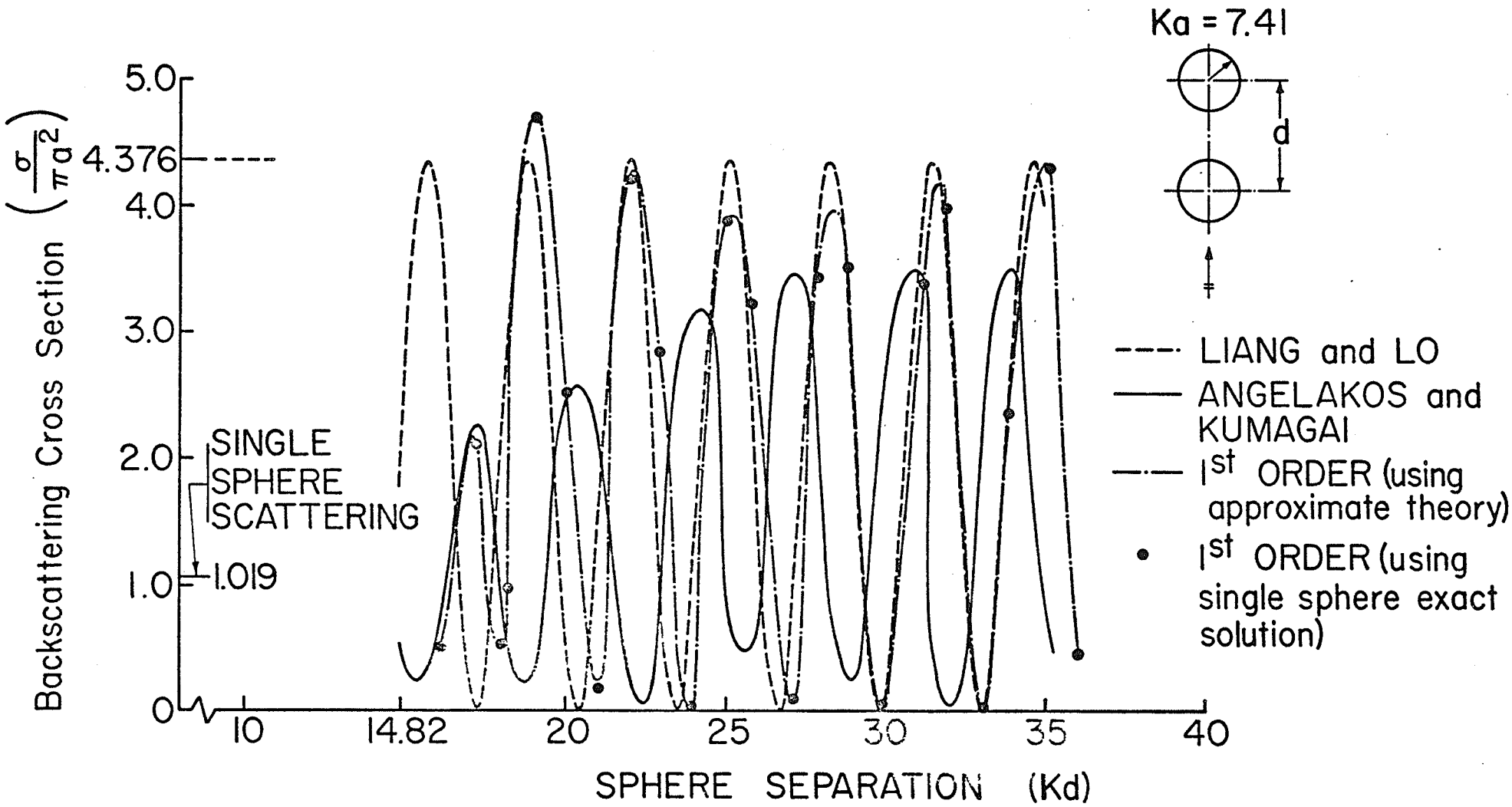

FIG. 2.8 Endfire Backscattering Cross Section vs Sphere Separation (Ka = 7.41)

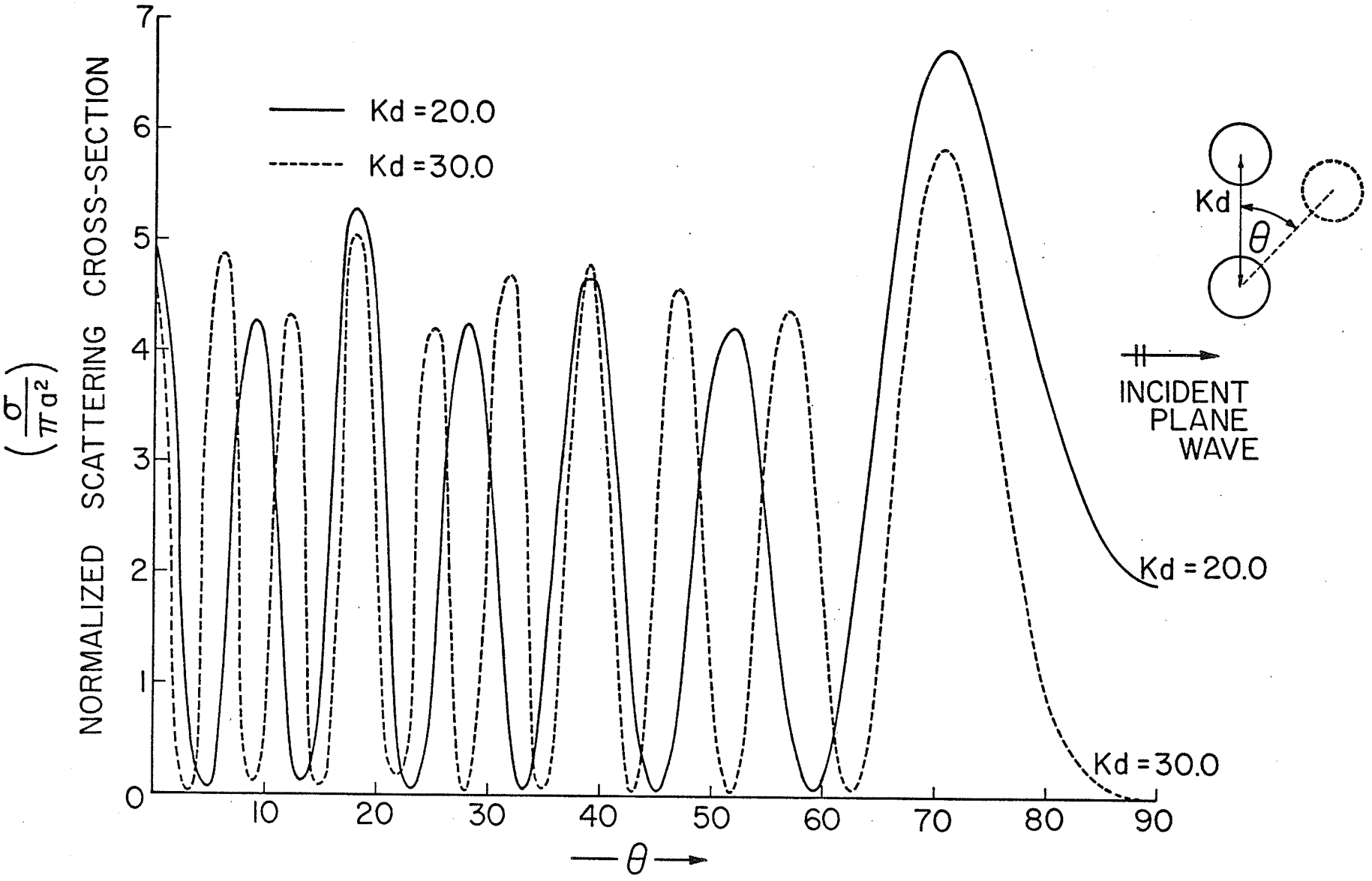

FIG. 2.9 Back Scattering Cross-section for Two Speres vs. Orientation Angle (Ka = 5.0)

CHAPTER III

EXTENSION TO THE IMPERFECTLY CONDUCTING SPHERE

3.1 Introduction

Chapter II has dealt with the ray optical scattering of plane waves by imperfectly conducting spheres. However, in practice the sphere usually has finite conductivity, surface roughness or may be coated with a layer of another material. Such a scatterer is of practical importance in various applications as described in Chapter V.

To consider the effect of finite conductivity, surface roughness, or coating on the scattering properties, these must be incorporated either directly or indirectly into the formulation of the problem. This is achieved most conveniently by the application of the Leontovich impedance boundary condition, which accounts for these imperfections in the form of an effective surface impedance as shown in this chapter.

Impedance boundary conditions have been extensively used in scattering and diffraction problems to consider the material composition and surface characteristics of the body. Various fundamental scatterers have been considered, with particular emphasis on the finitely conducting plane, cylinder and sphere which have exact solutions. However, dispite considerable effort, the scattering behaviour of spheres with an impedance boundary is not fully understood and various related questions remain unanswered. Thus the exact series solution given in Appendix A converges very slowly when the electrical radius of the sphere ka is large compared to unity, requiring lengthy computations even with present day computers. Furthermore, the series solution does not provide a physical

insight into the scattering behaviour and an alternative solution in a simple analytical form is hence desirable.

An asymptotic solution of the problem for large ka, using the method of Fock [88], together with creeping wave concepts in conjunction with the geometrical theory of diffraction, presents a possibility for overcoming both drawbacks of the exact solution. The procedure was used effectively in the previous chapter for the scattering by a perfectly conducting sphere and essentially the same method is used here to derive asymptotic expressions for the geometrical optics and creeping wave terms for both polarizations for the monostatic and forward scattered fields, as well as the bistatic field.

3.2 Formulation of the Problem

Consider a plane electromagnetic wave incident along the negative z direction on a sphere of radius a as shown in Fig. 2.1. If the electric field is parallel to the x axis, we have

$$E_x^i = \hat{x}\, E_o\, e^{jkr\cos\theta}$$
$$H_y^i = \hat{y}\, \frac{E_o}{\eta_o}\, e^{jkr\cos\theta} \tag{3.1}$$

where $k = 2\pi/\lambda$, $\eta_o = 120\pi$ and the $e^{-j\omega t}$ time dependence has been suppressed. The exact modal series expressions for the non-vanishing components of the scattered electric field from Appendix A are given as

$$E_\theta^s = j\, \frac{E_o e^{jkr}}{kr}\, \cos\phi\; p(\theta) \tag{3.2a}$$

and

$$E_\phi^s = -\, j\, \frac{E_o e^{jkr}}{kr}\, \sin\phi\; q(\theta) \tag{3.2b}$$

where

$$p(\theta) = \sum_{n=1}^{\infty} \frac{(2n+1)}{n(n+1)} \left[B_n \frac{\partial}{\partial \theta} P_n^1(\cos\theta) + C_n \frac{P_n^1(\cos\theta)}{\sin\theta} \right] \tag{3.3a}$$

$$q(\theta) = \sum_{n=1}^{\infty} \frac{(2n+1)}{n(n+1)} \left[B_n \frac{P_n^1(\cos\theta)}{\sin\theta} + C_n \frac{\partial}{\partial \theta} P_n^1(\cos\theta) \right] \tag{3.3b}$$

$$B_n = \frac{\hat{j}_n'(ka) + j\eta \hat{j}_n(ka)}{\hat{h}_n^{(1)'}(ka) + j\eta \hat{h}_n^{(1)}(ka)} \tag{3.3c}$$

$$C_n = \frac{\hat{j}_n'(ka) + j\delta \hat{j}_n(ka)}{\hat{h}_n^{(1)'}(ka) + j\delta \hat{h}_n^{(1)}(ka)} \tag{3.3d}$$

and

$$\eta = \frac{Z}{\eta_o} , \quad \delta = \frac{Y}{Y_o} = \frac{1}{\eta} \tag{3.3e}$$

where the prime notation denotes differentiation with respect to the argument. η and δ are the normalized values of the surface impedance Z and the admittance Y with respect to the corresponding free space values η_o and Y_o, respectively. The directions $\theta = 0$ and $\theta = \pi$ correspond to the forward and backscattering directions and $P_n^1(\cos\theta)$ are the Legendre functions defined before and

$$\hat{j}_n(x) = x\, j_n(x) \tag{3.4a}$$

$$\hat{h}_n^{(1)}(x) = x\, h_n^{(1)}(x) \tag{3.4b}$$

where $j_n(x)$ and $h_n^{(1)}(x)$ are spherical Bessel and Hankel functions defined in the previous chapter. In arriving at (3.2), the Leontovich impedance boundary condition [1]

$$\bar{E} - (\bar{E} \cdot \bar{n})\bar{n} = Z(\bar{n} \times \bar{H}) \tag{3.5}$$

has been applied as in the same manner for various scattering and propagation problems involving impedance boundaries.

To consider various surface conditions, the normalized impedance η is expressed in the form

$$\eta = |\eta| e^{j\xi} \tag{3.6}$$

where $\xi = -\pi/2$ for a purely capacitive surface, $\pi/2$ for an inductive surface, $\pi/4$ for a homogeneous conductor and generally assumes different values for lossy or corrugated surfaces.

The normalized bistatic scattering cross sections in the E and H planes are the main parameters of interest and are given by

$$\frac{\sigma_e}{\pi a^2} = \frac{4}{(ka)^2} |p(\theta)|^2 \tag{3.7a}$$

$$\frac{\sigma_h}{\pi a^2} = \frac{4}{(ka)^2} |q(\theta)|^2 \tag{3.7b}$$

respectively. In particular σ_b, σ_f, σ_θ will be used to denote the normalized back, forward and bistatic cross sections respectively.

To put equation (3.3) in a form suitable for the application of the Watson's transformation, we use the relationship

$$P_n^{-1}(\cos\theta) = -\frac{1}{n(n+1)} P_n^1(\cos\theta) \tag{3.8}$$

therein and obtain for $p(\theta)$ and $q(\theta)$ the following expressions

$$p(\theta) = -\sum_{n=1}^{\infty} (2n+1) \left\{ B_n \frac{\partial}{\partial\theta} P_n^{-1}(\cos\theta) + C_n \frac{P_n^{-1}(\cos\theta)}{\sin\theta} \right\} \tag{3.9a}$$

$$q(\theta) = -\sum_{n=1}^{\infty} (2n+1) \left\{ B_n \frac{P_n^{-1}(\cos\theta)}{\sin\theta} + C_n \frac{\partial}{\partial\theta} P_n^{-1}(\cos\theta) \right\} \tag{3.9b}$$

Note that it is adequate to work with one polarization, since the results for the other polarization may be obtained directly from these. Choosing, without loss of generality, the E plane expression, the series for $p(\theta)$ on transformation into a contour integral gives

$$p(\theta) = -\int_C \left\{ B_{\nu-\frac{1}{2}} \frac{\partial}{\partial\theta} P^{-1}_{\nu-\frac{1}{2}}(\cos\theta) + C_{\nu-\frac{1}{2}} \frac{P^{-1}_{\nu-\frac{1}{2}}(\cos\theta)}{\sin\theta} \right\} \frac{2\nu d\nu}{1 + e^{2j\nu\pi}} \tag{3.10}$$

where C is a path enclosing, in a clockwise sense, the zeros of $(1 + e^{2j\nu\pi})$ for $\nu > 0.5$ as shown in Fig. 3.1.

Writing the Bessel functions in $B_{\nu-\frac{1}{2}}$ and $C_{\nu-\frac{1}{2}}$ in terms of Hankel functions of the first and second kind and evaluating (3.10) by the theory of residues, we obtain two new integrals, the first of which reduces to zero since

$$\sum_{n=1}^{\infty} (n + \frac{1}{2}) P^{-1}_n(\cos\theta) = -\frac{1}{2} \operatorname{Cot}(\frac{\theta}{2}) \tag{3.11}$$

and $p(\theta)$ is hence given by

$$p(\theta) = -\int_{\infty - j\varepsilon}^{\infty + j\varepsilon} \left\{ D_{\nu-\frac{1}{2}} \frac{\partial}{\partial\theta} P^{-1}_{\nu-\frac{1}{2}}(\cos\theta) + G_{\nu-\frac{1}{2}} \frac{P^{-1}_{\nu-\frac{1}{2}}(\cos\theta)}{\sin\theta} \right\} \frac{\nu d\nu}{1 + e^{2j\nu\pi}} \tag{3.12a}$$

where

$$D_{\nu-\frac{1}{2}} = \frac{\hat{h}^{(2)'}_{\nu-\frac{1}{2}}(ka) + j\eta \hat{h}^{(2)}_{\nu-\frac{1}{2}}(ka)}{\hat{h}^{(1)'}_{\nu-\frac{1}{2}}(ka) + j\eta \hat{h}^{(1)}_{\nu-\frac{1}{2}}(ka)} \tag{3.12b}$$

$$G_{\nu-\frac{1}{2}} = \frac{\hat{h}^{(2)'}_{\nu-\frac{1}{2}}(ka) + j\delta \hat{h}^{(2)}_{\nu-\frac{1}{2}}(ka)}{\hat{h}^{(1)'}_{\nu-\frac{1}{2}}(ka) + j\delta \hat{h}^{(1)}_{\nu-\frac{1}{2}}(ka)} \tag{3.12c}$$

and ε is a small positive number which is eliminated when the contour

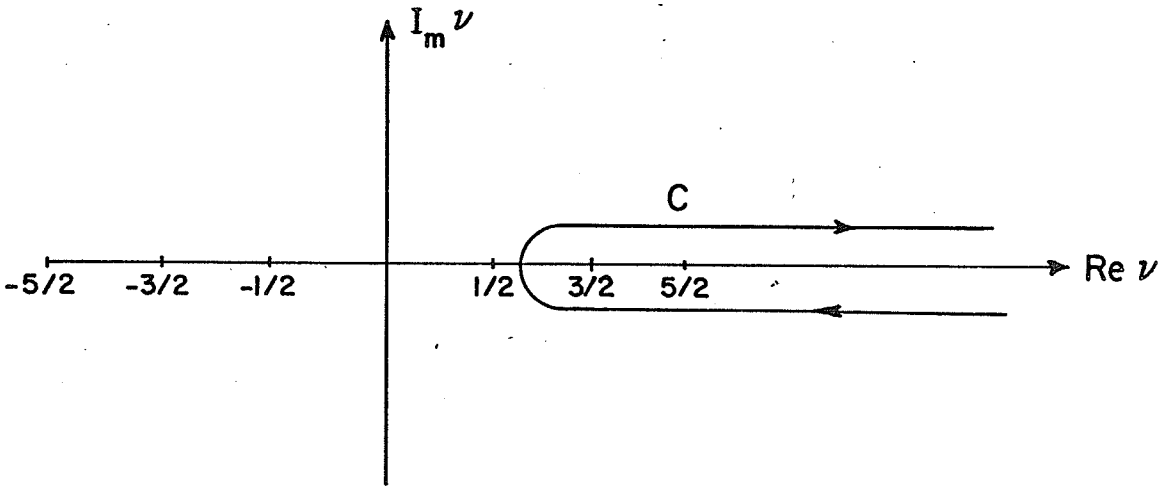

FIG. 3.1 INTEGRATION PATH C

runs just above the real axis.

A similar procedure for $q(\theta)$ leads to the form

$$q(\theta) = -\int_{\infty-j\varepsilon}^{\infty+j\varepsilon} \left\{ D_{\nu-\frac{1}{2}} \frac{P^{-1}_{\nu-\frac{1}{2}}(\cos\theta)}{\sin\theta} + G_{\nu-\frac{1}{2}} \frac{\partial}{\partial\theta} P^{-1}_{\nu-\frac{1}{2}}(\cos\theta) \right\} \frac{\nu d\nu}{1 + e^{2j\nu\pi}} \tag{3.12d}$$

and it remains to separate (3.12a) and (3.12d) into geometric optics and creeping wave terms.

This is done in the bistatic range of angles

$$\psi < \theta < \pi - \psi \quad ; \quad \psi = 0(\frac{1}{ka}) \tag{3.13}$$

where the forward and backscatter directions are excluded, since they correspond to caustics in the field.

It is convenient to express the Legendre functions in terms of the $E_m^{(1),(2)}(\nu,\theta)$ functions introduced by Logan [89], i.e.

$$(-1)^m 2P^{-m}_{\nu-\frac{1}{2}}(\cos\theta) = E_m^{(1)}(\nu,\theta) + E_m^{(2)}(\nu,\theta) \tag{3.14}$$

where the $E_m^{(1),(2)}(\nu,\theta)$ functions are defined explicitly by

$$E_m^{(1),(2)}(\nu,\theta) = \frac{\Gamma(\nu - m + \frac{1}{2})}{\Gamma(\nu + 1)} \sqrt{\frac{2}{\pi\sin\theta}}\, e^{\pm j(\nu\theta - \frac{\pi}{4} - \frac{m\pi}{2})}$$

$$\times\ {}_2F_1(\tfrac{1}{2}m,\ \tfrac{1}{2} - m,\ \nu + 1,\ \mp\frac{je^{\pm j\theta}}{2\sin\theta}) \tag{3.15}$$

and are convergent in the range $\pi/6 < \theta < 5\pi/6$. These functions possess asymptotic values for large ν and $\varepsilon_1 < \theta < \pi/6$ or $5\pi/6 < \theta < \pi - \varepsilon_1$, where $\varepsilon_1 > 0$ and has a modulus of 2π. The asymptotic relation is given by Macdonald's formula, i.e.

$$E_m^{(1),(2)} \simeq \frac{1}{\nu^m}\sqrt{\frac{\theta}{\sin\theta}}\, H_m^{(1),(2)}(\nu\theta) \tag{3.16}$$

where $H_m^{(1),(2)}(\nu\theta)$ denote the Hankel functions of order m. Expressing $(\sin\theta)^{-\frac{1}{2}}$ as $|\sin\theta|^{-\frac{1}{2}}$ for $0 < \theta < \pi$, and utilizing the fact that the (3.15) hypergeometric functions are periodic in θ with period π, we have for integer ℓ

$$e^{j\nu\ell\pi} E_m^{(1)}(\nu,\theta) = E_m^{(1)}(\nu,\ell\pi + \theta) \tag{3.17a}$$

and

$$e^{j\nu\ell\pi} E_m^{(2)}(\nu,\theta) = e^{j(m+\frac{1}{2})\pi} E_m^{(1)}(\nu,\ell\pi - \theta) \tag{3.17b}$$

Substituting (3.14) into (3.12a) and (3.12d) and splitting each resulting integrand into two parts, we obtain

$$p(\theta) = S_p^o(\theta) + S_p^c(\theta) \tag{3.18a}$$

$$q(\theta) = S_q^o(\theta) + S_q^c(\theta) \tag{3.18b}$$

where the superscripts "o" and "c" denote the geometric optics and creeping wave terms, respectively, and

$$S_p^o(\theta) = \frac{1}{2}\int_{-\infty+j\varepsilon}^{\infty+j\varepsilon} \left\{ D_{\nu-\frac{1}{2}} \frac{\partial}{\partial\theta} E_1^{(2)}(\nu,\theta) + G_{\nu-\frac{1}{2}} \frac{E_1^{(2)}(\nu,\theta)}{\sin\theta} \right\} \nu d\nu \tag{3.19}$$

$$S_p^c(\theta) = \frac{1}{2}\int_{-\infty+j\varepsilon}^{\infty+j\varepsilon} \left\{ D_{\nu-\frac{1}{2}} \left[\frac{\partial}{\partial\theta} E_1^{(1)}(\nu,\theta) \frac{1}{1+e^{2j\nu\pi}} - \frac{\partial}{\partial\theta} E_1^{(2)}(\nu,\theta) \frac{1}{1+e^{-2j\nu\pi}} \right] \right.$$

$$\left. + G_{\nu-\frac{1}{2}} \left[\frac{E_1^{(1)}(\nu,\theta)}{\sin\theta} \frac{1}{1+e^{2j\nu\pi}} - \frac{E_1^{(2)}(\nu,\theta)}{\sin\theta} \frac{1}{1+e^{-2j\nu\pi}} \right] \right\} \nu d\nu \tag{3.20}$$

while $S_q^o(\theta)$ and $S_q^c(\theta)$ are obtained from (3.19) and (3.20) by interchanging $D_{\nu-\frac{1}{2}}$ and $G_{\nu-\frac{1}{2}}$ in the integrands. Note that the creeping wave

terms decay exponentially as $\text{Im}\ \nu \to \infty$.

Since the operators $\frac{\partial}{\partial\theta}$ and $\frac{1}{\sin\theta}$ in (3.19) and (3.20) do not essentially affect the behaviour of $P^{-1}_{\nu-\frac{1}{2}}(\cos\theta)$ as a function of ν for $|\nu| \gg 1$, $\text{Im}\ \nu > 0$, we see from (3.16) that the asymptotic value of $E^{(1),(2)}_m(\nu,\theta)$ decays exponentially in ν as $e^{j\nu(\theta-\pi/2)}$. Closing the contours in the upper half plane, the contribution from the semi-circular path vanishes and the integrals can then be evaluated by the method of residues from the zeros (ν_n,ν_m) of $\hat{h}^{(1)'}_{\nu-\frac{1}{2}}(ka) + j\eta\hat{h}^{(1)}_{\nu-\frac{1}{2}}(ka)$ and $\hat{h}^{(1)'}_{\nu-\frac{1}{2}}(ka) + j\delta\hat{h}^{(1)}_{\nu-\frac{1}{2}}(ka)$ if the remainder of the integrands remain bounded. This is possible in this case since a path between two zeros can always be found where this condition holds. Hence we obtain

$$
\begin{aligned}
S^c_p(\theta) = {} & j\pi \sum_n U_{\nu-\frac{1}{2}}\Big|_{\nu=\nu_n} \Bigg[\frac{\partial}{\partial\theta} E^{(1)}_1(\nu,\theta)\, \frac{1}{1+e^{2j\nu\pi}} \\
& - \frac{\partial}{\partial\theta} E^{(2)}_1(\nu,\theta)\, \frac{1}{1+e^{-2j\nu\pi}}\Bigg] \\
& + j\pi \sum_m V_{\nu-\frac{1}{2}}\Big|_{\nu=\nu_m} \Bigg[\frac{E^{(1)}_1(\nu,\theta)}{\sin\theta}\, \frac{1}{1+e^{2j\nu\pi}} \\
& - \frac{E^{(2)}_1(\nu,\theta)}{\sin\theta}\, \frac{1}{1+e^{-2j\nu\pi}}\Bigg]
\end{aligned}
\tag{3.21}
$$

where

$$
U_{\nu-\frac{1}{2}} = \frac{\nu\left[\hat{h}^{(2)'}_{\nu-\frac{1}{2}}(ka) + j\eta\hat{h}^{(2)}_{\nu-\frac{1}{2}}(ka)\right]}{\frac{\partial}{\partial\nu}\left[\hat{h}^{(1)'}_{\nu-\frac{1}{2}}(ka) + j\eta\hat{h}^{(1)}_{\nu-\frac{1}{2}}(ka)\right]}
$$

$$
V_{\nu-\frac{1}{2}} = \frac{\nu\left[\hat{h}^{(2)'}_{\nu-\frac{1}{2}}(ka) + j\delta\hat{h}^{(2)}_{\nu-\frac{1}{2}}(ka)\right]}{\frac{\partial}{\partial\nu}\left[\hat{h}^{(1)'}_{\nu-\frac{1}{2}}(ka) + j\delta\hat{h}^{(1)}_{\nu-\frac{1}{2}}(ka)\right]}
$$

Hence it remains to evaluate $S_p^o(\theta)$ and $S_p^c(\theta)$ specifically for the monostatic, bistatic and forward scattering directions, using the above expressions.

3.3 The Monostatic Field

The monostatic or backscattered field will be considered first due to its importance and may be evaluated by introducing the transformation

$$\alpha = \pi - \theta \tag{3.22}$$

and the relation

$$E_1^{(1),(2)}(\nu,\theta) = e^{\pm j\nu\pi}\left[\mp jP^{-1}_{\nu-\frac{1}{2}}(\cos\alpha) + \frac{2}{\pi} Q^{-1}_{\nu-\frac{1}{2}}(\cos\alpha)\right] \tag{3.23}$$

where $Q^{-1}_{\nu-\frac{1}{2}}(\cos\theta)$ are the Legendre functions of the second kind. Substituting (3.22) and (3.23) into (3.21) leads to

$$S_p^c(\alpha) = -\pi \sum_n U_{\nu-\frac{1}{2}}\Big|_{\nu=\nu_n} \operatorname{Sec} \nu_n\pi \frac{\partial}{\partial\alpha} P^{-1}_{\nu_n-\frac{1}{2}}(\cos\alpha)$$

$$+ \pi \sum_m V_{\nu-\frac{1}{2}}\Big|_{\nu=\nu_m} \operatorname{Sec} \nu_m\pi \frac{P^{-1}_{\nu_m-\frac{1}{2}}(\cos\alpha)}{\sin\alpha} \tag{3.24}$$

which is finite for $\alpha = 0$. The expression for $S_q^c(\theta)$ may be obtained in a similar manner.

Substituting (3.23) into (3.19) we obtain

$$S_p^o(\alpha) = -\frac{1}{2}\int_{-\infty+j\varepsilon}^{\infty+j\varepsilon}\left\{D_{\nu-\frac{1}{2}}\left[j\frac{\partial}{\partial\alpha} P^{-1}_{\nu-\frac{1}{2}}(\cos\alpha) + \frac{2}{\pi}\frac{\partial}{\partial\alpha} Q^{-1}_{\nu-\frac{1}{2}}(\cos\alpha)\right]\right.$$

$$\left. - G_{\nu-\frac{1}{2}}\left[j\frac{P^{-1}_{\nu-\frac{1}{2}}(\cos\alpha)}{\sin\alpha} + \frac{2}{\pi}\frac{Q^{-1}_{\nu-\frac{1}{2}}(\cos\alpha)}{\sin\alpha}\right]\right\} e^{-j\nu\pi}\nu d\nu \tag{3.25}$$

and using the relations

$$P^{-1}_{-\nu-\frac{1}{2}}(x) = P^{-1}_{\nu-\frac{1}{2}}(x) \tag{3.26}$$

$$Q^{-1}_{-\nu-\frac{1}{2}}(x) = Q^{-1}_{\nu-\frac{1}{2}}(x) + \pi \tan(\nu\pi) P^{-1}_{\nu-\frac{1}{2}}(x) \tag{3.27}$$

we see that (3.25) reduces to the form

$$S^{o}_{p}(\alpha) = -\frac{1}{\pi}\int_{D}\left\{D_{\nu-\frac{1}{2}}\frac{\partial}{\partial\alpha}Q^{-1}_{\nu-\frac{1}{2}}(\cos\alpha) - G_{\nu-\frac{1}{2}}\frac{Q^{-1}_{\nu-\frac{1}{2}}(\cos\alpha)}{\sin\alpha}\right\}e^{-j\nu\pi}\nu d\nu$$

$$+\int_{\infty-j\varepsilon}^{0}\left\{D_{\nu-\frac{1}{2}}\frac{\partial}{\partial\alpha}P^{-1}_{\nu-\frac{1}{2}}(\cos\alpha) - G_{\nu-\frac{1}{2}}\frac{P^{-1}_{\nu-\frac{1}{2}}(\cos\alpha)}{\sin\alpha}\right\}\tan(\nu\pi)e^{-j\nu\pi}\nu d\nu \tag{3.28}$$

where the contour D is similar to C but intersecting the real ν axis between $-\frac{1}{2}$ and $+\frac{1}{2}$ as shown in Fig. 3.2. Evaluating the first integral on the right hand side of (3.28) in terms of the residues of $Q^{-1}_{\nu-\frac{1}{2}}(\cos\alpha)$, we obtain

$$S^{o}_{p}(\alpha) = -\frac{1}{2}\,\mathrm{Sec}^{2}(\alpha)e^{-2jka}\left(\frac{1-\eta}{1+\eta}\right) - \int_{\infty-j\varepsilon}^{0}\left\{D_{\nu-\frac{1}{2}}\frac{\partial}{\partial\alpha}P^{-1}_{\nu-\frac{1}{2}}(\cos\alpha)\right.$$

$$\left. - G_{\nu-\frac{1}{2}}\frac{P^{-1}_{\nu-\frac{1}{2}}(\cos\alpha)}{\sin\alpha}\right\}\tan(\nu\pi)e^{-j\nu\pi}\nu d\nu \tag{3.29}$$

Hence for the backscattering direction ($\alpha = 0$) we obtain

$$S^{o}_{p}(\pi) = -\frac{1}{2}\frac{(1-\eta)}{(1+\eta)}e^{-2jka} - \frac{1}{2}\int_{\infty-j\varepsilon}^{0}\left[D_{\nu-\frac{1}{2}} - G_{\nu-\frac{1}{2}}\right]\tan(\nu\pi)e^{-j\nu\pi}\nu d\nu \tag{3.30}$$

and

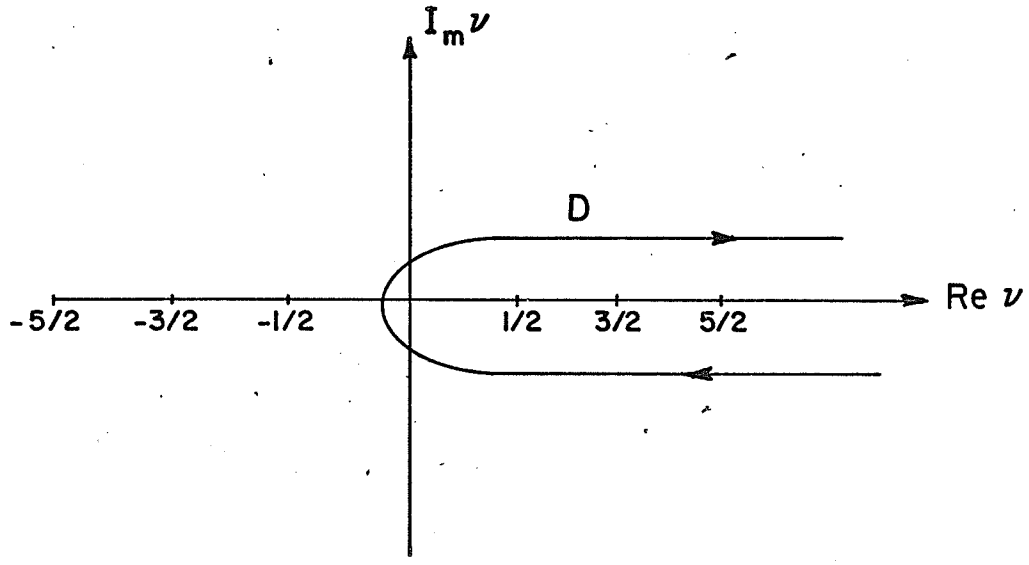

FIG. 3.2 INTEGRATION PATH D

$$S_p^c(\pi) = \frac{\pi}{2} \sum_n U_{\nu-\frac{1}{2}}\Big|_{\nu=\nu_n} \operatorname{Sec} \nu_n\pi - \frac{\pi}{2} \sum_m V_{\nu-\frac{1}{2}}\Big|_{\nu=\nu_m} \operatorname{Sec} \nu_m\pi \tag{3.31}$$

while the corresponding expressions for $S_q^c(\theta)\big|_{\theta=\pi}$ and $S_q^c(\theta)\big|_{\theta=\pi}$ are identical to (3.30) and (3.31), respectively, since $p(\pi) = q(\pi)$.

Using the Debye asymptotic formula [90] for the Hankel functions and evaluating the integrals in (3.30) directly, we obtain

$$S_p^o(\pi) = - j \frac{ka}{2} e^{-2jka} \left(\frac{1 - \eta}{1 + \eta}\right) \left[1 - \frac{j}{2ka} + \ldots\right] \tag{3.32}$$

which reduces to the corresponding expression for the perfectly conducting sphere when $\eta = 0$.

In order to evaluate the expression for the creeping wave term, it is convenient to resort to an Airy function series representation of the Hankel functions. Retaining the principal terms of the series for large values of the order and argument of the Hankel function, we obtain

$$\hat{h}^{(1)}_{\nu-\frac{1}{2}}(ka) \simeq - j \left(\frac{ka}{2}\right)^{1/6} W_1(t) \tag{3.33}$$

$$\hat{h}^{(1)\prime}_{\nu-\frac{1}{2}}(ka) \simeq j \left(\frac{ka}{2}\right)^{1/6} W_1'(t) \tag{3.34}$$

where $W_1(t)$ is the complex Airy function

$$W_1(t) = \sqrt{\pi} \left[\mathrm{Bi}(t) + j\, \mathrm{Ai}(t)\right] \tag{3.35a}$$

while t is related to ν by

$$\nu = ka + \tau t \quad , \quad \tau = \left(\frac{ka}{2}\right)^{1/3} \tag{3.35b}$$

Hence

$$S_p^c(\pi) = - j\tau\pi \left\{ \sum_{n=1}^{\infty} \frac{\nu_n \operatorname{Sec} \nu_n\pi}{(\beta_n + \eta^2\tau^2)[W_1(\beta_n)]^2} - \sum_{m=1}^{\infty} \frac{\eta^2 \nu_m \operatorname{Sec} \nu_m\pi}{(\tau^2 + \alpha_m\eta^2)[W_1(\alpha_m)]^2} \right\} \tag{3.36}$$

where α_m and β_m are the zeros of

$$W_1'(x) - j\eta\tau W_1(x) = 0 \tag{3.37a}$$

and

$$W_1'(x) - j\delta\tau W_1(x) = 0 \tag{3.37b}$$

respectively. Using the method of Streifer [49,91], the expressions for ν_n and ν_m are related to the zeros of $Ai'(-x)$ and $Ai(-x)$, denoted by γ_n and Ω_m, respectively, by the equations

$$\nu_n = ka + e^{j\pi/3}\tau\gamma_n - \frac{e^{j\pi/3}}{60\tau\gamma_n}(\gamma_n^3 - 9) + \frac{1}{1400\tau^3\gamma_n^3}(\gamma_n^6 - 7\gamma_n^3 + \frac{63}{4})$$

$$+ \frac{\tau^3\eta}{2\gamma_n^3}(\eta - \frac{j}{2\tau^3}) - j\frac{\eta}{10}(1 + \frac{1}{\gamma_n^3}) + \frac{j\eta\tau}{\gamma_n e^{j\pi/3}} - \frac{j\eta\tau}{10e^{2\pi j/3}\gamma_n^2}(1 - \frac{3}{2\gamma_n^3})$$

$$+ \frac{\eta}{e^{2\pi j/3}\gamma_n^3}(\frac{1}{3} - \frac{1}{2\gamma_n^2})(\frac{3j}{16\tau^2} - \frac{3\eta\tau}{4} - j\eta^2\tau^4)$$

$$+ \frac{\eta}{4e^{j\pi/3}\gamma_n^4}(\frac{7}{3} - \frac{5}{2\gamma_n^3})(\eta^3\tau^5 - j\eta^2\tau^2 - \frac{3\eta}{8\tau} + \frac{j}{16\tau^4})$$

$$- \frac{j\eta}{20\tau^2 e^{2\pi j/3}}(\frac{41\gamma_n}{126} + \frac{1}{5\gamma_n} - \frac{3}{10\gamma_n^5}) + \frac{\eta}{2e^{j\pi/3}\gamma_n}(\frac{3j}{16\tau^4} - \frac{3\eta}{4\tau} - j\eta^2\tau^2)$$

$$\cdot (\frac{1}{2\gamma_n^6} - \frac{7}{15\gamma_n^3} - \frac{11}{45}) + O(\tau^{-5}) \tag{3.38}$$

and

$$\nu_m = ka + \Omega_m e^{j\pi/3} + \frac{\Omega_m^2 e^{2j\pi/3}}{60\tau} + \frac{\Omega_m^3 - 10}{1400\tau^3} - \frac{j}{\delta} + \frac{1}{4\delta^2\tau^3}(1 - \frac{1}{\delta^2})$$

$$- j(\frac{1}{2} - \frac{1}{\delta^2})\frac{\Omega_m e^{j\pi/3}}{3\tau^2\delta} + \frac{j\Omega_m^2 e^{2\pi j/3}}{5\delta^3\tau^4}\left[\frac{\delta^3}{72} - \frac{13}{18}(\frac{j\delta^2}{4\tau^3} - \delta) - (\frac{1}{\delta} + \frac{3}{4\tau^3}\right]$$

$$+ O(\tau^{-5}) \tag{3.39}$$

where $\eta = 0[(ka)^{-2/3}]$, $\delta = 0(1)$ while γ_n and Ω_m have been tabulated by Logan [89] and others.

To obtain a physical interpretation of (3.36), we use the expansion

$$\text{Sec } \nu_n \pi = 2 \sum_{\ell=0}^{\infty} (-1)^{\ell} e^{j(2\ell+1)\pi\nu_n} \tag{3.40}$$

where the successive terms decrease exponentially and correspond to creeping wave terms decaying in amplitude due to radiation as they circle around the sphere. Because of this exponential decay, it is sufficient for large values of ka to retain the $\ell = 0$ term corresponding to creeping waves travelling half the circumference only. It may be shown that the first sum in (3.36) dominates and corresponds to E waves, while the second sum corresponds to H waves since their magnetic vectors are normal to the surface of the sphere.

3.4 The Bistatic Field

In order to evaluate the bistatic field in the range of the bistatic angle $\psi < \theta < \pi - \psi$ where $\psi = 0(1/ka)$, we use equations (3.19) and (3.21). A preliminary simplification can be made for $|\nu \sin\theta| > 1$ where $E_1^{(2)}(\nu,\theta)$ becomes predominantly exponential in nature and may be evaluated by the saddle point method. The saddle point in this case is at $\nu = ka \cos(\theta/2)$ and hence

$$E_1^{(2)}(\nu,\theta) = \sqrt{\frac{2}{\pi\nu\sin\theta}}\, e^{-j(\nu\theta-3\pi/4)} \text{cosec}\theta \left(1 - \frac{3j\cot\theta}{8\nu^2} + 0(\nu^{-3})\right) \tag{3.41}$$

$$\frac{\partial}{\partial\theta} E_1^{(2)}(\nu,\theta) = \sqrt{\frac{2}{\pi\nu\sin\theta}}\, e^{-j(\nu\theta-\pi/4} \left[1 - \frac{7j\cot\theta}{8\nu} + \frac{1}{128} \cdot (49 - 57\,\text{cosec}^2\theta) + 0(\nu^{-3})\right] \tag{3.42}$$

Using (3.41) and (3.42) together with the approximate expressions for $D_{\nu-\frac{1}{2}}$ and $G_{\nu-\frac{1}{2}}$ given in Appendix B, we proceed to evaluate (3.19) by the saddle point method for large $|\nu|$ and $|\nu \sin\theta| > 1$. For this we extend the path of integration from $0.5(\pi + \theta) - j\infty$ to $-0.5(\pi - \theta) + j\infty$ and we evaluate the integrand at the saddle point $\nu = ka \cos(\theta/2)$. This leads to a first approximation

$$S_p^o(\theta) = - j \frac{ka}{2}\left(\frac{1 - \eta}{1 + \eta}\right) e^{-2jka \sin \theta/2}\left[1 - \frac{j}{2ka \sin^3 \theta/2}\right.$$

$$\left. - \frac{7 \cos^2 \theta/2}{4ka^2 \sin^6 \theta/2} + \ldots\right] \tag{3.43}$$

and similarly

$$S_q^o(\theta) = - j \frac{ka}{2} \left(\frac{1 - \eta}{1 + \eta}\right) e^{-2jka \sin \theta/2}\left[1 + \frac{j \cos\theta}{2ka \sin^3 \theta/2} + \ldots\right] \tag{3.44}$$

where (3.43) and (3.44) reduce to the backscattered geometric optics field (3.32) for $\theta = \pi$.

A somewhat different procedure is used to derive the creeping wave expression in the bistatic range of θ. For this we use the relations

$$E_1^{(1)}(\nu,\theta) = j e^{j\nu\pi} E_1^{(2)}(\nu,\alpha) \tag{3.45}$$

$$E_1^{(2)}(\nu,\theta) = - j e^{-j\nu\pi} E_1^{(1)}(\nu,\alpha) \tag{3.46}$$

and the desired expression hence reduces to

$$S_p^c(\alpha) = - 2\pi \sum_n U_{\nu-\frac{1}{2}}\Big|_{\nu=\nu_n} \frac{e^{j\nu_n\pi}}{1 + e^{2j\nu_n\pi}} \frac{\partial}{\partial\alpha} P^{-1}_{\nu_n-\frac{1}{2}}(\cos\alpha)$$

$$+ 2\pi \sum_m V_{\nu-\frac{1}{2}}\Big|_{\nu=\nu_m} \frac{e^{j\nu_m\pi}}{1 + e^{2j\nu_m\pi}} \frac{P^{-1}_{\nu_m-\frac{1}{2}}(\cos\alpha)}{\sin\alpha} \tag{3.47}$$

which in the limit $\alpha = 0$ reduces to the backscattered creeping wave field (3.31). Furthermore, for $|\nu| >> 1$ and $\alpha < \pi$, the Legendre functions can be replaced by cylindrical Bessel functions using Macdonald's asymptotic formula

$$P^{-1}_{\nu-\frac{1}{2}}(\cos\alpha) \sim -\frac{1}{\nu}\left(\frac{\alpha}{\sin\alpha}\right)^{\frac{1}{2}} J_1(\nu\alpha) \tag{3.48}$$

where $J_1(x)$ represents the cylindrical Bessel function. Hence

$$S^c_p(\theta) = 2\pi \sum_n U_{\nu-\frac{1}{2}}\Big|_{\nu=\nu_m} \frac{e^{j\nu_n\pi}}{1 + e^{2j\nu_n\pi}} \left(\frac{\pi - \theta}{\sin\theta}\right)^{\frac{1}{2}} J_1'[\nu_n(\pi - \theta)]$$

$$- 2\pi \sum_m V_{\nu-\frac{1}{2}}\Big|_{\nu=\nu_m} \frac{e^{j\nu_m\pi}}{1 + e^{2j\nu_m\pi}} \left(\frac{\pi - \theta}{\sin\theta}\right)^{\frac{1}{2}} \frac{J_1[\nu_m(\pi - \theta)]}{\nu_m \sin\theta} \tag{3.49}$$

Following the Airy function representation of the Hankel function as used to derive (3.36), we reduce (3.49) to the form

$$S^c_p(\theta) = -j4\pi\tau \left(\frac{\pi - \theta}{\sin\theta}\right)^{\frac{1}{2}} \left\{ \sum_n \frac{\nu_n J_1'[\nu_n(\pi - \theta)] e^{j\nu_n\pi}}{(\eta^2\tau^2 + \beta_n)[W_1(\beta_n)]^2(1 + e^{2j\nu_n\pi})} \right.$$

$$\left. - \sum_m \frac{J_1[\nu_m(\pi - \theta)]\eta^2 e^{j\nu_m\pi}}{(\tau^2 + \eta^2\alpha_m)[W_1(\alpha_m)]^2 \sin\theta (1 + e^{2j\nu_m\pi})} \right\} \tag{3.50}$$

which is valid for all $\theta < \pi$ like the corresponding expression derived by Senior and Goodrich [71] for the perfectly conducting sphere. Similarly for the H polarization

$$S^c_q(\theta) = -j4\pi\tau \left(\frac{\pi - \theta}{\sin\theta}\right)^{\frac{1}{2}} \left\{ \sum_n \frac{J_1[\nu_n(\pi - \theta)] e^{j\nu_n\pi}}{(\eta^2\tau^2 + \beta_n)[W_1(\beta_n)]^2 \sin\theta (1 + e^{2j\nu_n\pi})} \right.$$

$$\left. - \sum_{m=1} \frac{\nu_m J_1'[\nu_m(\pi - \theta)]\eta^2 e^{j\nu_m\pi}}{(\tau^2 + \eta^2\alpha_m)[W_1(\alpha_m)]^2 (1 + e^{2j\nu_m\pi})} \right\} \tag{3.51}$$

The first and second sums in both (3.50) and (3.51) again represent contributions from E and H waves respectively. However, in $S_p^c(\theta)$, the contributions of the E waves are dominant since the rate of attenuation of the H waves is larger and the contribution of the H waves is normally negligible. A similar situation exists in $S_q^c(\theta)$ except for very large values of ka when the contribution of the E waves becomes dominant due to the behaviour of the roots ν_m. As θ tends to 0 or π, the amplitudes of the E and H waves become comparable due to the negative powers of $\sin\theta$ in (3.50) and (3.51) in the vicinity of these directions.

3.5 The Forward Scattered Field

The forward scattering direction ($\theta = 0$) is a true caustic of the diffracted rays which emerge from the shadow boundary ($\theta = \pi/2$) and travel parallel to each other to form a geometric optics wave in the far field. In addition, there is a contribution due to the creeping waves travelling in the E and H planes. In the vicinity of the caustic ($\theta = 0$), the amplitudes of the E and H type creeping waves become comparable unlike the monostatic and bistatic fields where the E type waves are dominant.

Since the functions $E_1^{(1),(2)}(\nu,\theta)$ become singular at $\theta = 0$, we use the original expression for $p(\theta)$ and $q(\theta)$ in (3.9) and (3.10) to obtain

$$p(0) = \int_c \left[B_{\nu-\frac{1}{2}} + C_{\nu-\frac{1}{2}}\right] \frac{\nu d\nu}{1 + e^{2j\nu\pi}} \tag{3.52}$$

and

$$q(0) = - p(0) \tag{3.53}$$

Considering the residue at $\nu = \frac{1}{2}$ we have

$$p(0) = \int_{D_1} \left[B_{\nu-\frac{1}{2}} + C_{\nu-\frac{1}{2}} \right] \frac{\nu d\nu}{1 + e^{2j\nu\pi}} - \frac{1}{2} \tag{3.54}$$

where D_1 passes through the origin in the ν plane as shown in Fig. 3.4.

Reflection of the lower part of path D_1 at the origin results in a new expression for $p(0)$ whose terms can be identified as geometric optics and creeping wave terms of the form

$$S_p^o(0) = \int_0^{ka} \nu d\nu - \frac{1}{2} + \int_{\infty - j\varepsilon}^{0} \frac{e^{-2j\nu\pi}}{1 + e^{-2j\nu\pi}} - \int_0^{\infty + j\varepsilon} \frac{e^{2j\nu\pi}}{1 + e^{2j\nu\pi}} \nu d\nu \tag{3.55}$$

and

$$S_p^c(0) = - \frac{1}{2} \int_{-\infty + j\varepsilon}^{\infty + j\varepsilon} \left[D_{\nu-\frac{1}{2}} + G_{\nu-\frac{1}{2}} \right] \frac{e^{2j\nu\pi}}{1 + e^{2j\nu\pi}} \nu d\nu$$

$$+ \frac{1}{2} \int_{-\infty}^{ka} \left[D_{\nu-\frac{1}{2}} + G_{\nu-\frac{1}{2}} \right] \nu d\nu + \int_{ka}^{\infty} \left[B_{\nu-\frac{1}{2}} + C_{\nu-\frac{1}{2}} \right] \nu d\nu \tag{3.56}$$

Expanding the integrands of the last two integrals in (3.55) as binomial series and retaining the leading terms we obtain after integration

$$S_p^o(0) = \frac{1}{2} \left[(ka)^2 - \frac{11}{12} \right] \tag{3.57}$$

where (3.55) and (3.57) are identical with the corresponding expressions for a perfectly conducting sphere. Furthermore, since the geometric optics term outweighs the creeping wave contribution, the forward scattered field

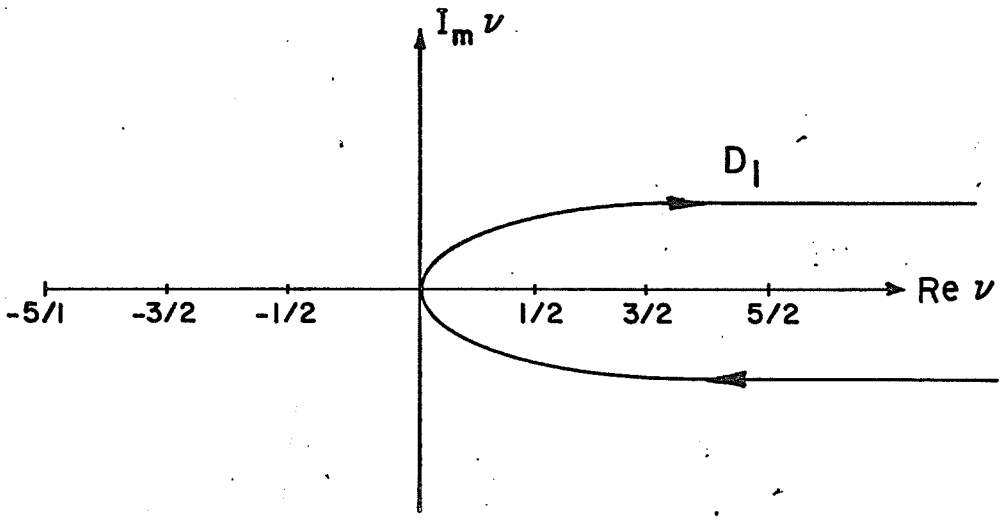

FIG. 3.3 INTEGRATION PATH D_1

is almost independent of the surface impedance of the sphere.

The integrals in (3.56) may be evaluated by the method of Senior and Goodrich [71] where the Bessel and Hankel functions and their derivatives are replaced by Airy functions. The final result is given by

$$S_p^c(0) = \left(\frac{1-\eta}{1+\eta}\right)\tau^4\left[.082972 + j\cdot 144019 + \frac{1}{\tau^2}(.385229 - j\cdot 667169) - \frac{.069342}{\tau^4} + 0(\tau^{-6})\right] + 2\pi\tau\left\{\sum_{n=1}^{\infty} \frac{\nu_n}{(\eta^2\tau^2 + \beta_n)[W_1(\beta_n)]^2(1 + e^{-2j\nu_n\pi})} + \sum_{m=1}^{\infty} \frac{\eta^2}{(\tau^2 + \alpha_m\eta^2)[W_1(\alpha_m)]^2(1 + e^{-2j\nu_m\pi})}\right\} \qquad (3.58)$$

where the terms in the square bracket may be interpreted as due to those creeping waves that have not progressed any appreciable distance around the sphere and are excited at the shadow boundary.

3.6 Numerical Results

In order to verify the accuracy of our approximate expressions, computations were performed using (3.52) and (3.36) for σ_b, (3.43) and (3.50) for σ_θ, (3.57) and (3.58) for σ_f and the results compared with those based on the exact solution. The results for σ_e are shown in Fig. 3.4 to Fig. 3.7 for various values of ka and normalized impedance corresponding to resistive, inductive and capacitive coatings as well as for a homogeneous conductor, while the H plane results are shown in Fig. 3.8 to Fig. 3.11. The curves indicate good agreement except near the forward scattering direction where (3.43) is not valid since the condition $ka \sin^3(\theta/2) \gg 1$ is not satisfied. Outside this region, it

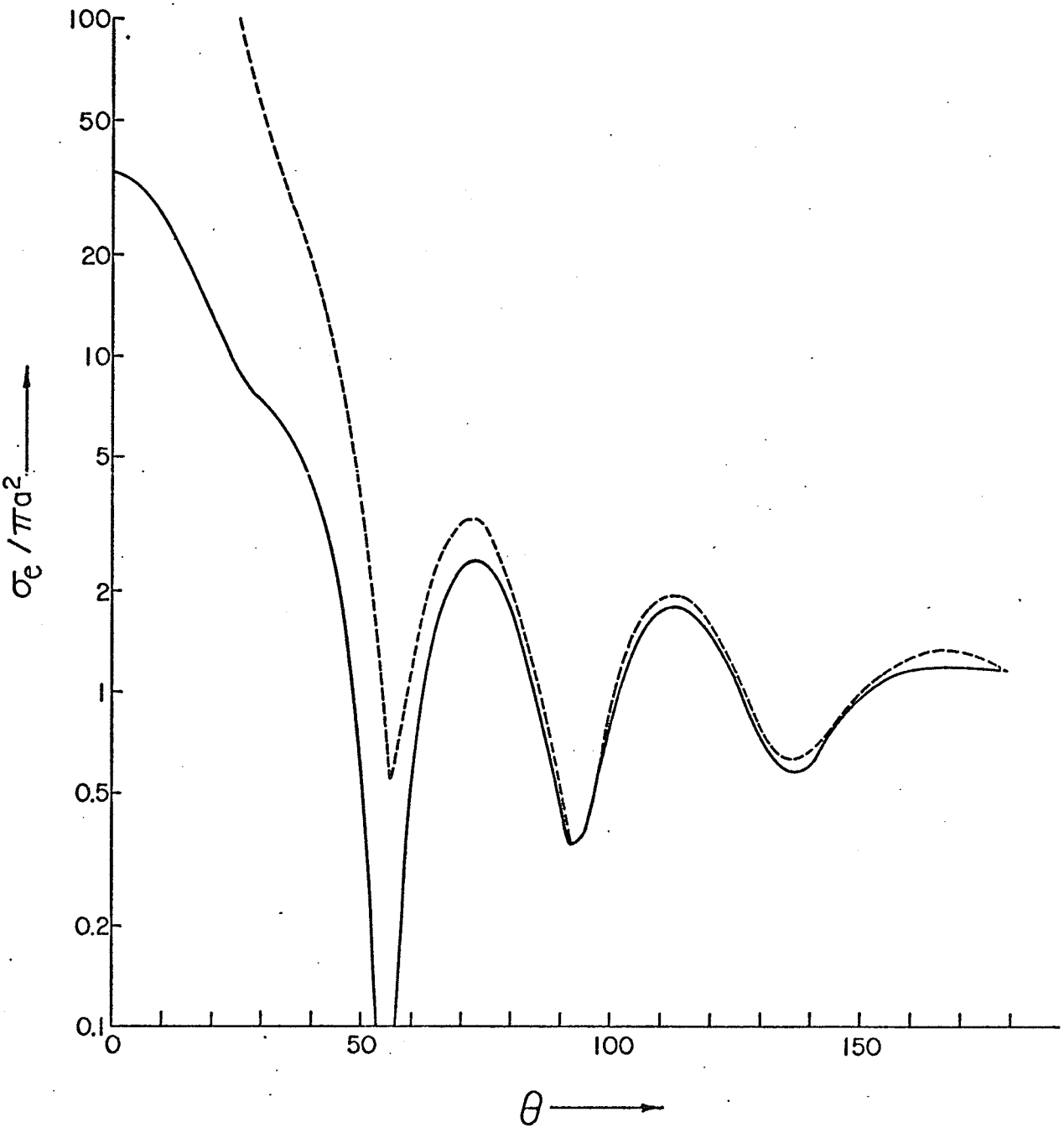

Fig. 3.4 E-Plane Scattering Cross-section $\sigma_e/\pi a^2$ vs. bistatic angle θ (ka = 5.0 η = 0.1) ——— exact solution, ---- ray solution

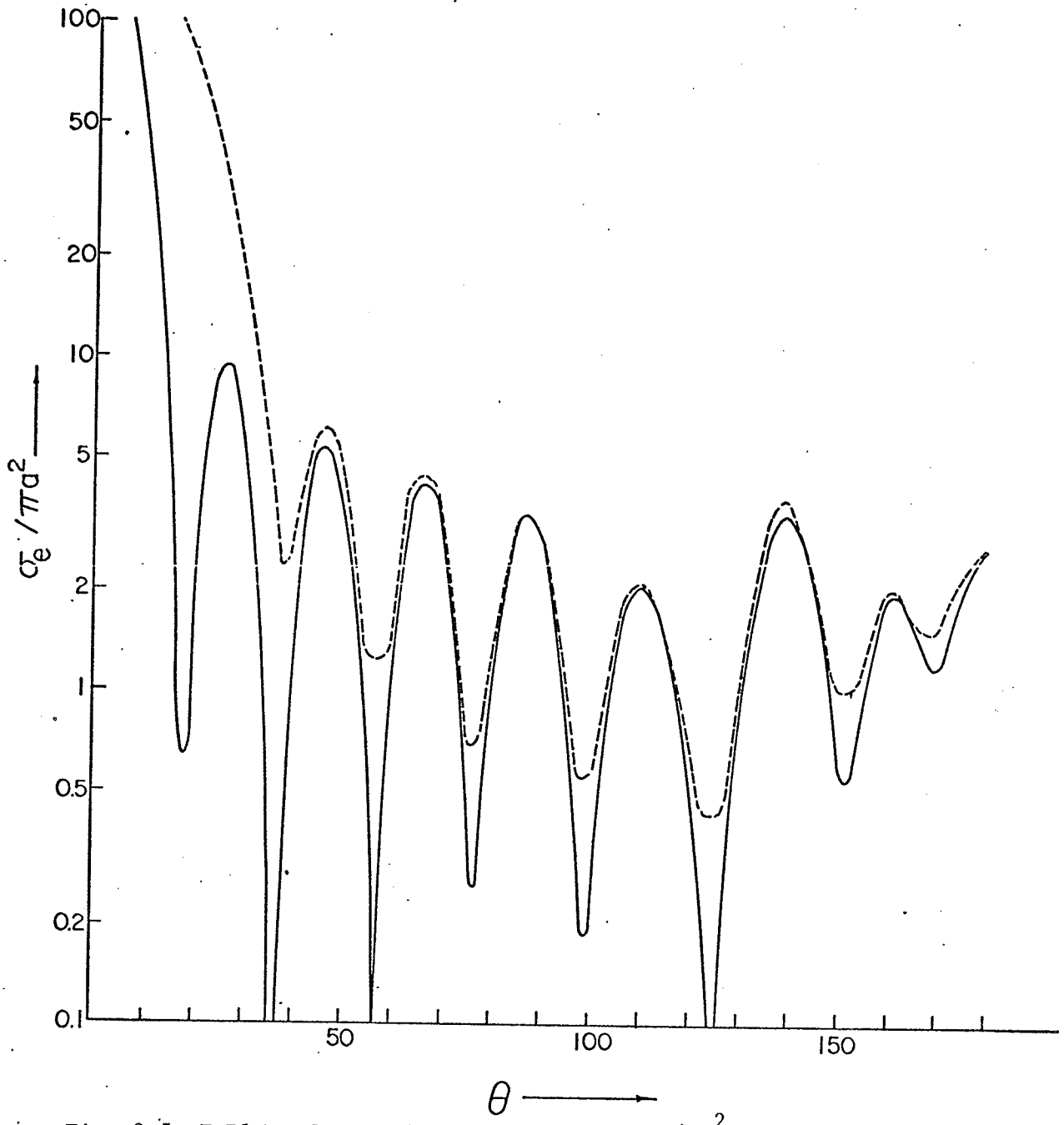

Fig. 3.5 E-Plane Scattering Cross-section $\sigma_e/\pi a^2$ vs. bistatic angle θ (ka = 8.0 η = .5j) —— exact solution, ---- ray solution

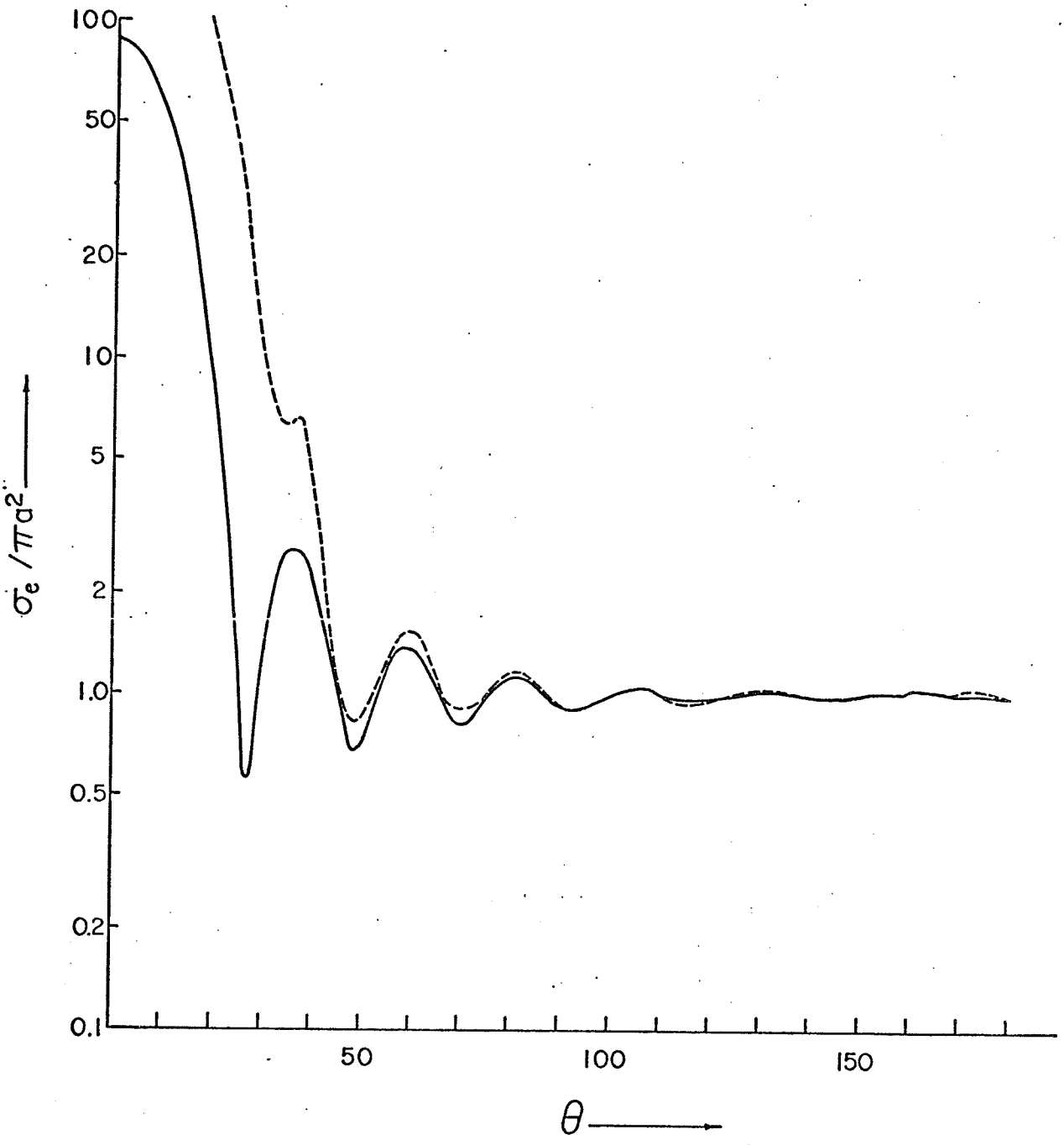

Fig. 3.6 E-Plane Scattering Cross-section $\sigma_e/\pi a^2$ vs. bistatic angle θ ($ka = 9.0$ $\eta = -.3j$) —— exact solution, ---- ray solution

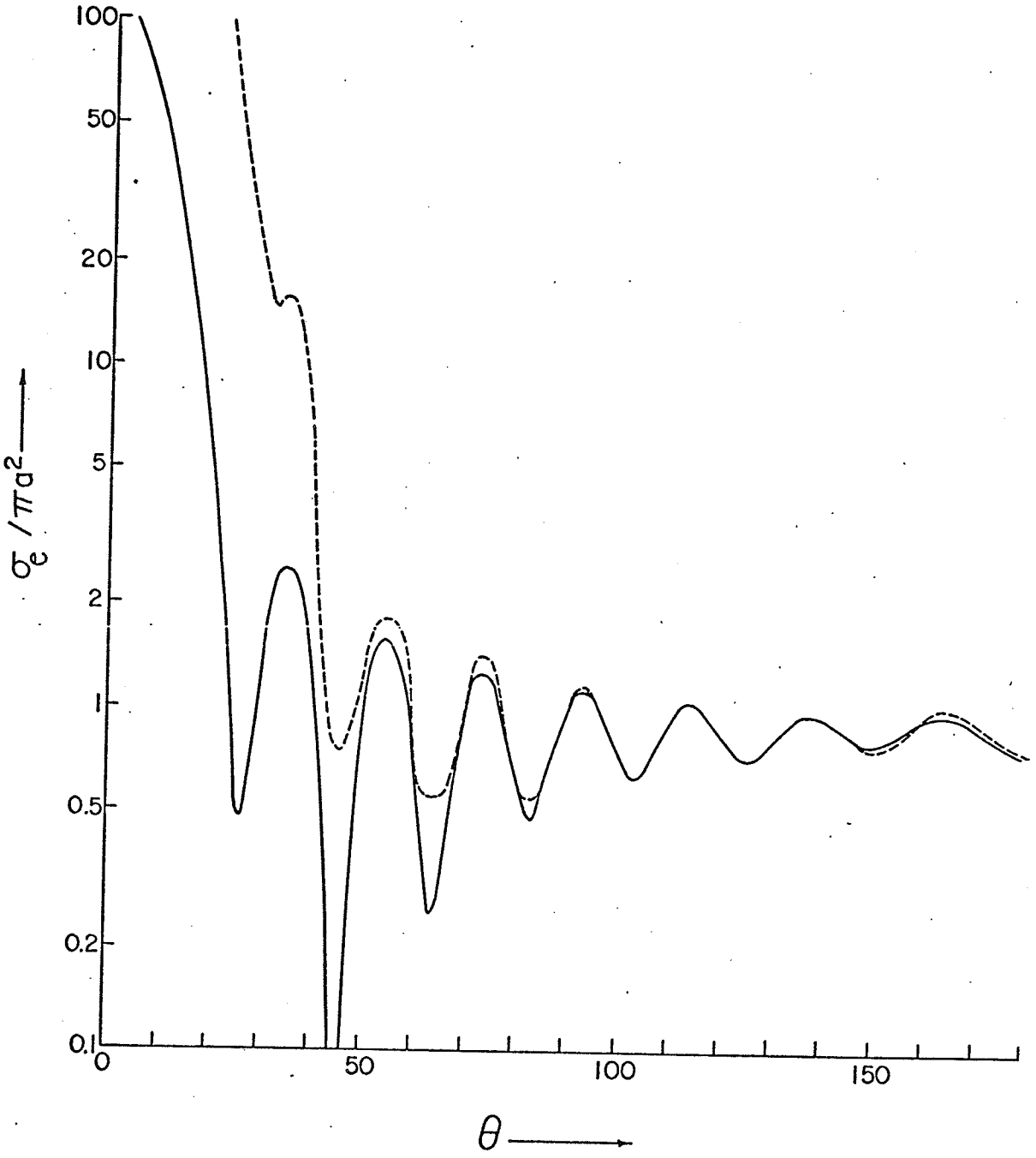

Fig. 3.7 E-Plane Scattering Cross-section $\sigma_e/\pi a^2$ vs. bistatic angle θ ($ka = 10.0 \quad \eta = .05e^{j\pi/4}$) ——— exact solution,---- ray solution

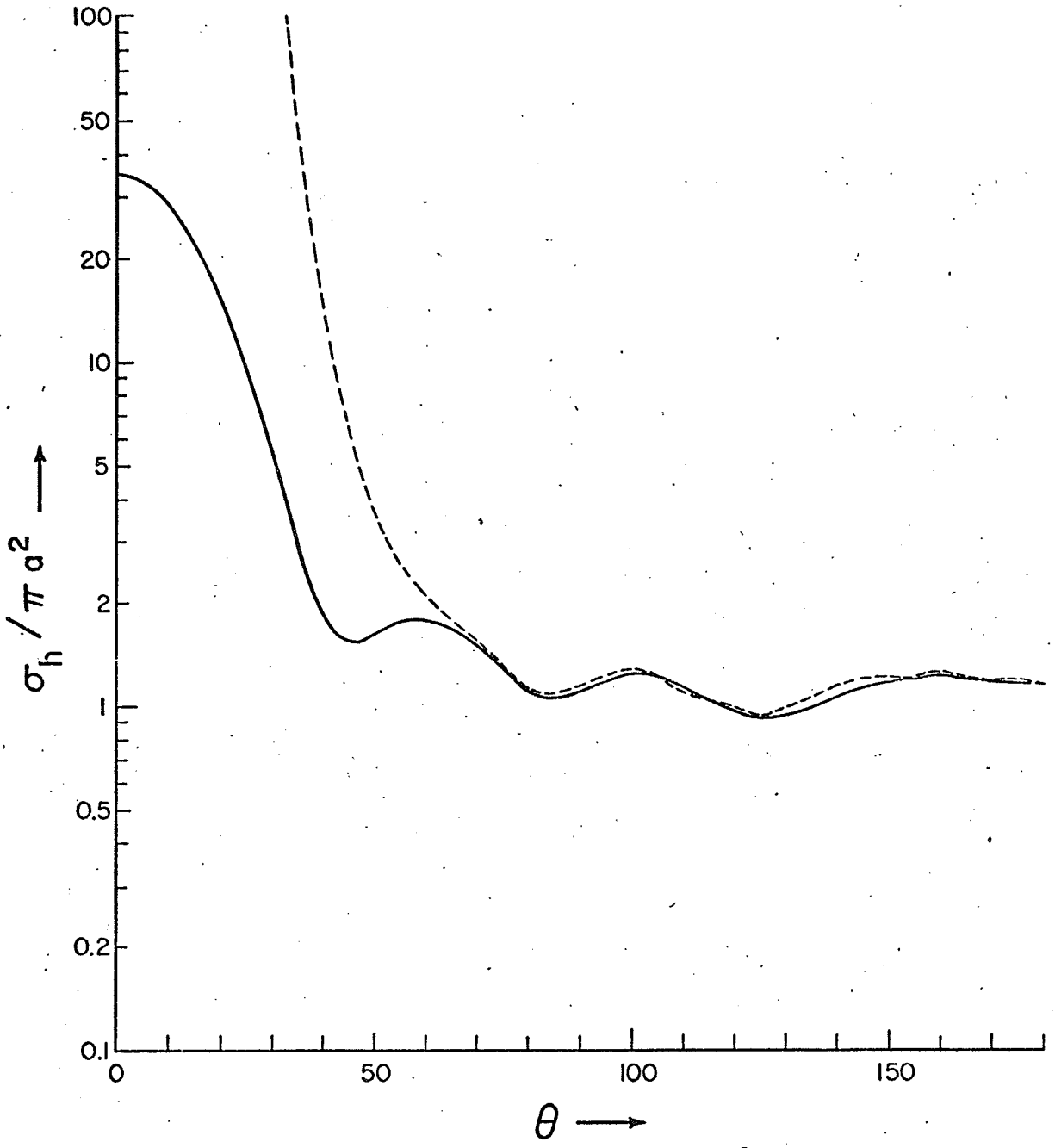

Fig. 3.8 H-Plane Scattering Cross-section $\sigma_e/\pi a^2$ vs. bistatic angle θ ($ka = 5.0 \quad \eta = 0.1$) —— exact solution, ---- ray solution

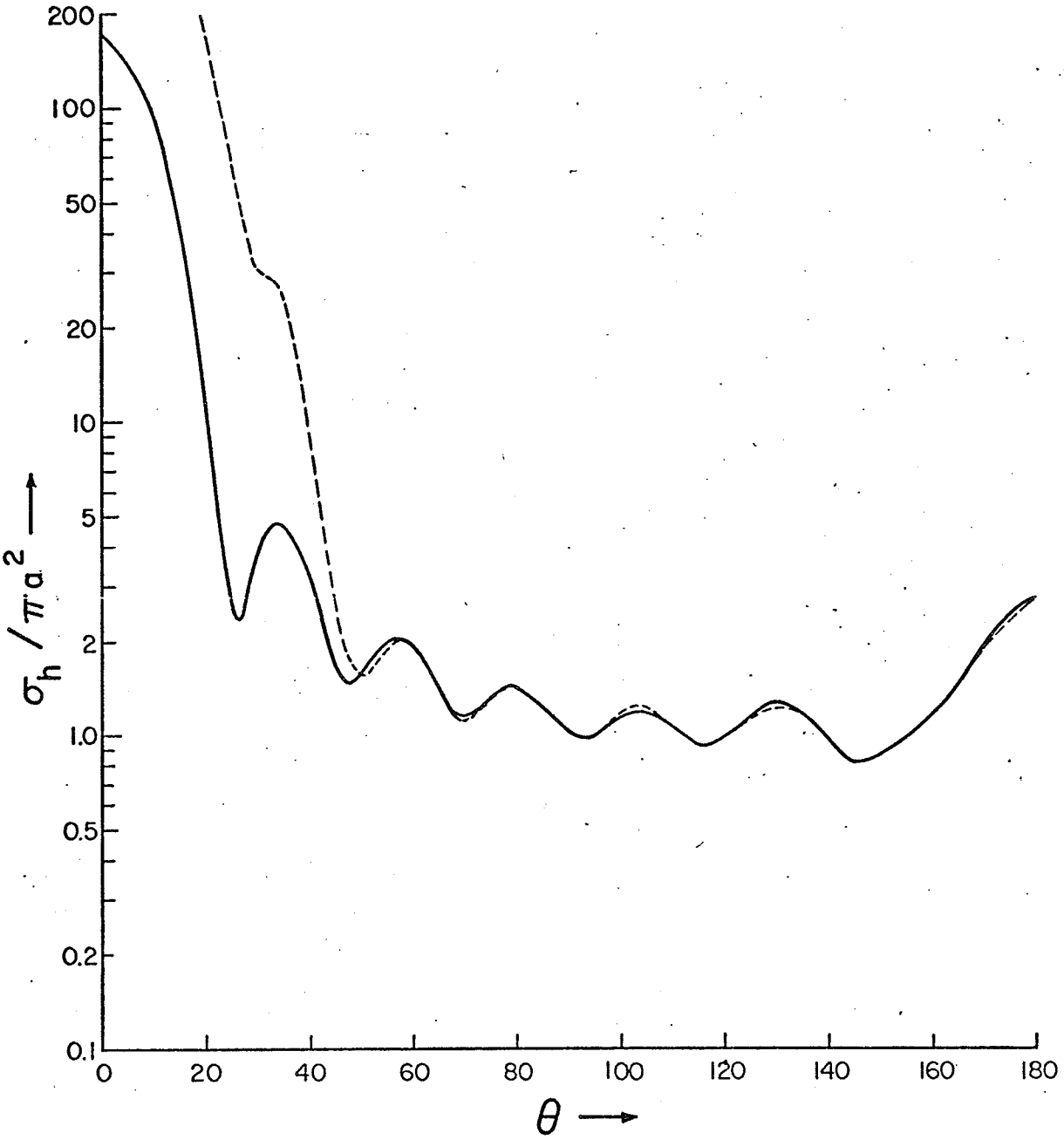

Fig. 3.9 H-Plane Scattering Cross-section $\sigma_e/\pi a^2$ vs. bistatic angle θ (ka = 8.0 η = .5j) ——— exact solution, ---- ray solution

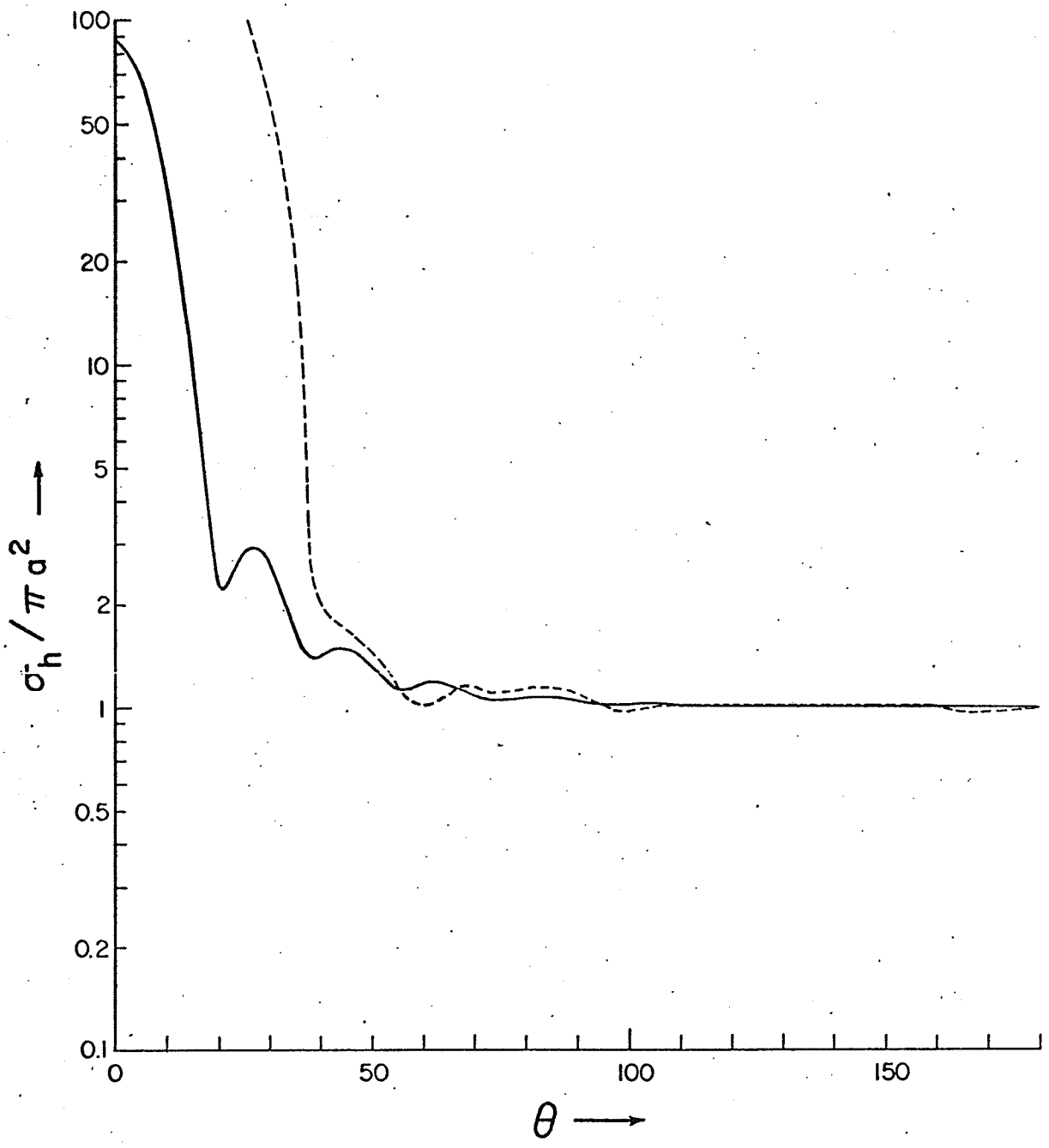

Fig. 3.10 H-Plane Scattering Cross-section $\sigma_e/\pi a^2$ vs. bistatic angle θ (ka = 9.0 η = -.3j) —— exact solution, ---- ray solution

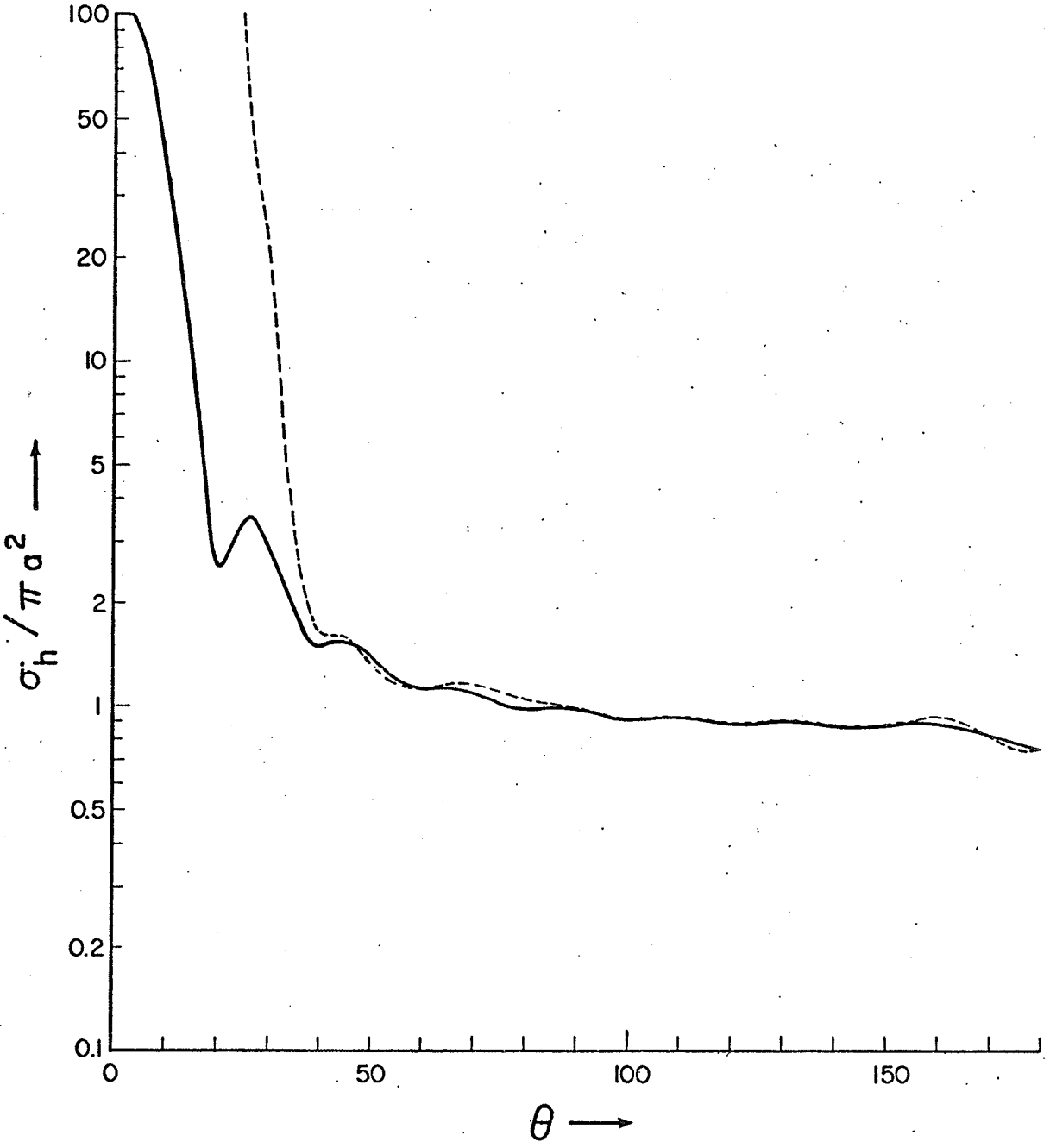

Fig. 3.11 H-Plane Scattering Cross-section $\sigma_e/\pi a^2$ vs. bistatic angle θ ($ka = 10.0 \quad \eta = .05e^{j\pi/4}$) —— exact solution, ---- ray solution

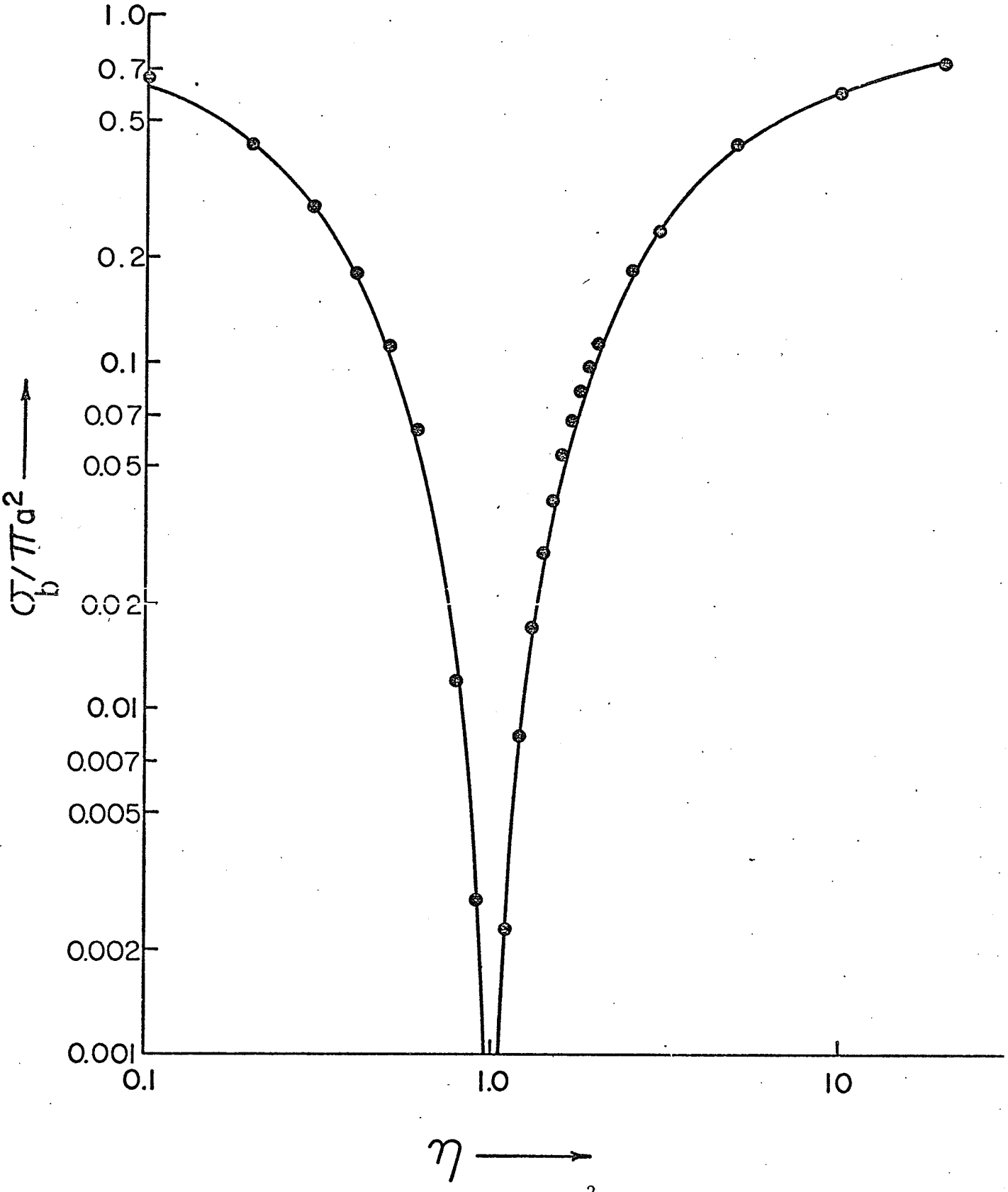

Fig. 3.12 Backscattering Cross-section $\sigma_b/\pi a^2$ vs. normalized surface impedance η. (ka = 10.0) —— exact solution, ···· ray solution

is evident that our ray solution is sufficiently accurate and requires minimum computation time compared to the exact solution which requires lengthy numerical computations of series of Bessel and Hankel functions. Furthermore, the ray solution shows clearly the dependence of σ_b and σ_f on ka which for $\eta \neq 1$ tend to 1 and $(ka)^2$ as $ka \to \infty$, respectively, and oscillate for smaller values of ka due to the creeping wave contribution.

Fig. 3.12 shows a plot of σ_b vs. η for $ka = 10$ based on (3.32) and (3.36) as well as the exact solution. Here we observe that σ_b decreases from its value for the perfectly conducting case (0.9292) to almost zero when $\eta = 1$ and increases beyond this point to its initial value. This is in contrast to the forward scattering case where σ_f is maximum at $\eta = 1$. Beyond this, σ_f drops off for any increase or decrease in η until the limiting cases of a perfect scatterer or a perfect absorber $(\eta = \infty)$ are reached where its value is 106.3. However, in general, no such statements can be made with respect to σ_θ since it is a function of θ and polarization.

Examination of the analytical results indicates that the ray optical method gives a physical insight into the scattering mechanisms by an imperfectly conducting sphere. Thus Fig. 3.12 indicates that for $\eta = 0$ (i.e. a perfectly conducting sphere) the dominant contribution to σ_b is due to the E waves. However, as η increases, the E waves become less dominant until $\eta = 1$ when the creeping wave contributions due to the E and H waves are of the same magnitude, but opposite in phase thus cancelling each other. Since the geometric optics terms for $\eta = 1$ is also zero from (3.32), the net result for σ_b is zero. This is in

agreement with a theorem proposed by Weston [91] for plane wave scattering by a general absorbing body which is invariant under a 90° rotation about any axis.

Analysis of the numerical data for σ_θ indicates that it is independent of polarization for $\eta = 1$. Furthermore, for E plane scattering, the values of σ_θ in the range $0 \leq \eta \leq 1$ correspond to the H plane values in the range $1 \leq \eta \leq \infty$. This shows that we have two ranges of η of interest and they are bounded by $\eta = 0$, $\eta = 1$ and $\eta = \infty$ which correspond to a perfect conductor, matched scatterer and perfect absorber, respectively. Hence, it is only necessary to derive the E or H plane solution for each range to obtain the complete data in both planes for all η.

A similar result holds for reactive coatings in the bistatic case. Thus for an inductive surface, the E plane scattering cross section σ_e in the range $0 < |\eta| \leq 1$ is identical to σ_h in the H plane for a capacitive coating with $|\eta|$ given by the reciprocal value and hence lying in the range $1 \leq |\eta| < \infty$. Therefore, it is sufficient to evaluate σ_e and σ_h in both ranges for either an inductive or a capacitive surface to obtain results for a purely reactive coating. These results suggest the possibility of extending Babinet's principle to three dimensions in the electromagnetic sense whereby a perfectly conducting sphere is complementary to a perfectly absorbing sphere. This result has also been verified for the two dimensional case of an imperfectly conducting cylinder although the numerical results have been omitted. It should be noted, however, that a perfect absorber is not truly a non-scatterer. This is because the total field at any point is the sum

of the incident and scattered field and this universally accepted definition of the scattered field entails the paradoxical consequence that a perfect absorber must reradiate as shown by Midgley [92]. Here reradiation provides for destructive interference with the incident field without which absorption is not possible.

A study of the scattering pattern for the bistatic cross section shows that the lobe structure is not significantly different from the perfectly conducting case except that the maxima and minima are altered with variations in η, while new lobes may appear mainly in the E plane. However, a method for controlling the lobe structure could be realized by choosing the appropriate impedance coating which may have to be a function of θ and ϕ.

Finally, it is interesting to note that the average value of the scattering cross sections in any direction or polarization for two isolated spheres of the same ka and coated with an impedance η and its complex conjugate η^*, respectively, is numerically equal to that of a sphere of the same ka and coated with a resistive impedance equal to the real part of η.

CHAPTER IV

NUMERICAL METHODS FOR IMPERFECTLY CONDUCTING BODIES

4.1 Introduction

The preceeding two chapters have considered the ray optical scattering by single and multiple, perfectly and imperfectly conducting spheres. The approach has been based on representing the scattered fields in terms of geometric optics and creeping wave terms through the application of Watson's transform to the exact boundary value series solution. The conventional ray procedure proposed by Levy and Keller [62] is to formulate the diffracted fields using mode decay and diffraction coefficients which are evaluated by comparison with the asymptotic solution of the exact solution. One inherent difficulty with this approach is that the mode diffraction coefficient is obtained by comparing two asymptotic representations of the same field, thus leading to breakdown along shadow regions. Another difficulty is due to the postulate that a creeping wave excites an infinite number of modes thus introducing an extra summation and requiring the appropriate decay and diffraction coefficients for each mode. Needless to say, the asymptotic expansion of the exact solution, if available, is fairly tedious and requires Watson's transformation for large characteristic dimension and is totally inadequate for smaller dimensions.

With the advent of fast digital computers, exact numerical solutions can be obtained for most bodies, particularly two dimensional, thus avoiding the need for exact analytical solutions and their asymptotic series representation. The basic advantage of numerical methods over

exact modal series solutions lies in the computational time required particularly when the characteristic dimension of the body is large. Thus the dependence of ray theory on mode theory would be no longer essential, particularly for bodies of complicated geometries. Furthermore, the computational difficulties introduced by the summation over excited modes may be overcome by the ray-numerical method proposed in this chapter. The method is established for the two dimensional case of perfectly conducting cylinders. In addition, other numerical methods are utilized to investigate the scattering by more complex structures as polygonal and dielectric coated cylinders and cavities with lossy walls.

4.2 The Ray-Numerical Technique

As the name implies, the method employs rays which depend on numerical solutions. In principle, the method postulates that a ray incident on a smooth curved surface suffers initial diffraction leading to one or several surface rays, which are transmission line type rays with a single propagation coefficient for each, before finally suffering a second diffraction at the point of emergence on finite bodies. The ray diffraction and propagation coefficients are independent of the conventional mode diffraction and decay coefficients. It is evident that the ray propagation coefficient is independent of the angle of incidence and observation.

In implementing this technique, the conventional ray formulation is maintained and the ray diffraction and propagation coefficients are introduced, instead of mode diffraction and decay coefficients, and are evaluated by comparison with exact numerical data based on a numerical

technique most appropriate for the body under consideration as illustrated in the next section.

4.2.1 Application to the Perfectly Conducting Cylinder

Consider a circular cylinder of radius a and a line source located at $Q(\rho,0)$ and parallel to the z axis, as shown in Fig. 4.1. The diffracted field at an observation point $P(r,\phi)$ is due to creeping rays emerging tangentially from the cylinder to pass through ρ, and is given by [62]

$$U_d(\rho,r,\phi) = (8\pi k)^{-\frac{1}{2}}(r^2 - a^2)^{-\frac{1}{4}}(\rho^2 - a^2)^{-\frac{1}{4}}e^{\{-jk[(\rho^2-a^2)^{\frac{1}{2}}+(r^2-a^2)^{\frac{1}{2}}]-j\,\pi/4\}}$$

$$\cdot \left[\sum_m D_m^2 \frac{e^{\{(-jka-a\xi_m)\phi\}} + e^{\{(-jka-a\xi_m)(2\pi-\phi)\}}}{1 - e^{\{-2\pi(-jka+a\xi_m)\}}}\right.$$

$$\left. \cdot\, e^{\{-(-jka+a\xi_m)(\cos^{-1}(a/r)+\cos^{-1}(a/\rho))\}}\right] \qquad (4.1)$$

which is a rapidly convergent series since the creeping rays decay in amplitude as they progressively encircle the cylinder. In this expression ξ_m represents the decay coefficient and D_m the diffraction coefficient, of the mth mode excited by the incident ray. Comparing (4.1) with the asymptotic expansion of the exact solution for large ka yields D_m and ξ_m [62], i.e.

$$\xi_m = -jk + j\,\tau_m a^{-1} \qquad (4.2)$$

$$D_m = e^{-\pi j/8}\left(\frac{2\pi}{k}\right)^{\frac{1}{4}}\left[\frac{\Omega\, h^{(2)}_{\tau_m}(ka)}{\frac{\partial}{\partial\tau}\Omega\, h^{(2)}_{\tau_m}(ka)}\right]^{\frac{1}{2}} \qquad (4.3)$$

where τ_m and Ω are given in [93].

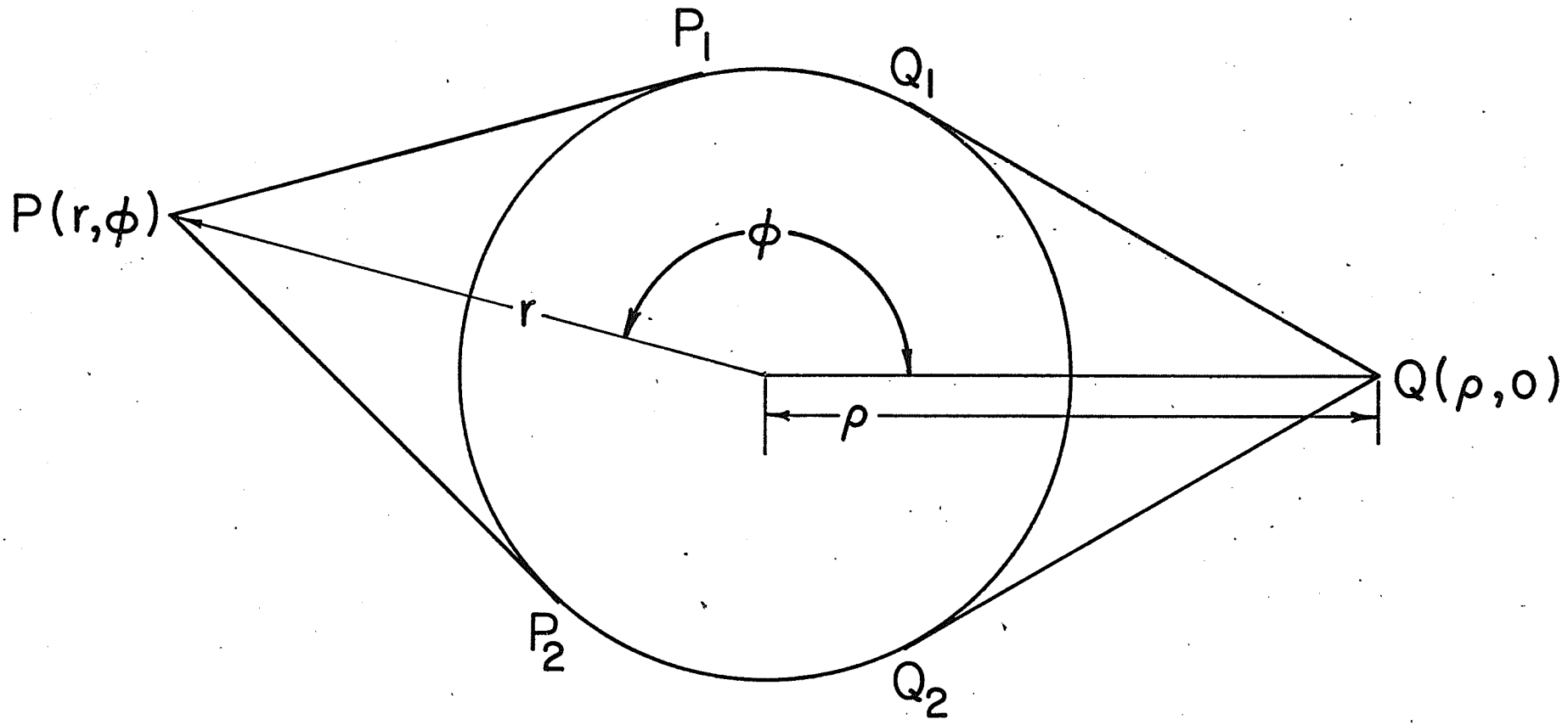

FIG. 4.1 CIRCULAR CYLINDER SCATTERING GEOMETRY

Eliminating the mode diffraction and decay coefficients and introducing ray diffraction and propagation coefficients, D and γ, instead, the form of (4.1) suggests that the diffracted field can be written in the form

$$U_d(\rho,r,\phi) = \frac{(r^2 - a^2)^{-\frac{1}{4}}}{k} (\rho^2 - a^2)^{-\frac{1}{4}} e^{\{-jk[(\rho^2-a^2)^{\frac{1}{2}}+(r^2-a^2)^{\frac{1}{2}}]-j\,\pi/4\}}$$

$$\cdot \left[D \frac{e^{\{-(jka+\gamma)\phi\}} + e^{\{-(jka+\gamma)(2\pi-\phi)\}}}{1 - e^{\{-2\pi(jka+\gamma)\}}} \right.$$

$$\left. \cdot e^{\{(jka+\gamma)[\cos^{-1}(a/r)+\cos^{-1}(a/\rho)]\}} \right] \qquad (4.4)$$

To obtain the coefficients D and γ, a numerical procedure is followed. The diffracted field is evaluated in the shadow region, where the scattered field consists of only the diffracted field, using the exact solution [94]. If U_1 and U_2 represent the fields at a pair of shadow region points (r,ϕ_1) and (r,ϕ_2), respectively, the ratio of the fields at these points is given by

$$\frac{U_1(\rho,r,\phi_1)}{U_2(\rho,r,\phi_2)} = \frac{e^{\{-(jka+\gamma)\phi_1\}} + e^{\{-(jka+\gamma)(2\pi-\phi_1)\}}}{e^{\{-(jka+\gamma)\phi_2\}} + e^{\{-(jka+\gamma)(2\pi-\phi_2)\}}} \qquad (4.5)$$

Hence, a numerical evaluation of the complex zeros of (4.5) gives the solution for γ and substitution of this into (4.4) results in the value of D. However, (4.5), being a transcendental equation, has many roots and for a unique value of γ, equation (4.5) is solved again for some other combination of aspect angles in the shadow region. The root common to both cases gives the value of γ. Alternately, the value of γ may be obtained if the angle of observation is fixed but either ρ

or r is varied. Hence

$$\frac{U_1(\rho,r_1,\phi)}{U_2(\rho,r_2,\phi)} = \frac{e^{\{(jka+\gamma)[\cos^{-1}(a/r_1)+\cos^{-1}(a/\rho)]\}}}{e^{\{(jka+\gamma)[\cos^{-1}(a/r_2)+\cos^{-1}(a/\rho)]\}}} \tag{4.6}$$

and by reciprocity

$$\frac{U_1(\rho_1,r,\phi)}{U_2(\rho_2,r,\phi)} = \frac{e^{\{(jka+\gamma)[\cos^{-1}(a/r)+\cos^{-1}(a/\rho_1)]\}}}{e^{\{(jka+\gamma)[\cos^{-1}(a/r)+\cos^{-1}(a/\rho_2)]\}}} \tag{4.7}$$

The method described above was employed to evaluate D and γ for the principal polarizations for various values of ka and the resulting tables are given in Appendix C. The results show that as the cylinder size increases, the propagation coefficient γ and the diffraction coefficient D increase and in the limit, as $ka \to \infty$, γ is infinite and the diffracted field vanishes. The computer program used to obtain the complex zeros of the transcendental equations (4.5) to (4.7) was compiled by Oczkowski [95] and evaluates the complex zeros and poles of a function in a given range. The advantages of this subroutine are that no derivatives are calculated and the order of the poles and zeros is also found. Finally, Fig. 4.2 compares the diffracted fields calculated by using (4.4), for both polarizations in illuminated and shadow region, and good correspondence is obtained with that computed using the formulation of Levy and Keller [62], which adequately establishes the principle of the ray-numerical formulation.

4.3 The Transformation Matrix Approach

In the previous section, the ray-numerical technique was established

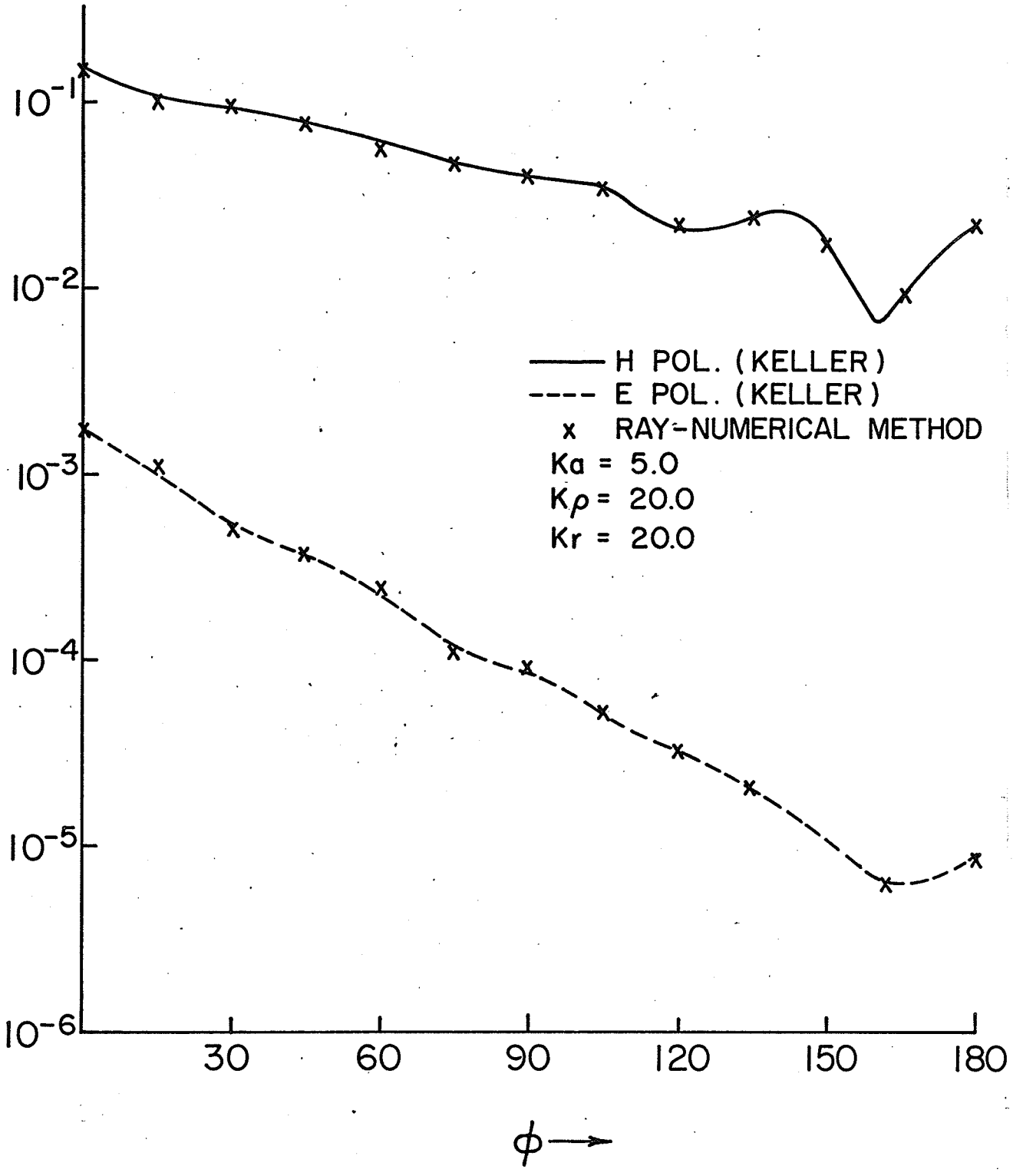

FIG. 4.2 DIFFRACTED FIELD FOR THE CIRCULAR CYLINDER

for the perfectly conducting circular cylinder. To extend the procedure to the imperfectly conducting circular cylinder the equations derived above still apply. However, exact numerical results are difficult to obtain for large ka from the exact solution and hence fast numerical techniques are required to deal with this and other geometries, particularly where exact solutions are not available.

The transformation matrix method [96-98] is based on a scattering matrix, analogous to that used in transmission line theory, and is used to formulate the problem of scattering by a cylinder of polygonal cross section and arbitrary surface impedance, in Appendix D. Expressing Maxwell's equations in the transform space, first order coupled differential equations satisfied by the field components are obtained and are used to evaluate the elements of a scattering matrix, which relate the far field to that on the surface of the scatterer. As a result, matrix equations which satisfy the Leontovich impedance boundary conditions in the transform space are obtained for the scattered field.

For the case of the circular cylinder of radius a, normalized surface impedance η and illuminated by an incident plane wave, the metric coefficients h in Appendix D are unity. Neglecting terms of the order of $1/\rho$ and $1/\rho^2$ in the differential equations for $I_{\pm}^n$ and $O_{\pm}^n$, obtained from (D.1) and (D.4), we have

$$\frac{\partial I_{\pm}^n}{\partial \rho} = jkI_{\pm}^n \quad \text{or} \quad I_{\pm}^n = c\, e^{jk\rho} \tag{4.8}$$

$$\frac{\partial O_{\pm}^n}{\partial \rho} = -jkO_{\pm}^n \quad \text{or} \quad O_{\pm}^n = c\, e^{-jk\rho} \tag{4.9}$$

where c is a constant. Letting $V^n = I_{\pm}^n + O_{\pm}^n$ and $U^n = I_{\pm}^n - O_{\pm}^n$, we

obtain from (D.6)

$$V^n = c_1 H_n^{(1)}(k\rho) + c_2 H_n^{(2)}(k\rho) \tag{4.10}$$

$$U^n = c \frac{1}{jk} \frac{\partial V^n}{\partial \rho} \tag{4.11}$$

From these equations, the matrices $S(\rho,\rho_o)$ and $P(\rho,\rho_o)$ of (D.6) can be obtained and the scattered field evaluated to obtain the resulting normalized scattering widths for the E and H polarizations. These are given by

$$\frac{\sigma_e}{\pi a} = \frac{4}{\pi ka} \left| \sum_{n=0}^{\infty} \varepsilon_n \frac{J_n(ka) + j\eta J_n'(ka)}{H_n^{(2)}(ka) + j\eta H_n^{(2)'}(ka)} \cos(n\phi) \right|^2 \tag{4.12}$$

$$\frac{\sigma_h}{\pi a} = \frac{4}{\pi ka} \left| \sum_{n=0}^{\infty} \varepsilon_n \frac{J_n'(ka) - j\eta J_n(ka)}{H_n^{(2)'}(ka) - j\eta H_n^{(2)}(ka)} \cos(n\phi) \right|^2 \tag{4.13}$$

$$\varepsilon_n = \begin{cases} 1 & n = 0 \\ 2 & n > 0 \end{cases}$$

as shown in Appendix E.

In the case of a regular polygon of N sides, each of length 2a, the transformation from the $z'(x + jy)$ plane to the transform $t(\theta + j\beta)$ plane is given by

$$\frac{dz'}{dt} = M[\cos(N \frac{t}{2})]^{2/N} \tag{4.14}$$

where M depends on the size of the polygon and its orientation in the z' plane. For a square, $M = j\, a/2L$, $L = 0.423607$, as shown by Bickley [99]. Solving for the metric coefficients, two coupled differential equations are obtained for $I_{\pm}^n$ and $O_{\pm}^n$, i.e.

$$\frac{dI_{\pm}^{n}}{d\rho} = \frac{j}{2\rho}\left\{\left[k\rho - \frac{n^2}{k\rho} + j + k\rho f(s)\right]I_{\pm}^{n} + \left[-k\rho + \frac{n^2}{k\rho} - j + k\rho f(s)\right]O_{\mp}^{n} + \left[\frac{k\rho g(s)}{2}\right]\left[\sum_{L} I_{\pm}^{n+L} + O_{\mp}^{n+L}\right]_{L=\pm N} + \ldots\right\} \tag{4.15}$$

$$\frac{dO_{\pm}^{n}}{d} = \frac{j}{2\rho}\left\{\left[k\rho + \frac{n^2}{k} - j - k\rho f(s)\right]I_{\pm}^{n} + \left[-k\rho + \frac{n^2}{k} + j - k\rho f(s)\right]O_{\mp}^{n} - \left[\frac{k\rho g(s)}{2}\right]\left[\sum_{L} I_{\pm}^{n+L} + O_{\mp}^{n+L}\right]_{L=\pm N} + \ldots\right\} \tag{4.16}$$

as shown in Appendix F. These equations are nonlinear, but may be solved numerically to obtain the transformation matrix and the scattered fields evaluated by the application of the boundary conditions.

Using (4.12) and (4.13) computations were performed to study the scattering behaviour of imperfectly conducting circular cylinders. Fig. 4.3 and Fig. 4.4 show the scattering width vs. ϕ for $ka = 5$ and E and H polarizations. The curves correspond to a normalized surface impedance of $\eta = 0$, corresponding to the perfectly conducting case, and $\eta = 0.1, 0.1e^{j\pi/2}, 0.1e^{-j\pi/2}, 0.1e^{j\pi/4}$ corresponding to resistive, inductive, capacitive and complex impedances, respectively. These results indicate that the effect of a small real, imaginary or complex surface impedance is not significant as far as the scattering pattern is concerned. For the above ka value, and a wide range of η, two definite ranges of normalized impedance for the forward ($\phi = 0$) and back ($\phi = \pi$) scattering are identified, where one corresponds to $0 \leq \eta \leq 1$ and the other to $1 \leq \eta \leq \infty$, as shown in Figs. 4.5 and 4.6. Examination of these curves shows that for a purely resistive surface,

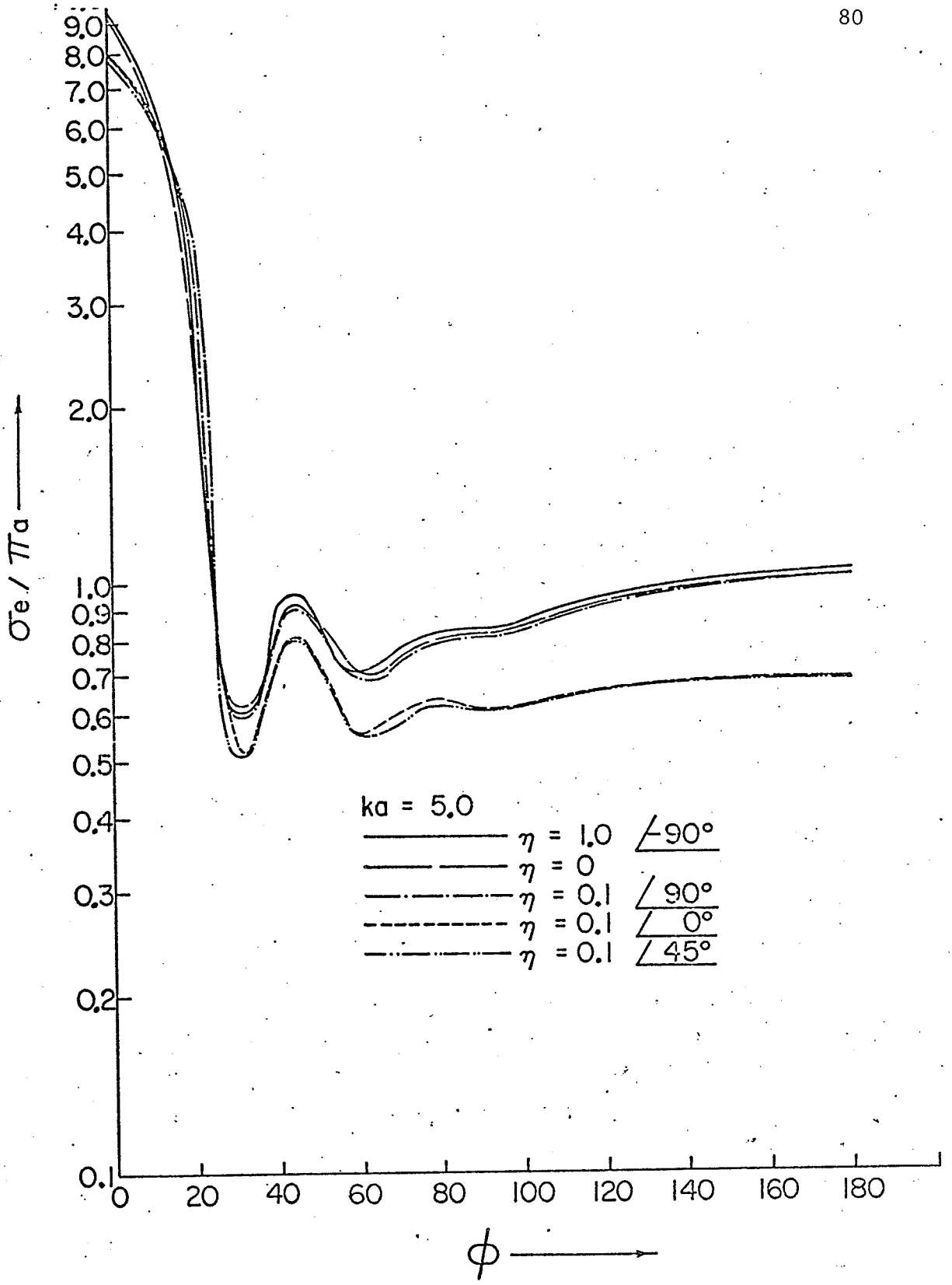

Fig. 4.3 E Polarization bistatic scattering widths for a circular cylinder (ka = 5.0) for various surface impedances

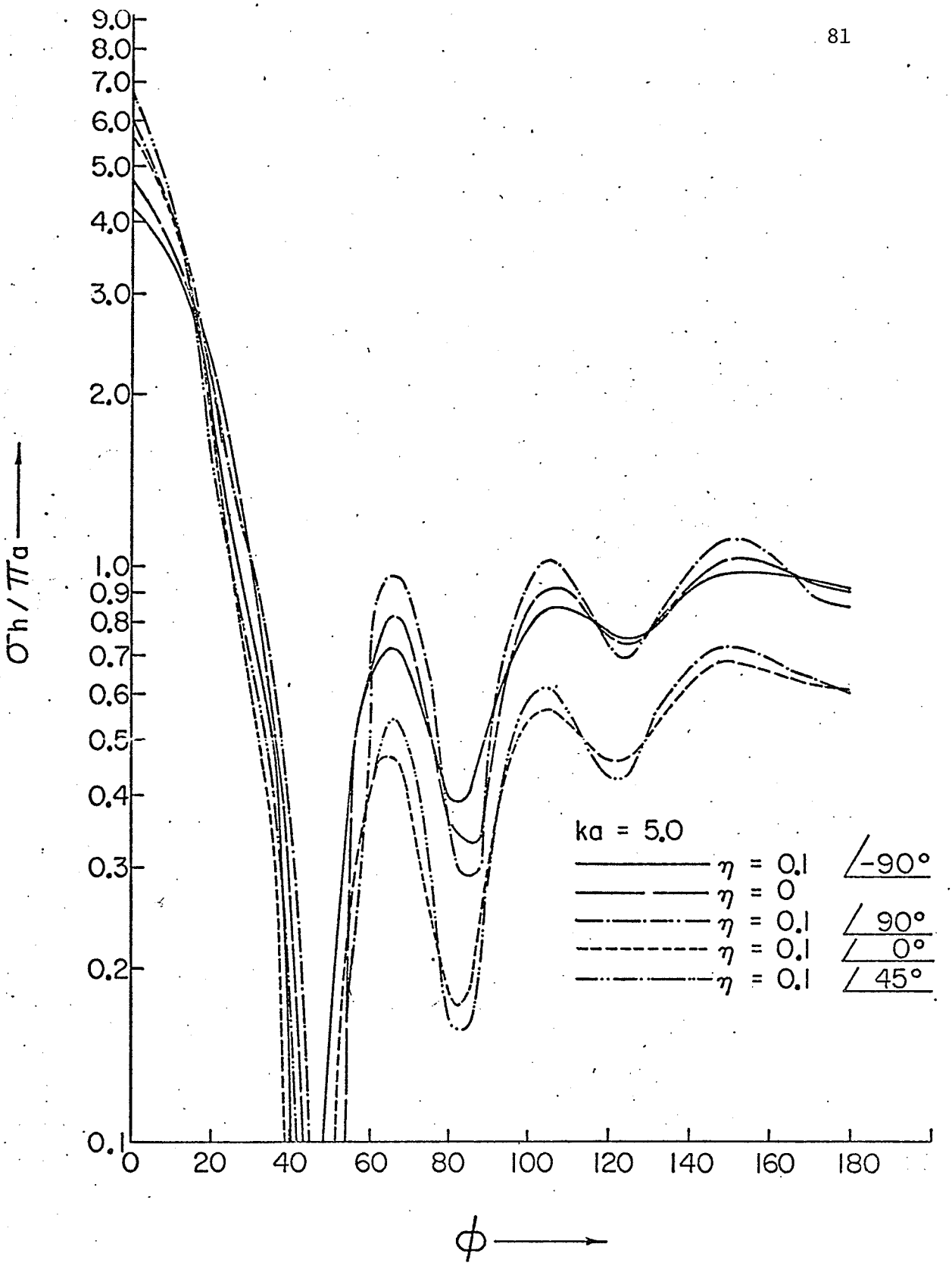

Fig. 4.4 H Polarization bistatic scattering widths for a circular cylinder (ka = 5.0) for various surface impedances

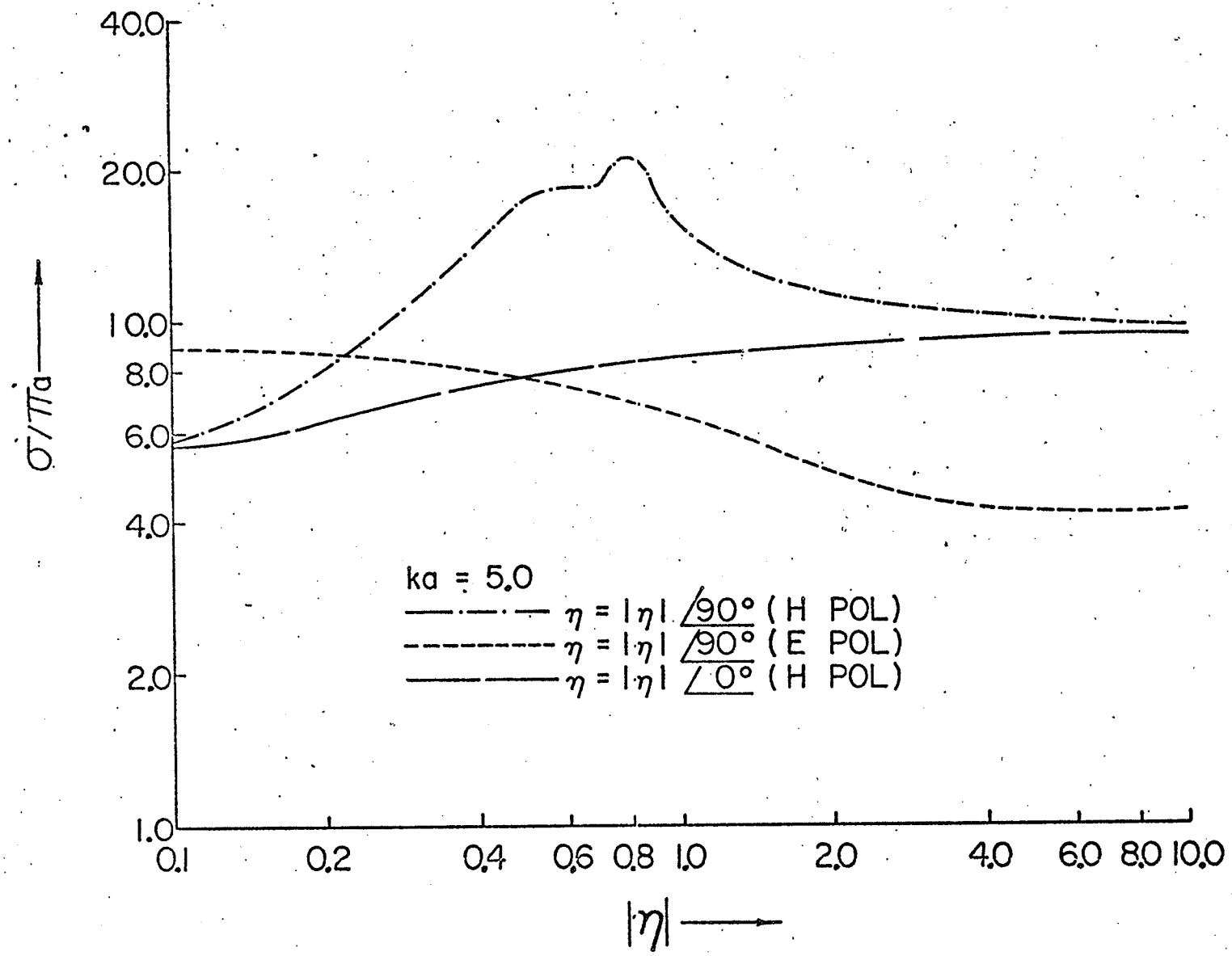

Fig. 4.5 Forward scattering widths versus surface impedance for a circular cylinder (ka = 5.0)

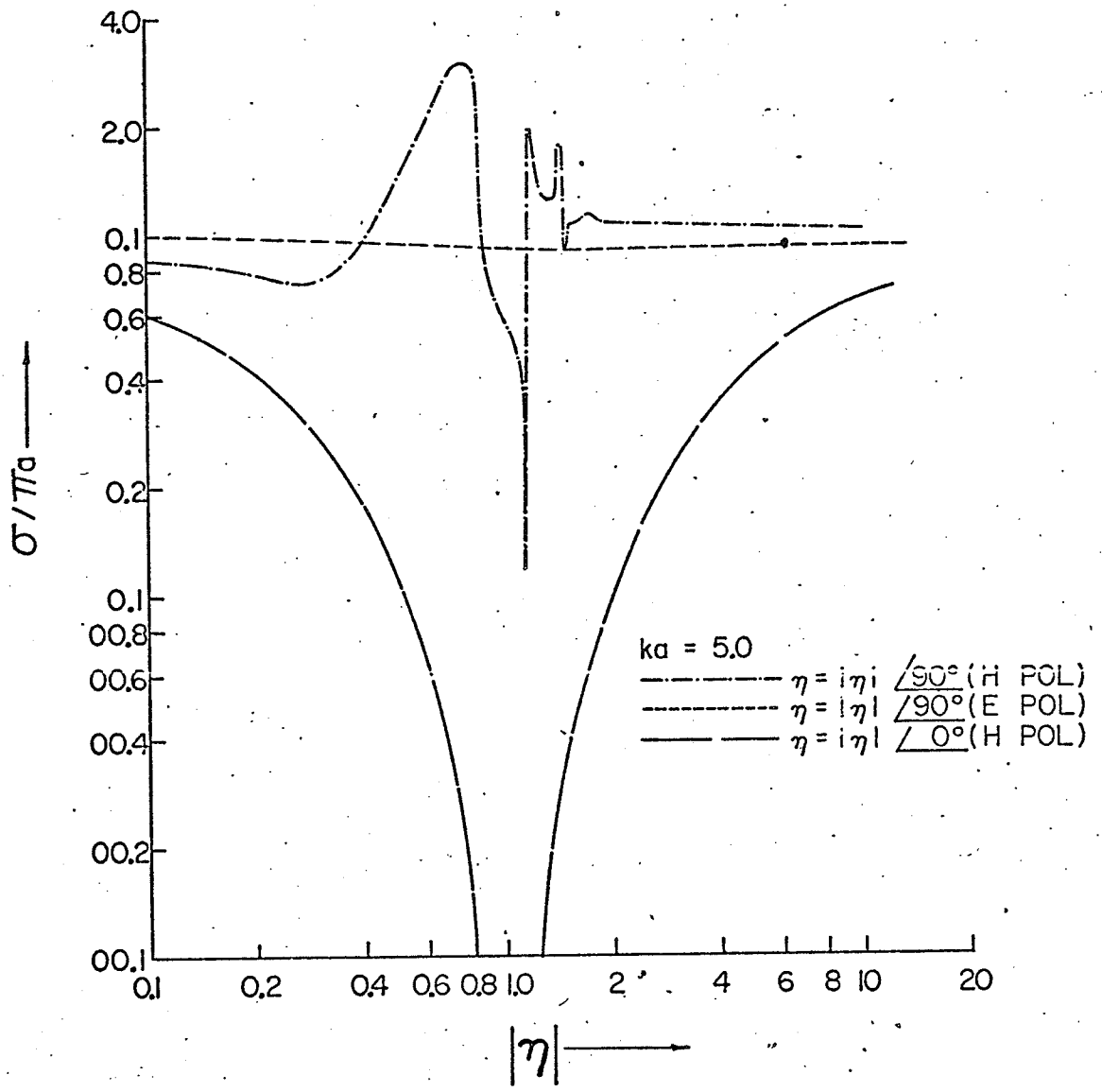

Fig. 4.6 Backscattering widths versus surface impedance for a circular cylinder (ka = 5.0).

the E polarization scattering width in the first range is identical to the corresponding H polarization results in the second range for the reciprocal value of η. For a purely inductive (or capacitive) surface, the E polarization scattering width in the first range is identical to the corresponding result for the H polarization and a purely capacitive (or inductive) surface in the second range. Hence a complete plot for either an inductive or capacitive impedance in both ranges and polarization gives all the results for both impedance types. Thus in Figs. 4.5 and 4.6 only plots for either case are shown.

Further examination of Fig. 4.5 shows that the forward scattering width is not significantly altered from the perfectly conducting case, except when the surface is a reactance and η is close to unity. For a resistive surface, on the other hand, the backscattering width decreases monotonically with increasing η until $\eta = 1$ when it almost vanishes as may be seen from the term $(1 - \eta)/(1 + \eta)$ in (D.12) and (D.14). Beyond this value of η, the curve rises in a symmetrical manner and tends towards the value for a perfectly absorbing cylinder.

The effect of variations in ka on the forward and backscattering width for both polarizations and $|\eta| = 0.5$ is shown in Figs. 4.7 and 4.8. Here we observe that although the forward scattering width increases almost monotonically with increasing ka, the backscattering width has an oscillatory behaviour unlike the case when the surface is perfectly conducting.

For the case of a square cylinder of $ka = 1.0$ and $|\eta| = 0.1$, the E polarization scattering width is compared with that for a perfectly conducting cylinder in Fig. 4.9. Only the results for

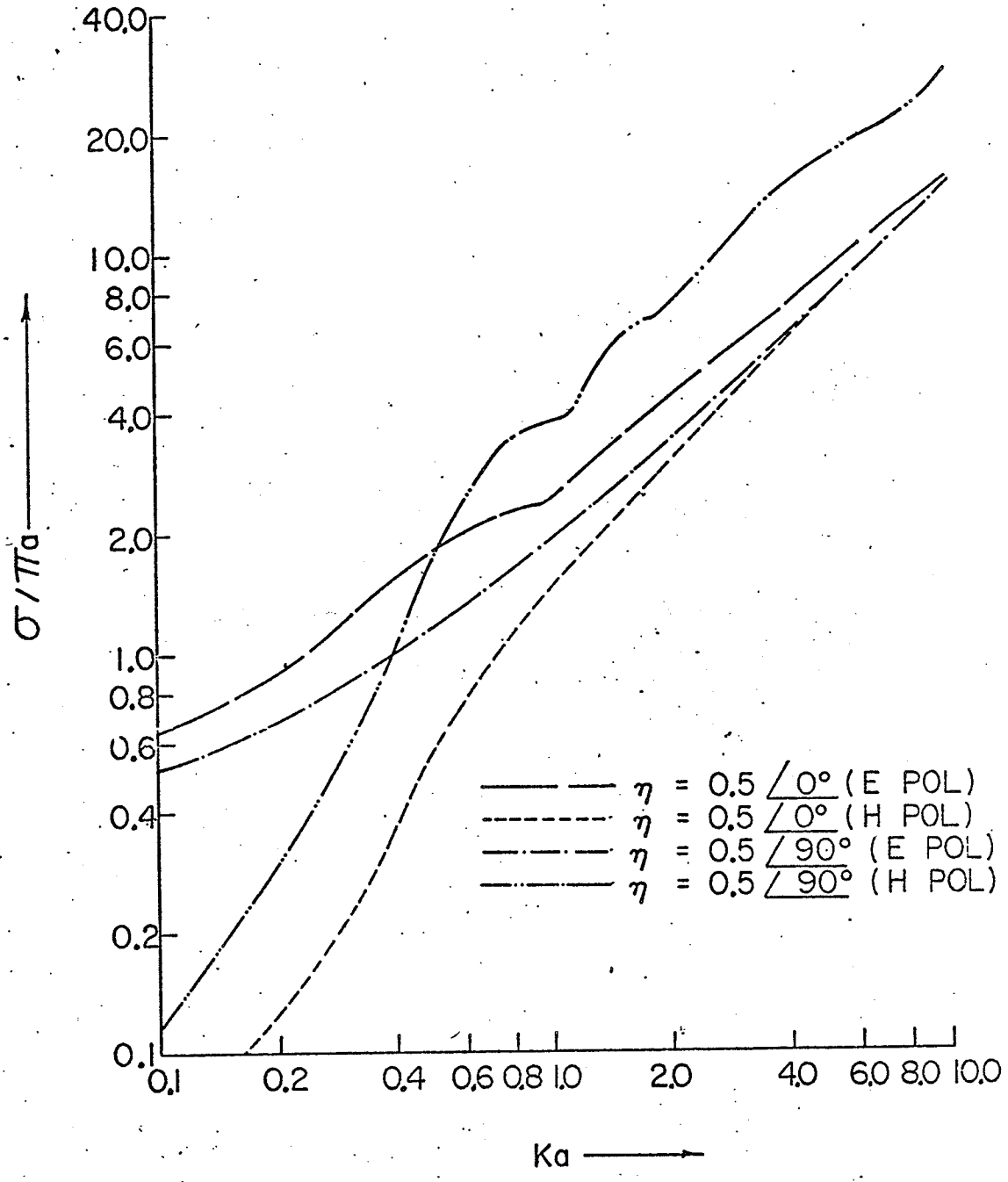

Fig. 4.7 Forward scattering widths versus ka for a circular cylinder and $|\eta| = .5$

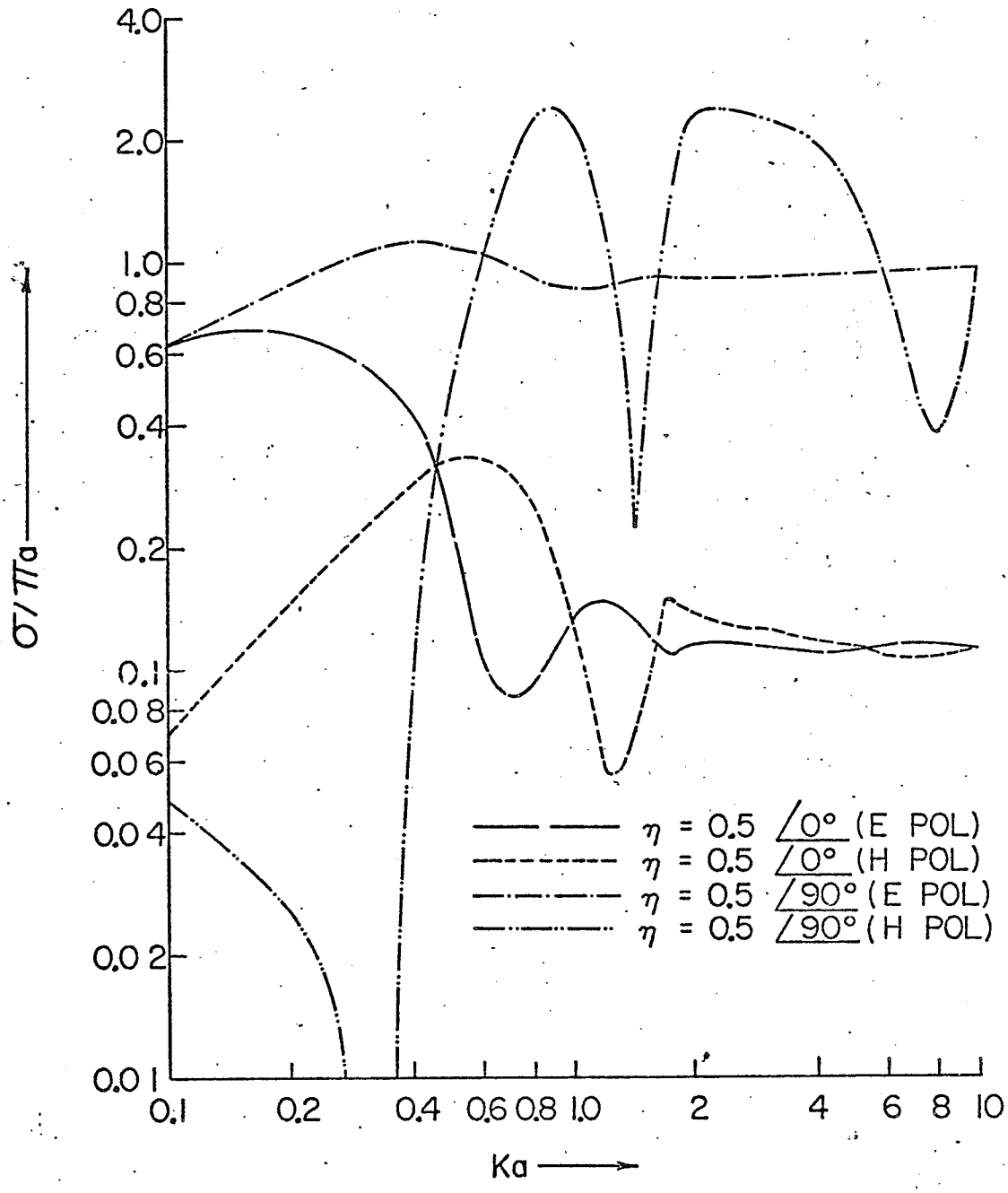

Fig. 4.8 Backscattering widths versus ka for a circular cylinder and $|\eta| = .5$

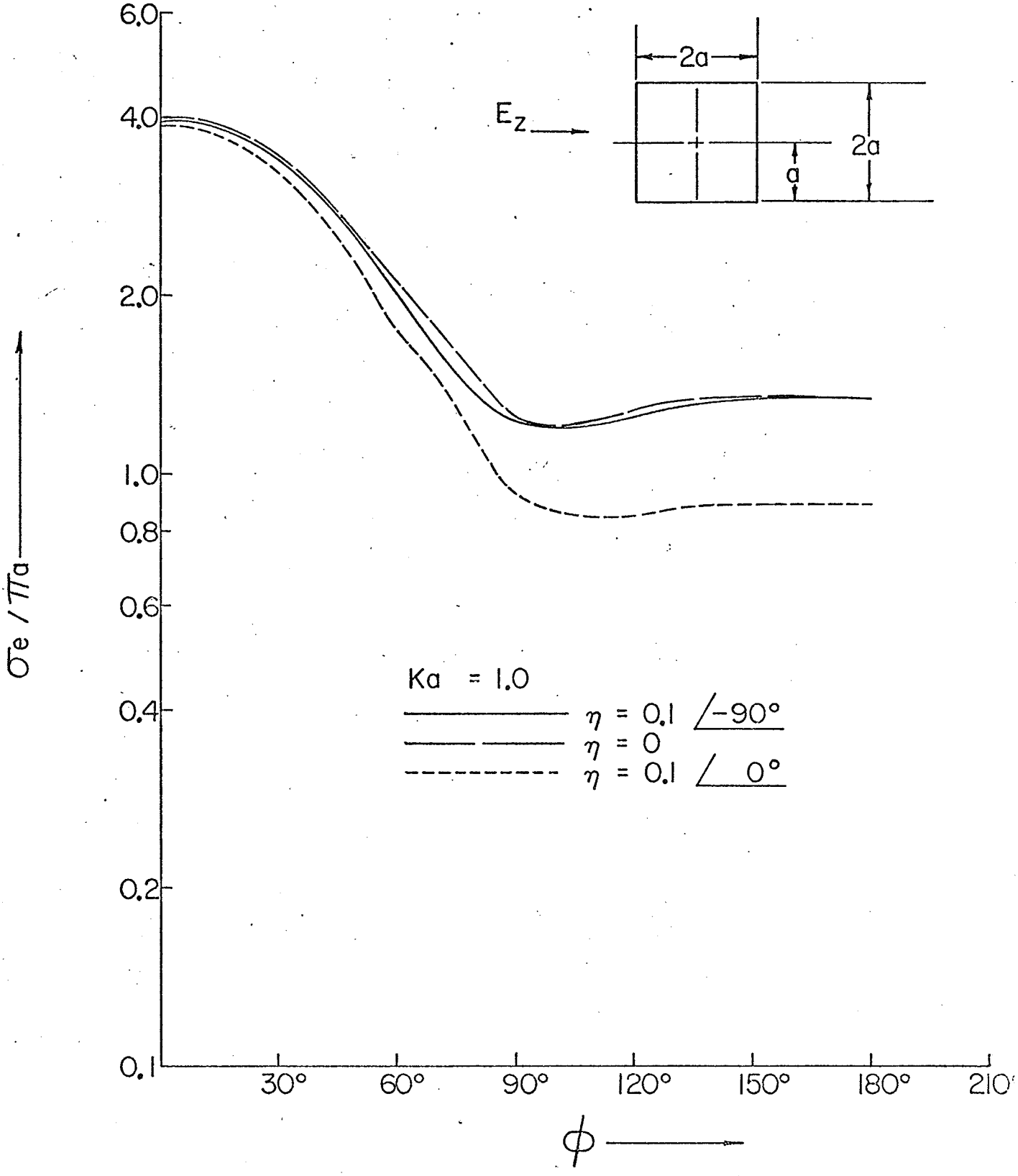

Fig. 4.9 E polarization bistatic scattering widths for a square cylinder (ka = 1.0) for various surface impedances

resistive and capacitive surfaces are shown, since the inductive and homogeneous conductor cases are almost identical, respectively. Here again we note that the scattering behaviour is not significantly altered for inductive and capacitive surfaces as long as $|\eta|$ is small. Also the reciprocal behaviour for the two ranges of normalized impedance is again observed as shown in Figs. 4.10 and 4.11 for $ka = 0.5$. However, unlike the case of the circular cylinder, the forward scattering width is significantly dependent on the surface impedance. The minimum back-scattering width for a resistive surface corresponds to $\eta = .66$ instead of $\eta = 1.0$ which is largely due to the phase of the various interference waves.

In the case of the square cylinder, the ray diagram for grazing incidence is shown in Fig. 4.12. Employing the principles of Section 4.2.1, and the ray formulation of Morse [100] in terms of unknown diffraction and propagation coefficients at the edges, equations may be set up using the numerical results obtained above. However, in this case, the number of unknown diffraction and propagation coefficients is large, thus requiring the simultaneous solution of multivariable transcendental equations. Varying the angles of incidence and observation, these coefficients may be determined and plotted as a function of aspect angle to obtain a least squares fit and hence a simple functional representation for the coefficients.

4.4 The Scattering Phase Shift Technique

Though the transformation matrix technique is ideal for bodies whose cross section is transformable to a circle, it is inadequate to

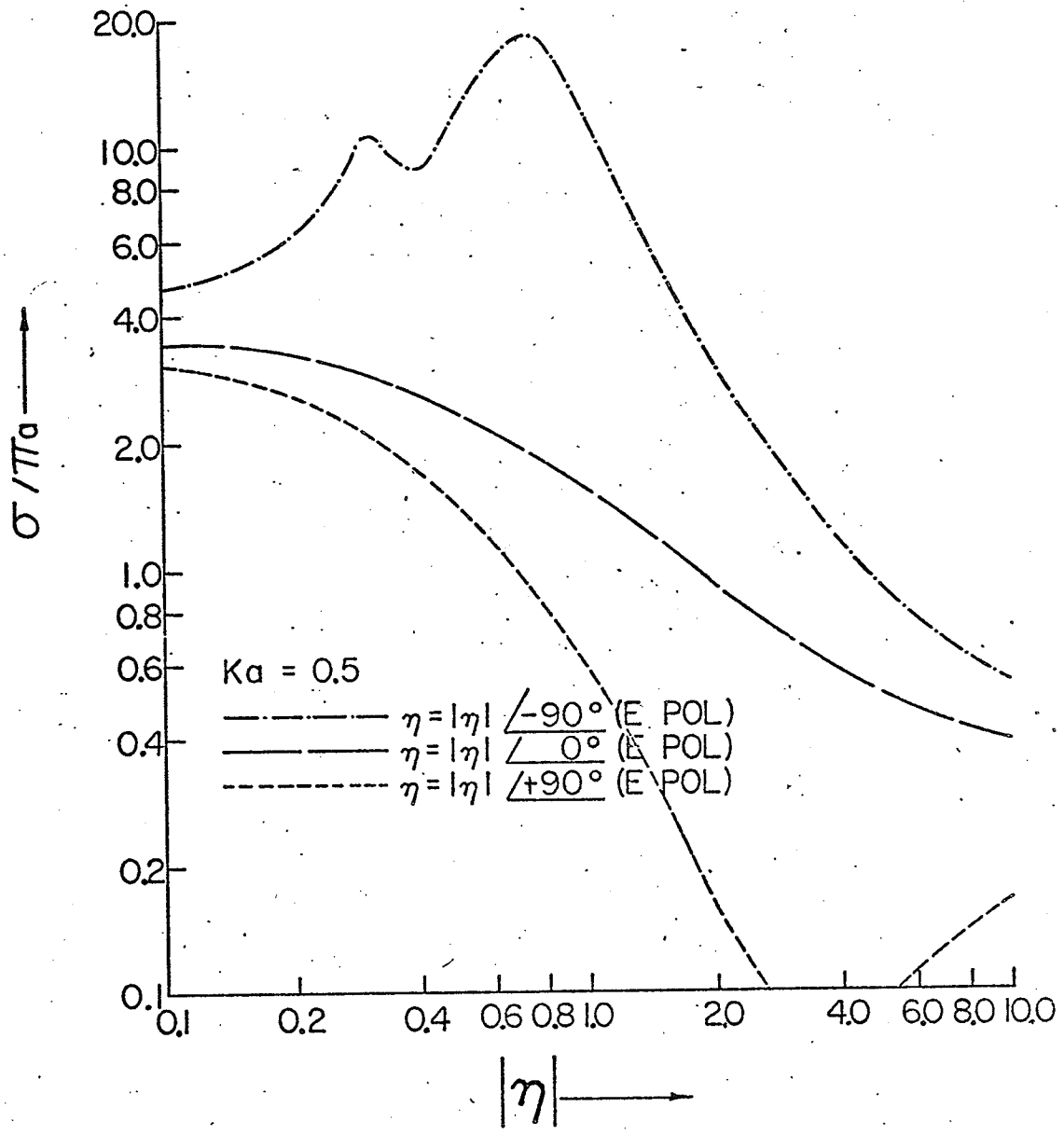

Fig. 4.10 Forward scattering width versus surface impedance for a square cylinder (ka = .5)

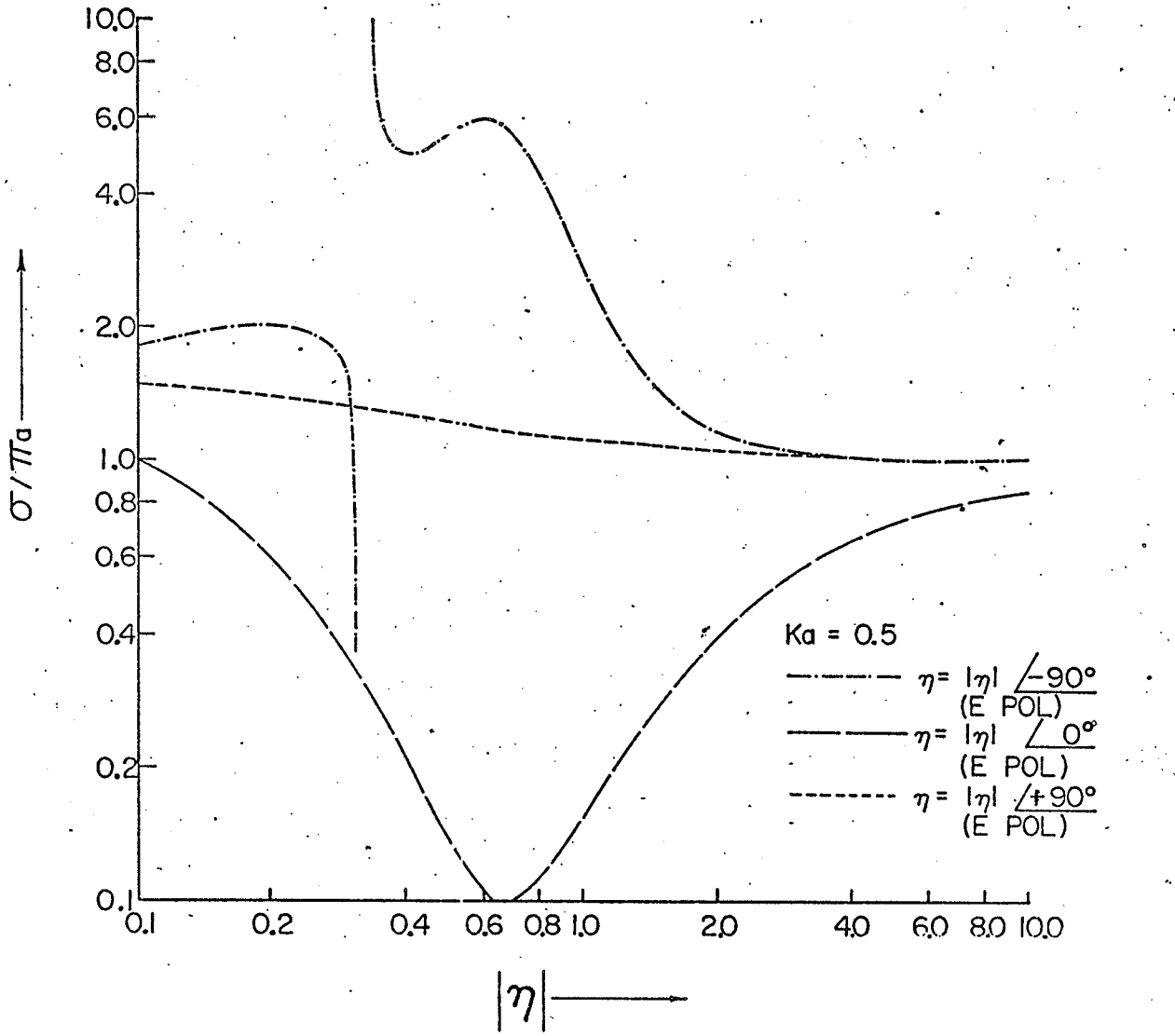

Fig. 4.11 Backscattering width versus surface impedance for a cylinder (ka = .5)

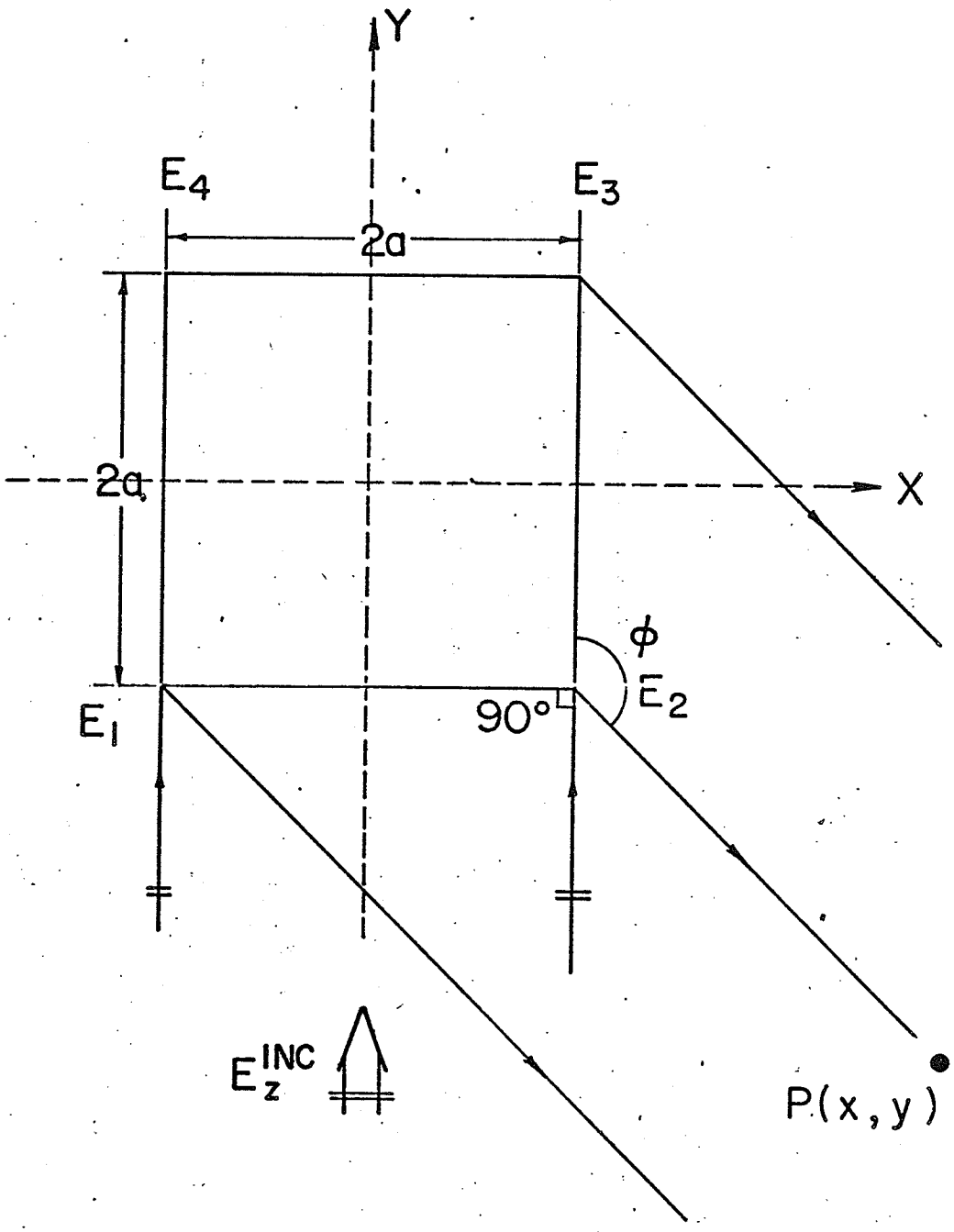

Fig. 4.12 Ray diagram for grazing incidence on a square cylinder

treat even the circular cylinder when it is coated with an inhomogeneous dielectric, due to the excessive computation time required for a reasonable accuracy. This problem is of interest in the scattering from space vehicles during re-entry and in the design of microwave lenses, and hence an alternate method of solution is desirable.

The procedure used here is based on the phase-shift method of Brysk and Buchanan [101] and Shafai [102] and involves the derivation of differential equations for the radial functions from the wave equation and the vector potential, as described in Appendix G. Two auxillary functions related to the phase and amplitude of the radial function are then defined and lead to two first order differential equations. The phase equation is independent of the amplitude and its solution is adequate for finding the fields outside the scatterer, the initial phase values being obtained from the boundary conditions. Since a first order differential equation is numerically solvable to any desired degree of accuracy, the method is highly effective for treating imperfectly conducting cylinders with radially inhomogeneous dielectric coatings.

Consider a circular cylinder of radius a, surface impedance η and coated with a radially inhomogeneous dielectric layer of permittivity $\varepsilon(\rho)$ and outer radius b. To obtain the scattered fields for both polarizations, it is adequate to solve (G.21) and (G.23) subject to the initial phase shifts obtained by applying the boundary conditions at the interface $\rho = a$. For a perfectly conducting cylinder, the initial phase shifts are given by

$$\delta_n(a) = \begin{cases} -\tan^{-1}[J_n(ka)/Y_n(ka)] & \text{for TM modes} \quad (4.17) \\ -\tan^{-1}[J_n'(ka)/Y_n'(ka)] & \text{for TE modes} \quad (4.18) \end{cases}$$

which are real angles in this case.

For the imperfectly conducting cylinder, the initial phase shifts may be assumed complex due to the surface losses, unlike the case of the perfectly conducting cylinder. At this surface, the Leontovich boundary condition (D.8) must be satisfied and hence we obtain

$$\delta_n(a) = - \tan^{-1} \left[\frac{J_n(ka) + j\eta\, J_n'(ka)}{Y_n(ka) + j\eta\, Y_n'(ka)} \right] \quad \text{for TM modes} \qquad (4.19)$$

$$\delta_n(a) = - \tan^{-1} \left[\frac{J_n'(ka) - j\eta\, J_n(ka)}{Y_n'(ka) - j\eta\, Y_n(ka)} \right] \quad \text{for TE modes} \qquad (4.20)$$

Knowing these values for both polarizations, the phase functions δ_n are obtained from a numerical integration of equations (G.21) and (G.23) for any specified dielectric inhomogeniety while the scattered field is evaluated using (G.10).

The differential equations for the phase functions were solved using the fourth order Runge Kutta method [103]. Figures 4.13 to 4.15 present results for the imperfectly conducting dielectric coated cylinder for $ka = 2.0$, $kb = 3.0$, $\eta = 0.5$ and ε varying as $(k\rho)^{-1}$, $(k\rho)^{-2}$ and $\exp(-k\rho)$, respectively. The results clearly indicate that the significant variations in the amplitude of the main scattering lobe as well as the number and polar positions of the side lobes may be attributed to the dielectric coating of the imperfectly conducting cylinder. This is in contrast to the results obtained without a dielectric coating where no significant deviations from the perfectly conducting cylinder were observed.

When the thickness $(b - a)$ of the dielectric is very small,

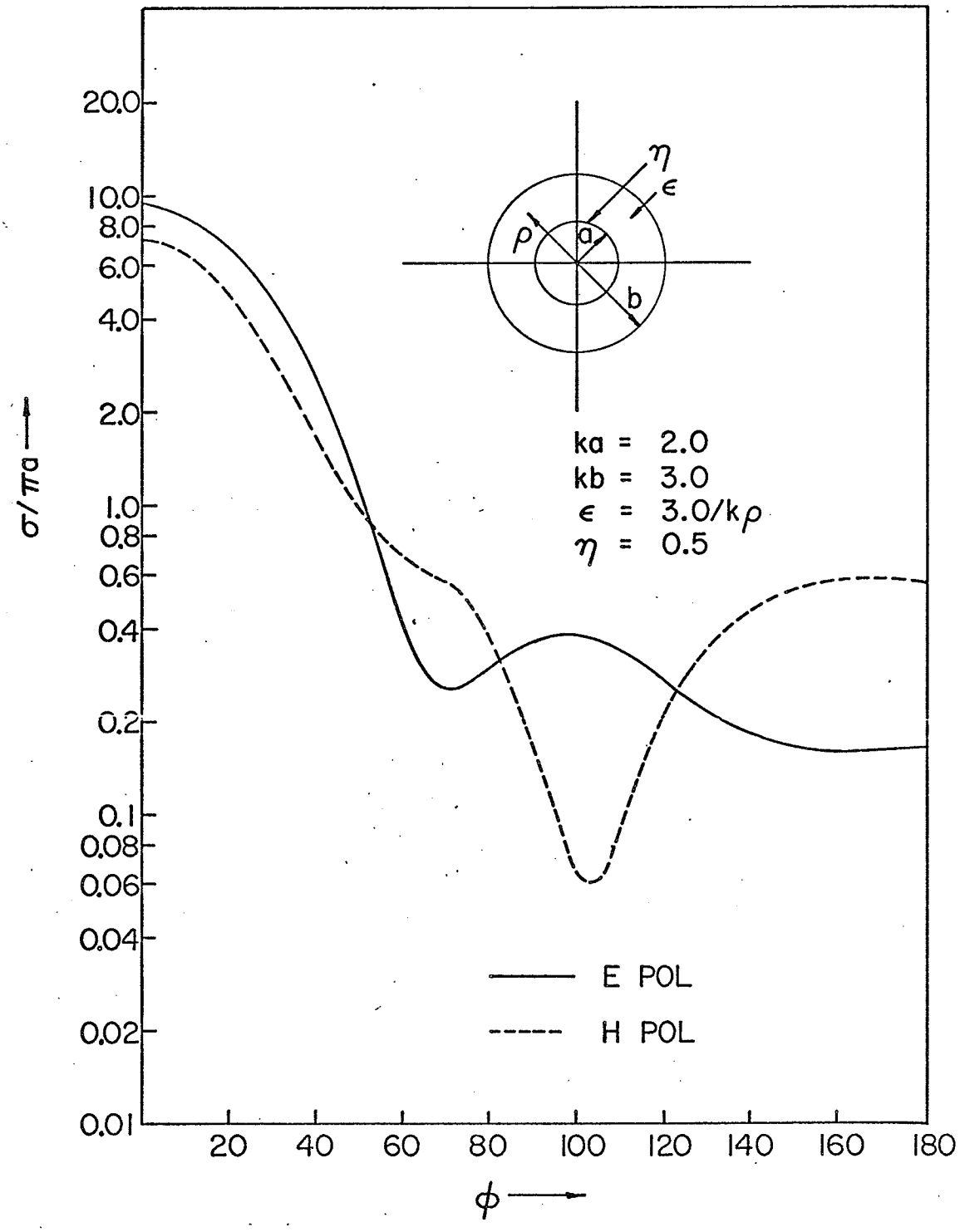

Fig. 4.13 Scattering width vs. ϕ for an impedance cylinder coated with a radially inhomogeneous dielectric

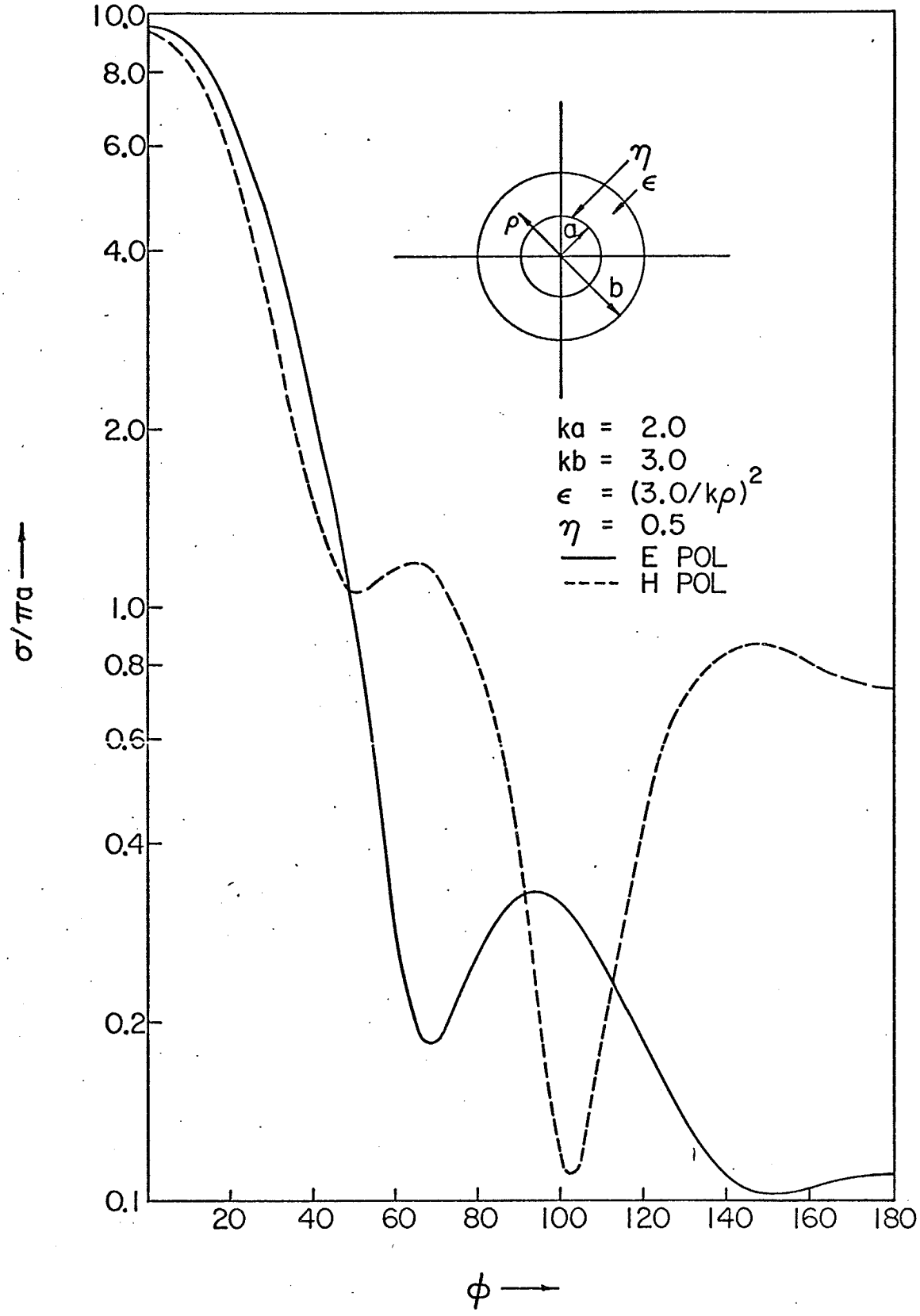

Fig. 4.14 Scattering width vs. ϕ for an impedance cylinder coated with a radially inhomogeneous dielectric

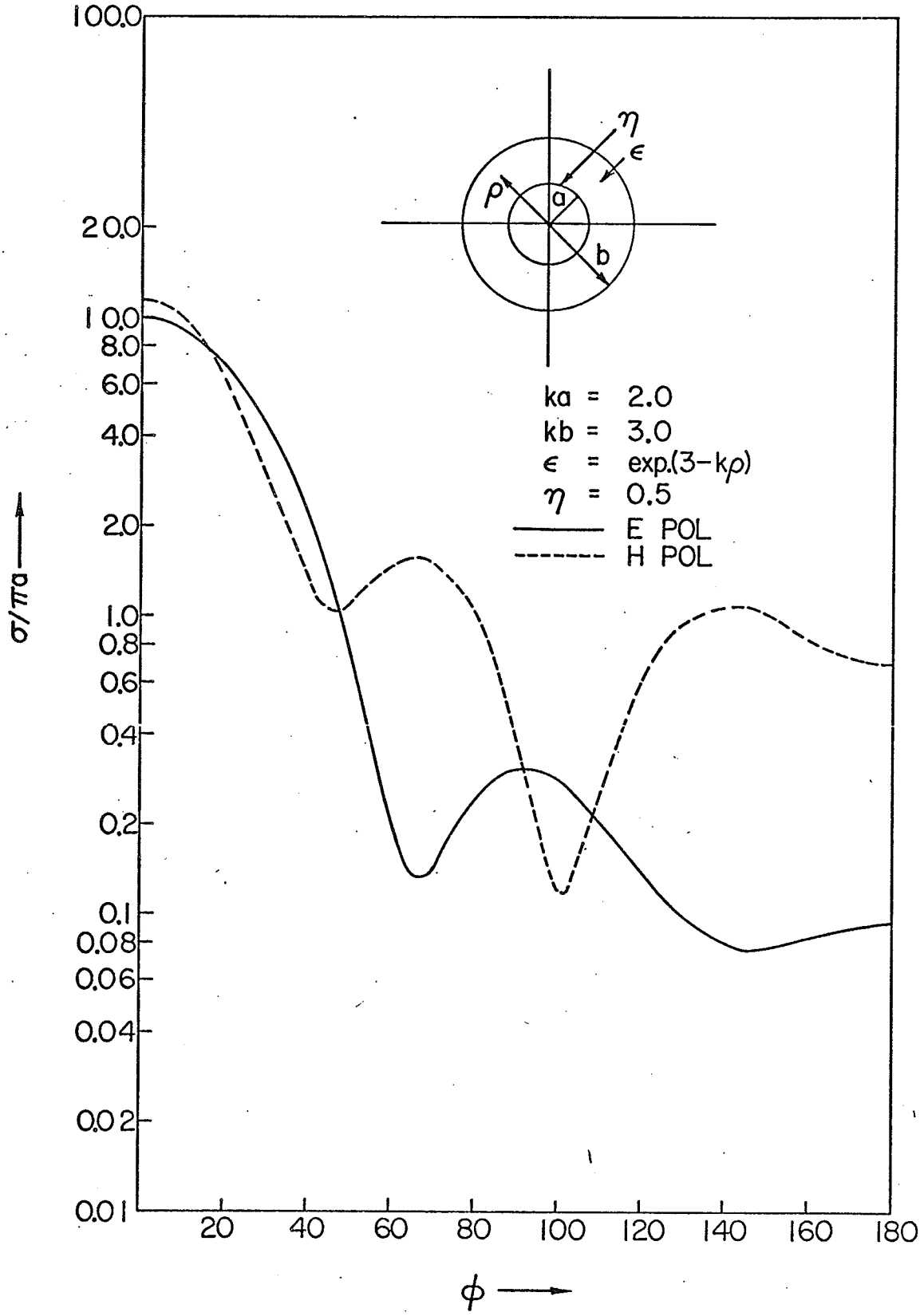

Fig. 4.15 Scattering width vs. ϕ for an impedance cylinder coated with a radially exponential dielectric

the cylinder may be viewed as being imperfectly conducting with an equivalent value of η. In this case, the ray-numerical procedure of Section 4.2.1 is easily applied and new diffraction and propagation coefficients determined. For larger thicknesses, it becomes necessary to consider various types of rays, e.g. the specular, axial, glory and stationary or rainbow rays in the dielectric together with reflection effects at the metal cylinder, thereby making the analysis considerably involved.

4.5 Methods for Imperfectly Conducting Cavities

Up to now we have treated the exterior travelling wave problem in presence of imperfectly conducting scatterers. In this section, the problem of imperfectly conducting cavities is briefly dealt with, as such structures are of great practical use in cavities for frequency meters, test chambers, microwave tubes and beam accelerator designs.

For the analysis of the rectangular cavity where all the walls are imperfectly conducting, the perturbation approach of Karbowiak [17], as given in Appendix H, is most practical for values of η near zero. The method leads to simple expressions for the propagation constant, Q factor and bandwidth such that conclusions as to the behaviour of these parameters are easily made without computations.

Appendix I presents the boundary value solution for the eigenvalues of a spherical cavity with an impedance wall. The Q factor and bandwidth are easily evaluated using the method of Appendix H. Figures 4.16 and 4.17 show the eigenvalues of a spherical resonator with imperfectly conducting walls for both TM and TE modes based on

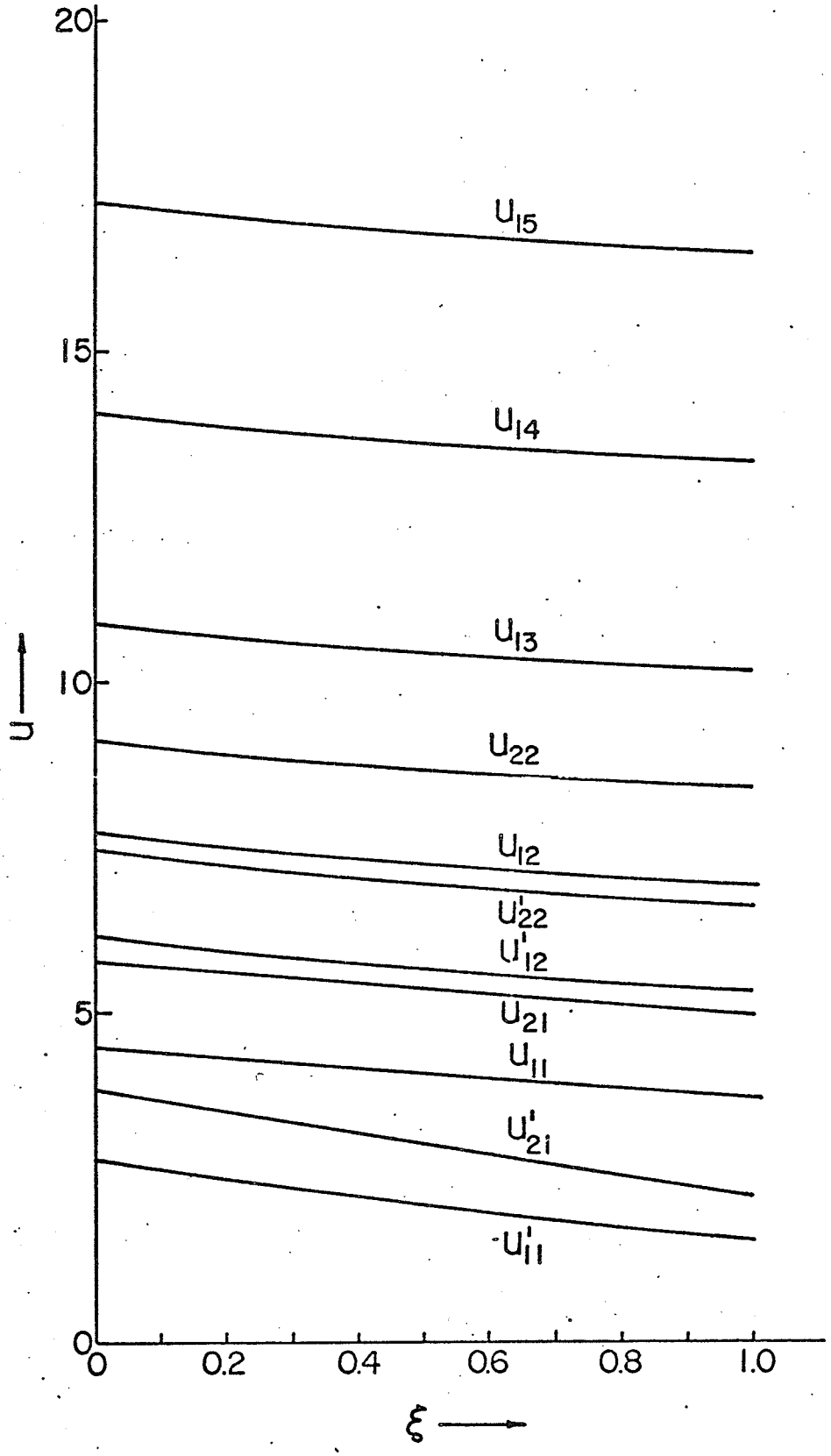

Fig. 4.16 Eigenvalues for a spherical resonator TM case

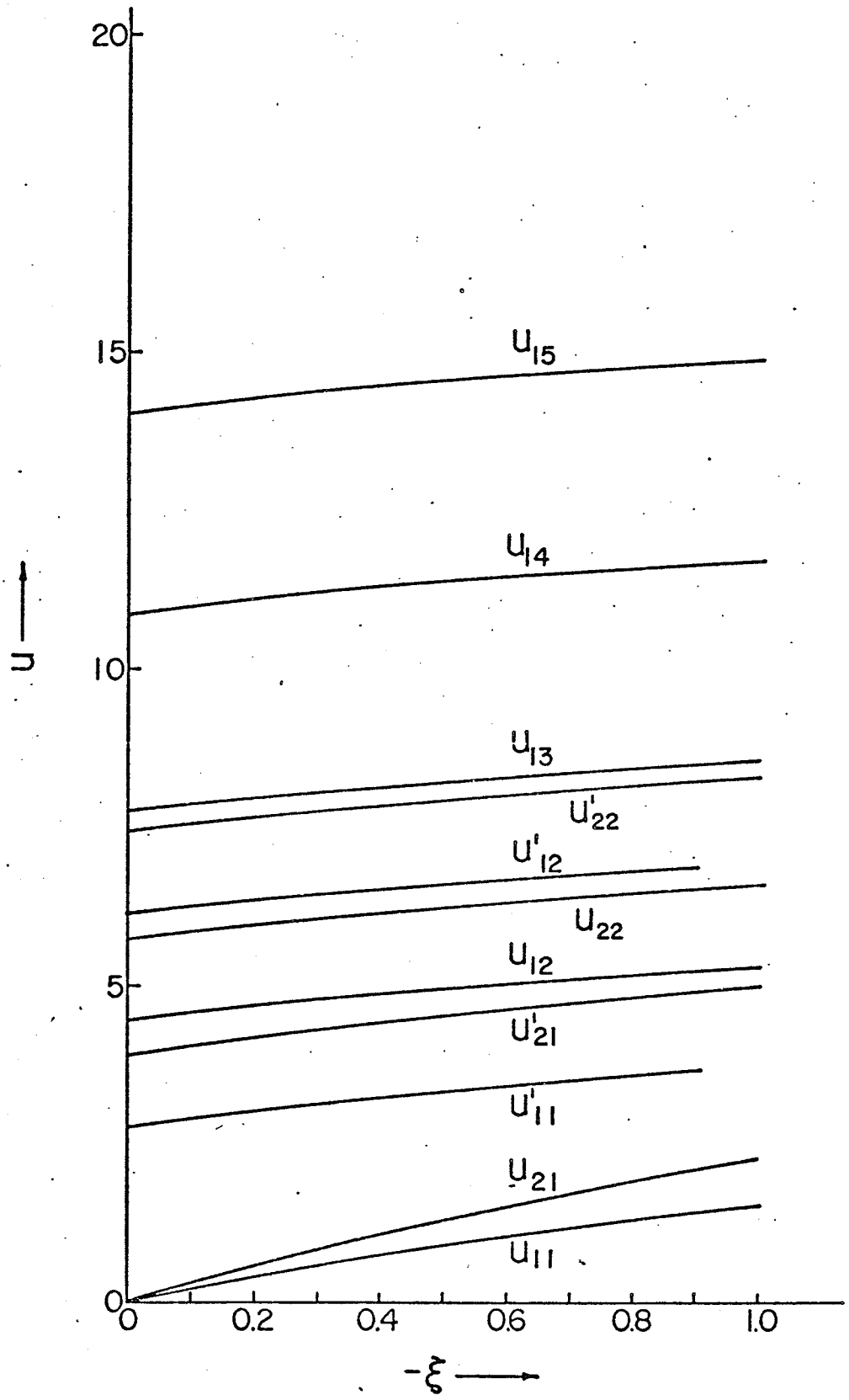

Fig. 4.17 Eigenvalues for a spherical resonator TE case

equations (I.7) and (I.8). The results indicate that the reactive impedance results in a frequency shift while the bandwidth depends on the real impedance. An inductive wall is seen to decrease the resonant frequency while a capacitive wall increases it. These properties are exhibited by both rectangular and spherical types. For a spherical cavity with capacitive walls, the TE mode, which is a perturbation of the zero value of the zero frequency static mode, is seen to be the dominant mode unlike the perfectly conducting cavity where the TM mode is dominant.

Though the ray optical method for a spherical cavity is considerably involved, the rectangular cavity can be analyzed using the method of Maurer and Felsen [104]. Simplification of the method may be realized by using the ray-numerical technique to determine the reflection coefficients required in this case.

CHAPTER V

SUGGESTED APPLICATIONS OF THE RESULTS

5.1 Introduction

Besides the academic interest in the problem of scattering from imperfectly conducting targets, such bodies are of importance in a number of potential applications. Two problems which have been of constant interest in electromagnetic scattering are the radar cross section reduction and enhancement, which are important in tracking aircraft, missiles, etc. in flight. Various methods have been proposed and implemented for the control of radar cross section, e.g. target shaping, addition of reflectors to the body and application of absorbing materials to the surface as treated in this thesis.

While the method of body shaping is theoretically possible, it, nevertheless, suffers from certain practical difficulties. In the design of an aircraft or missile, the shape is normally constrained by other variables and factors, and the problem of radar cross section reduction or enhancement, becomes of secondary importance. Furthermore, in the low frequency or Rayleigh region, shaping is ineffective since the cross section is dependent primarily on body volume rather than shape, and hence alternative techniques of approach must be applied, e.g. the method of impedance loading.

The method of impedance loading is based on the principle of disturbance of the current distribution on the surface of the body using discrete impedances at various points on the body. The cross section at a specific aspect angle and frequency can be either increased or

decreased by this method. However, it has been used primarily in cross section reduction, while radar reflectors provide a more convenient method of enhancing the cross section over a wide frequency band and for a large range of aspect angles, since the impedance loading method is highly sensitive to both frequency and aspect angle.

The results of the previous chapters show that the radar cross section may be reduced or enhanced by coating the surface with an absorbent material thicker than the skin depth. The reduction in cross section in this case is achieved by a combination of absorption and redirection of the scattered rays while the enhancement is achieved by constructive interference of the rays. It is not surprising that the development of these materials has occupied researchers in many countries over the last few decades. Ideally, the best suited material would be a paint like substance effective at all polarizations and over a broad range of frequencies and angles of incidence. At present, no such ideal material exists and the practical type of absorber used in a particular situation is dependent on the frequency, target shape and dimensions, bandwidth requirements and physical limitations such as weight, thickness, strength, environment, etc.

Practical absorbers are also in use in the design of "High Performance Shielded Antennas" [105], where a high directivty pattern is achieved through the use of a cylindrical metal shield on the rim of the parabolic dish to attenuate side and back radiation. The shield is lined with a long life broadband radio frequency absorbent material which reduces stray reflection and diffraction at the edges of the shield. A precision contour and a resonant absorbent strip along critical

portions of the primary reflector combine to control the aperture field.

Besides the capability of the control of scattering pattern by imperfectly conducting spheres as shown in Chapter III, this, in conjunction with the formulation for the scattering by multiple spheres, is of interest in a wide variety of problems. The scalar problem is of interest in acoustics and in the detection of voids by ultrasonic waves. The vector problem is also of interest in studying propagation through rain, study of sols, air pollution, meteorology, etc. However, two novel applications which result from this study, and are of considerable interest in high microwave power technology, are the possibility of the construction of (i) a high power density microwave anechoic chamber, and (ii) a high power density differential microwave power meter and will be dealt with in the next two sections.

5.2 Microwave Absorbing Chamber

Since absorbent materials may be used to control the radar cross section of scatterers, it is possible to construct low and high power anechoic chambers using a three dimensional array of lossy bodies. Thus Figures 3.4 to 3.11 show how the radar cross section is decreased with absorber coatings, while Fig. 3.12 depicts in particular the reduction in backscattering cross section with η. The lower backscatter obtainable using such bodies indicates the potential superiority of the use of arrays of such bodies over the conventional commercial pyramidal absorbers commonly used.

In the proposed arrangement, the incident power is partly absorbed at each element surface and partly redirected in other directions. The

scattered energy is further rescattered by other spheres in the array and consequently absorbed. The process of multiple scattering and absorption continues till finally all the energy is absorbed and a satisfactory quiet zone is obtained.

For low microwave power densities, the incident power is of the order of milliwatts and hence ordinary spheres with absorber coatings would suffice. However, for high microwave power densities, it would be necessary to construct an absorption chamber consisting of water loads. The water would be contained in plastic spheres with facilities for water circulation to remove heated water. Such a chamber may be useful for testing microwave power equipment in a shielded environment or for exposing food and other material samples to high density plane wave fields.

A computer program utilizing the multiple sphere ray scattering formulation of Chapter II, together with the monostatic, bistatic and forward scattering results for a single impedance sphere given in Chapter III, could be prepared to optimize the size, surface impedance and location of each sphere in the array. Use of the ray technique will make the computer program tractable, resulting in a considerable saving of computer time and a sufficiently accurate evaluation of the field distribution. For large separation between the spheres (i.e. $kd > \lambda$), a first order interaction is sufficient and the accuracy of this approximation increases as kd increases. Further simplifications in the computer program will be possible with the use of a matrix formulation, as in the analysis of antenna arrays.

With the present day trend of using microwave power for

innumerable industrial processes, a high microwave power anechoic chamber is of considerable interest to modern industry. The conventional absorber pyramidal structures used in the low power chambers are inadequate to deal with the problem, due to their inability to dissipate heat due to high incident microwave energy, and as such are a fire hazard. Hence the proposed scheme has considerable merit, since the absorbent material being used is water which has a greater thermal capacity, and the constant circulation of water removes the possibility of any over-heating. Finally, the cost of such a chamber would be extremely low in comparison to the conventional chamber, since plastic bodies or inflatable structures are easily fabricated at low cost and the absorbent material is just plain water. On the other hand, presently used low power absorbers in microwave anechoic chambers are not readily applicable at high power and the development of such a material itself would entail considerable research and expense.

5.3 Differential Microwave Power Meter

The fact that a sphere coated with an absorbent material, causes dissipation of some of the incident microwave energy on its surface, can be used to advantage in the construction of a high density microwave power meter. This dissipation of energy is primarily due to the creeping waves which attenuate when they travel over the sphere surface, as shown previously, and as such provides a direct measure of the incident power. Further, the sphere is also the ideal body for the construction of such a power meter, since it is the only body which enjoys three dimensional symmetry and is, therefore, free of polarization problems.

The proposed schematic of the differential power meter is shown in Fig. 5.1 and consists of two identical spheres enclosing a non-compressible gas of low time constant and high coefficient of thermal expansion, connected through a U column of mercury or other liquid. One sphere is used for power density monitoring while the other is a compensating sphere. Both spheres and stems are protected by windshields while the stems and compensating sphere are also shielded by electro-magnetic screens. The compensating sphere corrects for the effect of variations in the ambient temperature, while the multiple scattering between both spheres is accounted for in the scale calibration. The choice of liquids in the stem is dependent on the power density to be measured. Mercury would be useful at high power levels, while water, alcohol or other thermometric liquids would be suitable at low power densities. A visual indication of the power level could be obtained by using a liquid crystal solution or anhydrous Calcium Sulphate.

The power meter works on the simple principle of a differential manometer. The incident energy causes creeping waves to be set up on the sphere surface which are attenuated as they travel thus heating the enclosed gas in the probing sphere. The expansion of the gas forces the liquid column down and also the indicator, which registers the incident energy density level.

Though various types of microwave power density meters are commercially available and utilize different methods for monitoring the power density level, they are restricted to low power densities and, as such, are unsuitable for present day needs due to the very high density levels used in various industrial applications. The differential

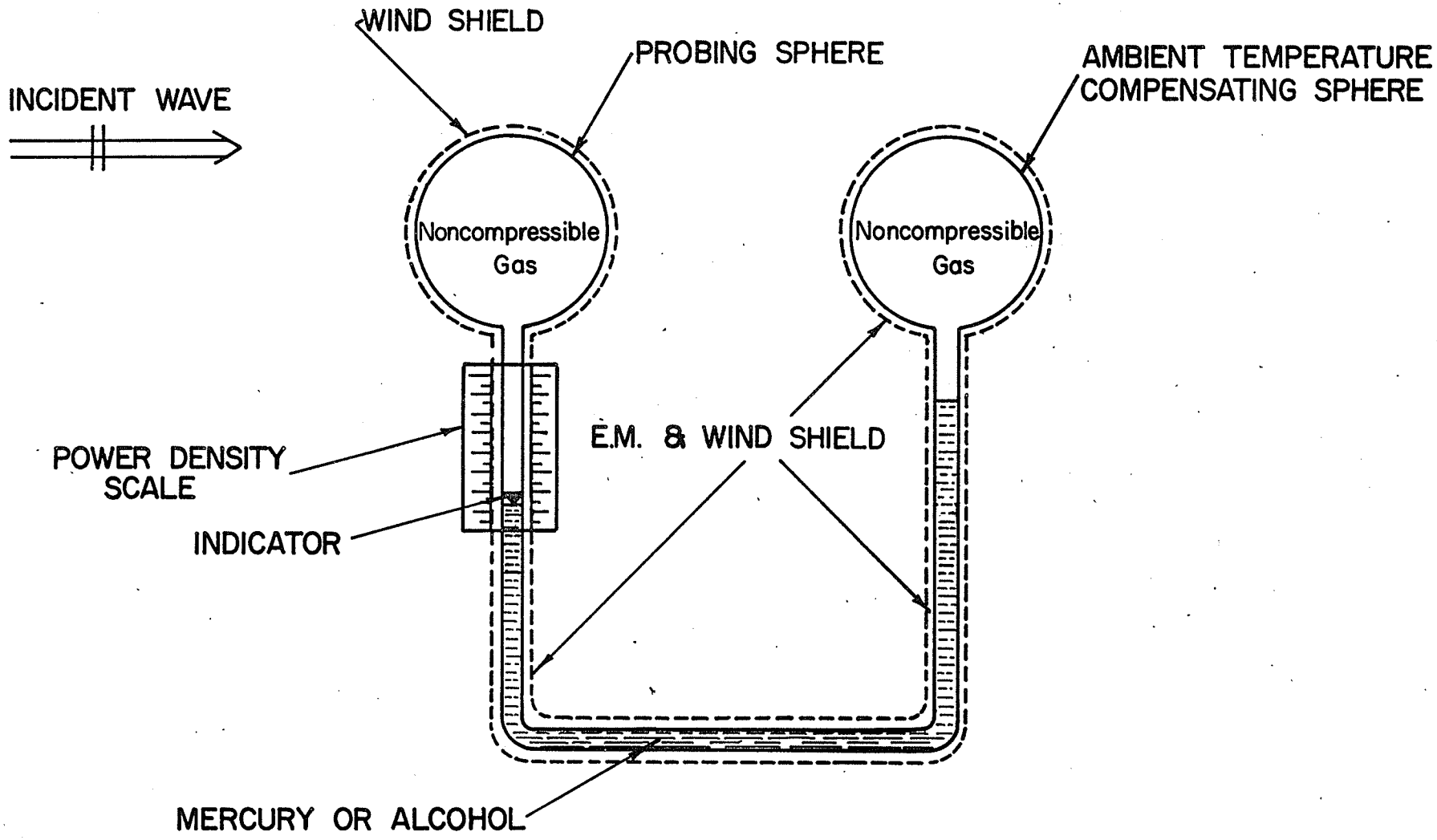

FIG. 5.1 SCHEMATIC OF HIGH MICROWAVE POWER DIFFERENTIAL POWER METER

microwave power meter presents an effective method of monitoring high power densities and can also be used as a safety meter for radiation monitoring, with the indicator designed as in the maximum-minimum thermometers, such that the maximum level in the region probed is indicated. Finally, the device could be positioned permanently in industrial equipment for indication of power level available for heating and processing various materials.

CHAPTER VI

DISCUSSIONS AND CONCLUSIONS

6.1 Discussion

The ray optical scattering by a perfectly conducting sphere is investigated in Chapter II, to establish the applicability of the ray method for spheres. The previous expressions by Senior and Goodrich [71] were corrected, for the monostatic, bistatic and forward scattered fields and analyzed for accuracy in Tables 2.1 and 2.2 and Figures (2.2a), (2.2b) and (2.2c). Good agreement is obtained between these results and those obtained from the Mie series exact solution in the backward and forward scattering directions. In the bistatic range of angles, the creeping wave term (2.5b) is not valid in the range $\psi \leq \theta \leq \pi - \psi$, $\psi = 0(ka)^{-1}$ while the geometrical optics term (2.5a) is only valid when $ka \cos^3(\theta/2) >> 1$. In order to extend the solution over a larger range of bistatic angles, the geometrical optics term must be improved and this was found possible by using Erukhimovich's geometric optics term (2.10), as illustrated in Figs. 2.3 and 2.4.

These limitations on the solution for the perfectly conducting sphere prevent the direct use of the solution in the scattering by multiple spheres except for the principal cases of the broadside and endfire scattering. Thus for solutions involving arbitrary angles of incidence and observation, the exact results for the single sphere must be used. In formulating the ray optical scattering by multiple spheres, other difficulties are also encountered. Although the scattering phenomenon involves multiple interactions, examination of (2.13) shows

that first order interactions are of much greater significance than the higher order terms, as illustrated in Figs. 2.7 and 2.8. Furthermore, the solution is inadequate for spheres being very close to each other or touching, but this can be overcome by the Zitron-Karp formulation [79]. This requires the expansion of the scattered field in terms of plane waves and their derivatives, and the solution for the region from the position where the spheres are touching to that when they are apart by approximately the larger sphere diameter can be obtained using this method. It is evident that the method becomes quite involved when considering an arbitrary distribution of spheres, unless mode caustic-caustic interactions [85] in conjunction with a scattering matrix approach are employed to reduce the computations required.

Having considered the limitations for single and multiple conducting spheres, the ray method is applied to imperfectly conducting spheres by imposing the Leontovich impedance boundary condition. When the characteristic dimension ka is small, little need be done to improve the Mie series in (3.2) from a computational point of view, since the series can be truncated after a few terms. However, as ka increases the series is tedious to compute. The ray optical formulation eliminates this difficulty, resulting in simple expressions for computational purposes and requiring considerably less computation time, particularly when ka is much larger than unity. The solution is obtained as the sum of a geometric optics contribution and a series of creeping rays which decay as they travel around the sphere, and hence only one or at most two such rays need be considered.

Examination of the results for σ_e and σ_h in Figures 3.4 to 3.11

indicates good agreement with the exact solution for an imperfectly conducting sphere except near the forward scattering direction, where (3.43) is not valid since the condition $ka \sin^3 \theta/2 \gg 1$ is violated. Furthermore, the ray solution shows clearly the dependence of σ_b and σ_f on ka, which for $\eta \neq 1$ tend to unity and $(ka)^2$ as $ka \to \infty$, respectively, and oscillate for smaller values of ka due to the creeping wave contribution. It is shown that the forward scattering cross section is increased, relative to the perfectly conducting sphere, for an inductive coating in the range $0 < |\eta| \leq 1$ or a capacitive coating in the range $1 \leq |\eta| < \infty$ and decreased for all other reactive coatings. On the other hand, the backscattering cross section is always below that of the perfectly conducting sphere and vanishes completely for $\eta = 1$, as shown in Fig. 3.12. This behaviour of σ_f and σ_b is attributed to the phase relationship between the E and H waves in (3.36) and (3.58) which determine the constructive or destructive interference of the creeping waves. For purely resistive coatings, the scattering cross section in any direction is below that of the perfectly conducting case due to power dissipation on the sphere surface, as is evident from (3.43) and (3.50). The behaviour is similar for a complex impedance coating except when the real part is sufficiently small, where the outcome is essentially determined by the reactive term.

Analysis of (3.43) and (3.50) shows that σ_θ is independent of polarization for $\eta = 1$, which is the dividing point between the two specific ranges of impedance $0 \leq |\eta| \leq 1$ and $1 \leq |\eta| \leq \infty$. The results for a specific impedance in either range are found adequate to determine completely the behaviour for the reciprocal impedance in the other.

This is the underlying concept for the possible extension of Babinet's principle to three dimensions and imperfectly conducting bodies while reducing computation time for the complete range of η to one-half. These results have been verified for the two dimensional case of the imperfectly conducting cylinder as well, as shown in Figs. 4.5 and 4.6.

Comparison of Figures 2.2b and 3.4 shows that the lobe structure is not significantly altered due to surface imperfections, though new lobes may appear mainly in the E plane. The lobe structure could be controlled by coating the sphere surface along specific directions. It should be noted that the reactive nature of most coating materials changes with frequency in the sense that they are not inductive or capacitive at all frequencies.

It is evident that the geometric optics terms for the backscattering (3.30) and bistatic scattering (3.43) reduce to the corresponding results for the perfectly conducting case when $\eta = 0$, except for the geometric optics expression (3.57) which is identical to that for the perfectly conducting sphere. Since this forms the dominant contribution to the forward scattered field, the latter is not significantly altered except for small capacitive or large inductive impedances, as shown in Figs. 3.5 and 3.6.

A survey of the results obtained by ray theory indicates that the method cannot be easily applied to other geometries without resorting to other methods. The ray method has been based on representing the scattered fields in terms of geometric optics and creeping wave terms through the application of Watson's transformation and/or for asymptotic expansions to the exact solution. A creeping wave is assumed to excite

an infinite number of modes, thus requiring an infinite summation in calculating the field and the evaluation of appropriate decay and diffraction coefficients. The ray numerical method of section 4.2 is postulated to overcome these difficulties by defining ray diffraction and propagation constants, which are evaluated by comparison of the numerical results for the diffracted field with the corresponding field expression involving the unknown coefficients. Thus in the case of the circular cylinder, the coefficients derived using equations (4.5), (4.6) and (4.7) predict accurately the diffracted field, as shown in Fig. 4.2.

Though the ray-numerical procedure is demonstrated effectively for the circular cylinder, its application to other geometries is hindered by the lack of numerical results and two methods for cylindrical scatterers are suggested. The first is the transformation matrix approach which is shown to be ideal for a cylindrical scatterer whose cross section can be mapped conformally into a circle. The technique eliminates edge singularities and gives good accuracy for bodies for which a transformation exists. As such it is an attractive alternative to the integral equation approach of Andreasen [44]. The technique is applied to the imperfectly conducting circular cylinder and various interesting results are obtained. Two definite ranges of impedance $0 \leq |\eta| \leq 1$ and $1 \leq |\eta| \leq \infty$ already identified for the sphere are also observed from Fig. 4.6 for the circular cylinder. The scattering cross section tends to zero as may be seen from the term $(1 - \eta)/(1 + \eta)$ in (D.12) and (D.14) in the same manner as for the imperfectly conducting sphere. Furthermore, the forward scattering width is not significantly different from the perfectly conducting case, except when the surface is reactive

and η close to unity.

The method is also illustrated for a square cylinder as a particular case of a polygonal structure and the results are given in Figs. 4.9, 4.10 and 4.11. In this case we observe from Fig. 4.11 that for $\eta = 1$ there is a finite backscattering width unlike the case of the circular cylinder. For $ka = 0.5$, a minimum in the backscattering occurs at $\eta = 0.66$, mainly due to the phase of the various interfering waves. For the forward direction, the value of η for a maximum forward field is approximately predicted by the Hansen-Woodyard condition [44].

The second method is the phase shift method which was introduced since the transformation matrix technique requires excessive computation time for a reasonable accuracy, as illustrated in section 4.3 for a cylinder coated with an inhomogeneous dielectric, due to the large number of integration steps required. In this case the phase shift method is more suited since it involves the numerical solution of a first order differential equation which, in principle, can be solved to any desired degree of accuracy. The equation for the phase function (G.21) is adequate to define completely the scattered field while the boundary conditions form the initial conditions for this equation. The results in Figures 4.13 to 4.15 show that the significant variations in the amplitude of the main scattering lobe as well as the number and polar positions of the side lobes may be attributed to the dielectric coating of the imperfectly conducting cylinder.

In considering the interior problem of imperfectly conducting cavities, which form essential components of various microwave devices, the rectangular cavity with such walls may be treated by using the

perturbation method as long as η is small. The conclusions from equation (H.12) that the reactive part of the surface impedance is responsible for the change in resonant frequency, while the bandwidth depends on the surface resistance of the walls, are also borne out by the results for the spherical cavity based on the boundary value approach. It is interesting to note that for a spherical cavity with a capacitive wall, the TE_{m01} mode, which is a perturbation of the zero frequency static mode, is dominant as shown in Fig. 4.17, unlike the perfectly conducting cavity where the TM_{m11} mode is dominant.

Finally, in the analysis of the imperfectly conducting sphere, the possibility of radar cross section reduction and surface absorption suggest certain practical applications. Two of these are the high power anechoic chamber and the high density microwave power meter discussed in detail in Chapter V.

6.2 Conclusions

The ray optical solution for the scattering of plane electromagnetic waves from a perfectly conducting sphere has been analyzed for accuracy and its range of applicability extended by modifying the geometrical optics term. In this form the solution predicts accurately the fields for the backscattering, forward scattering and $\theta = 90°$ directions, which make its use possible for scattering by multiple spheres in the endfire and broadside configuration. For the multiple sphere problem the formula developed predicts more accurately the scattering from two identical spheres, for any arbitrary angle of incidence and observation, than has been possible previously. The

model is simpler and permits easy interpretation of the phenomena of many body scattering. Furthermore, one finds that first order interaction terms are of much greater importance than the higher order terms.

The success of the ray optical formulation for the scattering by single and multiple perfectly conducting spheres, within certain bounds imposed by the asymptotic approximation, gives confidence in the extension of the method to the imperfectly conducting sphere. In this case it is shown that the ray optical formulation leads to results which compare favourably with the exact solution in the forward and backscattering directions as well as the bistatic range of angles, except in the vicinity of the forward direction. Furthermore, the method is shown to eliminate the computational difficulties of the exact solution and requires considerably less computation time.

Further extension of the ray optical technique to other imperfectly conducting bodies is shown to be limited due to the paucity of diffraction and decay coefficients for such bodies. In attempting to overcome this difficulty, the ray-numerical procedure is proposed. The method leads to an elimination of the summation required to consider the different modes excited at the body surface, and considerably simplifies the computations. The method is demonstrated for the circular cylinder and shows considerable promise. However, extension of the method to other geometries requires numerical results for the diffracted field, and hence for cylindrical structures, the transformation matrix technique and the phase shift method are developed. These methods are numerically accurate and apply to a wide range of cylindrical scatterers.

The transformation matrix technique applied to the imperfectly

conducting circular cylinder shows that for the cylinder, as in the case of the imperfectly conducting sphere, two definite ranges of impedance are identified, $0 \leq |\eta| \leq 1$ and $1 \leq |\eta| \leq \infty$, where the results for a specific impedance in either range determine the complete behaviour for the other range. The forward scattering for both geometries is not significantly altered over the value for the perfectly conducting case, except when the sphere surface impedance is inductive in the range $0 \leq |\eta| \leq 1$ or capacitive in the range $1 \leq |\eta| \leq \infty$, and for the cylinder when the reactance is near unity. Furthermore, the scattering cross section in both cases vanishes for $\eta = 1$ and the backscattering cross section is always lower than the value for the perfectly conducting case. For the case of the square cylinder, the forward scattering is significantly dependent on the impedance for large ka, unlike the circular cylinder.

The phase shift method requires the numerical integration of a first order differential equation for the solution of the fields and is a convenient method for dielectric coated cylinders.

The perturbation method proposed for the rectangular cavity with imperfectly conducting walls and the boundary value solution for the spherical cavity lead to general conclusions about cavities with reactive walls. An inductive wall decreases the resonant frequency while a capacitive wall increases it. The reactive part of the surface impedance is responsible for the change in resonant frequency, while the surface resistance affects the bandwidth. In the case of the spherical cavity with a capacitive wall, a new fundamental mode is created which is a perturbation of the zero value of the zero frequency static mode.

Finally, applications suggested by the results and described in Chapter V are of considerable industrial and scientific interest and may lead to effective solutions for high density power meters and microwave anechoic chambers.

6.3 Suggestions for Future Research

In the course of this thesis, various interesting problems have arisen that have been only briefly dealt with. Thus, though attempts have been made to improve the geometric optics term for the perfectly conducting sphere, no suitable expression, valid over the complete bistatic range, has been obtained. Similarly, the creeping wave term requires improvement near and at a shadow boundary. Furthermore, the solution for the scattering by two spheres could be extended to the scattering by an array of spheres, using a scattering matrix formulation as used in the analogous problem of radiation by an antenna array.

In the solution for imperfectly conducting spheres, there is again need for improving the geometric optics term. Furthermore, the solution for the pulse scattering by lossy spheres may be obtained by taking the inverse Laplace transform of the CW solution given in Chapter III. This solution would be of interest for purposes of radar detection. Also, the solution for an imperfectly conducting sphere in a weakly ionized plasma is of interest in radio astronomy and space communications.

Finally, the ray-numerical method proposed in Chapter IV has been applied only to the case of the circular cylinder and should be extended to other geometries.

APPENDIX A

BOUNDARY VALUE SOLUTION FOR AN IMPERFECTLY CONDUCTING SPHERE

Consider a sphere of radius a of surface impedance Z, with centre at the origin of a spherical system of coordinates (r,θ,ϕ) as shown in Fig. 2.1. A plane wave is incident on the sphere from the negative z axis and is defined by

$$E_x^i = E_o e^{jkz} = E_o e^{jkr\cos\theta} \tag{A-1}$$

$$H_y^i = \frac{E_o}{\eta_o} e^{jkz} = \frac{E_o}{\eta} e^{jkr\cos\theta} \tag{A-2}$$

where the time factor $e^{-j\omega t}$ has been suppressed and $\eta_o = 120\pi$. The total field is the sum of the TM and TE waves and the field components can be written in terms of the electric and magnetic potentials A and F, [94] respectively as

$$E_r = \frac{1}{\sigma - j\omega\varepsilon}\left(\frac{\partial^2}{\partial r^2} + k^2\right)A \tag{A-3}$$

$$E_\theta = \frac{1}{(\sigma - j\omega\varepsilon)r}\frac{\partial^2 A}{\partial r\partial\theta} - \frac{1}{r\sin\theta}\frac{\partial F}{\partial\phi} \tag{A-4}$$

$$E_\phi = \frac{1}{(\sigma - j\omega\varepsilon)r\sin\theta}\frac{\partial^2 A}{\partial r\partial\phi} + \frac{1}{r}\frac{\partial F}{\partial\theta} \tag{A-5}$$

$$H_r = -\frac{1}{j\omega\mu}\left(\frac{\partial^2}{\partial r^2} + k^2\right)F \tag{A-6}$$

$$H_\theta = +\frac{1}{r\sin\theta}\frac{\partial A}{\partial\phi} - \frac{1}{j\omega\mu r}\frac{\partial^2 F}{\partial r\partial\theta} \tag{A-7}$$

$$H_\phi = -\frac{1}{r}\frac{\partial A}{\partial\theta} - \frac{1}{j\omega\mu}\frac{1}{r\sin\theta}\frac{\partial^2 F}{\partial r\partial\phi} \tag{A-8}$$

Using the well known addition theorm

$$e^{-jkr\cos\theta} = \sum_{n=0}^{\infty} (-j)^n (2n+1) \frac{\hat{j}_n(kr)}{kr} P_n(\cos\theta) \tag{A-9}$$

we obtain

$$E_r^i = \cos\phi \sin\theta E_x^i = -\frac{E_o\cos\phi}{jkr} \frac{\partial}{\partial\theta} (e^{jkr\cos\theta}) \tag{A-10}$$

$$= -j \frac{E_o\cos\phi}{(kr)^2} \sum_{n=1}^{\infty} (-j)^{-n}(2n+1)\hat{j}_n(kr)P_n^1(\cos\theta) \tag{A-11}$$

where the Legendre function is defined by

$$P_n^1(\cos\theta) = -\frac{\partial}{\partial\theta} P_n(\cos\theta) \tag{A-12}$$

Hence the magnetic vector potential A^i is given by

$$A^i = -\frac{E_o\cos\phi}{\mu\omega} \sum_{n=1}^{\infty} a_n \hat{j}_n(kr)P_n^1(\cos\theta) \tag{A-13}$$

where $a_n = (-j)^{-n} \frac{(2n+1)}{n(n+1)}$

Similarly the electric vector potential F^i is given by

$$F^i = -\frac{E_o\sin\phi}{k} \sum_{n=1}^{\infty} a_n \hat{j}_n(kr)P_n^1(\cos\theta) \tag{A-14}$$

and for $r > a$ we have

$$\begin{aligned} A &= A^i + A^s \\ F &= F^i + F^s \end{aligned} \tag{A-15}$$

where the superscript s is associated with the scattered field. Since the scattered field must behave as an outgoing wave at infinity, A^s and F^s must contain the spherical Hankel functions in place of the Bessel functions. Thus

$$A = \sum_{n=1}^{\infty} A_n = - \frac{E_o \cos\phi}{\omega\mu} \sum_{n=1}^{\infty} \left[a_n \hat{j}_n(kr) + b_n \hat{h}_n^{(2)}(kr) \right] P_n^{(1)}(\cos\theta) \tag{A-16}$$

and

$$F = \sum_{n=1}^{\infty} F_n = - \frac{E_o \sin\phi}{k} \sum_{n=1}^{\infty} \left[a_n \hat{j}_n(kr) + c_n \hat{h}_n^{(2)}(kr) \right] P_n^{(1)}(\cos\theta) \tag{A-17}$$

where b_n and c_n are coefficients yet to be determined. Using the Leontovich impedance boundary condition at $r = a$,

$$\bar{E} - (\bar{E} \cdot \hat{i}_r)\hat{i}_r = Z(\hat{i}_r \times \bar{H}) \tag{A-18}$$

where $\hat{i}_r$ is the outward normal, we obtain

$$\left. \begin{aligned} - \frac{1}{j\omega\varepsilon_o} \frac{\partial A_n}{\partial r} &= Z\, A_n \\ - \frac{1}{j\omega\mu_o} \frac{\partial F_n}{\partial r} &= Y\, F_n \end{aligned} \right|_{r=a} \tag{A-19}$$

and hence we obtain for the coefficients

$$b_n = - \frac{(-j)^{-n}(2n+1)}{n(n+1)} \frac{(\hat{j}_n'(ka) + j\eta\hat{j}_n(ka))}{(\hat{h}_n^{(2)'}(ka) + j\eta\hat{h}_n^{(2)}(ka))} \tag{A-20}$$

$$c_n = - \frac{(-j)^{-n}(2n+1)}{n(n+1)} \frac{(\hat{j}_n'(ka) + j\delta\hat{j}_n(ka))}{(\hat{h}_n^{(2)'}(ka) + j\delta\hat{h}_n^{(2)}(ka))} \tag{A-21}$$

where $k = \omega\sqrt{\mu_o\varepsilon_o}$, $\eta = \frac{Z}{\eta_o}$ and $\delta = Y\eta_o$.

The scattered fields for $kr \gg 1$ are then given by

$$E_\theta^s = j \frac{E_o e^{jkr}}{kr} \cos\phi\, p(\theta) \tag{A-22}$$

$$E_\phi^s = - j \frac{E_o e^{jkr}}{kr} \sin\phi\, q(\theta) \tag{A-23}$$

where

$$p(\theta) = \sum_{n=1}^{\infty} \frac{(2n+1)}{n(n+1)} \left[B_n \frac{d}{d\theta} P_n^1(\cos\theta) + C_n \frac{P_n'(\cos\theta)}{\sin\theta} \right] \tag{A-24}$$

$$q(\theta) = \sum_{n=1}^{\infty} \frac{(2n+1)}{n(n+1)} \left[B_n \frac{P_n'(\cos\theta)}{\sin\theta} + C_n \frac{d}{d\theta} P_n^1(\cos\theta) \right] \tag{A-25}$$

and

$$B_n = \frac{\hat{j}_n'(ka) + j\eta \hat{j}_n(ka)}{\hat{h}_n^{(2)'}(ka) + j\eta \hat{h}_n^{(2)}(ka)} \tag{A-26}$$

$$C_n = \frac{\hat{j}_n'(ka) + j\delta \hat{j}_n(ka)}{\hat{h}_n^{(2)'}(ka) + j\delta \hat{h}_n^{(2)}(ka)} \tag{A-27}$$

APPENDIX B

ASYMPTOTIC EXPANSION OF $D_{\nu-\frac{1}{2}}$ AND $G_{\nu-\frac{1}{2}}$

The expressions for $D_{\nu-\frac{1}{2}}$ and $G_{\nu-\frac{1}{2}}$ defined in (3.12b) and (3.12c) may be approximated by using the Debye asymptotic expansion of the spherical Hankel functions and their derivatives for large orders and arguments [90], i.e.

$$\hat{h}^{(1)}_{\nu-\frac{1}{2}}(\rho) = \sqrt{\operatorname{cosec}\ \beta}\ e^{j\rho(\sin\beta-\beta\cos\beta)-j\ \pi/4} \sum_{m=0}^{\infty} \frac{(m-\frac{1}{2})!}{(-\frac{1}{2})!} \left(\frac{-2j}{\rho\sin\beta}\right)^m A_m \tag{B-1}$$

$$\hat{h}^{(1)'}_{\nu-\frac{1}{2}}(\rho) = \sqrt{\sin\beta}\ e^{j\rho(\sin\beta-\beta\cos\beta)+j\ \pi/4} \sum_{m=0}^{\infty} \frac{(m-\frac{1}{2})!}{(-\frac{1}{2})!} \left(\frac{-2j}{\rho\sin\beta}\right)^m \left(B_m + \frac{A_{m-1}}{2m-1}\right) \tag{B-2}$$

where

$$\rho = ka = \nu\ \mathrm{Sec}\beta \tag{B-3}$$

$$A_o = B_o = 1 \tag{B-4}$$

$$A_1 = \frac{1}{8}\left(1 + \frac{5}{3}\ \mathrm{Cot}^2\beta\right) \tag{B-5}$$

$$A_2 = \frac{1}{128}\left(3 + \frac{154}{9}\ \mathrm{Cot}^2\beta + \frac{385}{27}\ \mathrm{Cot}^4\beta\right) \tag{B-6}$$

$$B_1 = -\frac{7}{8}\left(1 + \frac{1}{3}\ \mathrm{Cot}^2\beta\right) \tag{B-7}$$

$$B_2 = -\frac{1}{273}\left\{23 + \frac{238}{3}\ \mathrm{Cot}^2\beta + O(\mathrm{Cot}^4\beta)\right\} \tag{B-8}$$

etc. where the higher order terms are generated by the recurrence relationship given by Watson [90]. The corresponding expressions for the Hankel functions of the second kind are given by the complex

conjugates of (B-1) and (B-2). Substituting in (3.12b) and retaining the leading terms of the binomial expansion for the denominator for $\eta < 1$ we obtain on simplification

$$D_{\nu-\frac{1}{2}} = -je^{-2j\rho(\sin\beta-\beta\cos\beta)}\left\{1 + \frac{2j}{\rho\sin\beta}(1 + B_1 + j\eta\rho)\right.$$

$$- \frac{2}{(\rho\sin\beta)^2}\left[-\frac{3\eta A_2}{\sin\beta} + (1 + j\rho\eta + B_1)^2 + \frac{\eta A_1}{\sin\beta}(1 + j\eta\rho + B_1)\right]$$

$$+ \frac{j2}{(\rho\sin\beta)^3}\left[3(B_2 + \frac{A_1}{3})(1 + j\eta\rho + B_1) + \frac{6\eta A_2}{\sin\beta}(1 + j\eta\rho + B_1)\right.$$

$$+ \frac{3\eta^2 A_1 A_2}{\sin\beta} - 15(B_3 + \frac{A_2}{5} - \frac{\eta A_3}{\sin\beta}) - (1 + j\eta\rho + B_1 + \frac{7A_1}{\sin\beta})^2$$

$$\left.\left. \cdot (1 + j\eta\rho + B_1)\right] + O(\rho\sin\beta)^{-4}\right\} \qquad \text{(B-9)}$$

A similar procedure may be used to approximate $G_{\nu-\frac{1}{2}}$ except that if $\eta < 1$ then $\delta > 1$. $G_{\nu-\frac{1}{2}}$ is first rewritten in the form

$$G_{\nu-\frac{1}{2}} = \frac{\hat{h}^{(2)}_{\nu-\frac{1}{2}}(\rho) - j\eta\,\hat{h}'^{(2)}_{\nu-\frac{1}{2}}(\rho)}{\hat{h}^{(1)}_{\nu-\frac{1}{2}}(\rho) - j\,\hat{h}'^{(1)}_{\nu-\frac{1}{2}}(\rho)} \qquad \text{(B-10)}$$

before the binomial expansion is applied to the denominator. Proceeding in the same manner used to derive (B-9), we obtain

$$G_{\nu-\frac{1}{2}} = je^{-2j\rho(\sin\beta-\beta\cos\beta)}\left\{1 + \frac{j}{\rho\sin\beta}\left[A_1 + \eta\sin\beta(B_1 + 1) + j\eta\rho\sin^2\beta\right]\right.$$

$$+ \frac{1}{(\rho\sin\beta)^2}\left[3(A_2 + \eta\sin\beta(B_2 + \frac{A_1}{3}))\right.$$

$$\left.\left. - \left[A_1 + \eta\sin\beta(B_1 + 1) + j\eta\rho\sin^2\beta\right]^2\right]\right.$$

$$+\frac{j}{(\rho\sin\beta)^3}\left\{6\left[A_1+\eta\sin\beta(B_1+1)+j\eta\rho\sin\beta\right]\right.$$

$$\cdot\left[A_2+\eta\sin\beta(B_2+\frac{A_1}{3})\right]-15\left[A_3+\eta\sin\beta(B_3+\frac{A_2}{5})\right]$$

$$\left.-\left[A_1+\eta\sin\beta(B_1+1)+j\eta\rho\sin^2\beta\right]^3\right\}+0(\rho\sin\beta)^{-4}\Bigg\}$$

(B-11)

where $D_{\nu-\frac{1}{2}}$ and $G_{\nu-\frac{1}{2}}$ reduce to the corresponding expressions for the perfectly conducting sphere when $\eta = 0$.

APPENDIX C

TABLES OF D AND γ FOR A PERFECTLY CONDUCTING CYLINDER

Table C-1 D and γ for parallel polarization

ka	D	γ/radian
5	0.702 - j0.0924	-1.905 - j1.100
6	0.723 - j0.0952	-2.024 - j1.169
7	0.742 - j0.0977	-2.132 - j1.230
8	0.758 - j .0999	-2.228 - j1.286
9	0.774 - j0.1019	-2.317 - j.1338
10	0.787 - j0.1037	-2.400 - j1.386
11	0.800 - j0.1050	-2.478 - j1.431
12	0.812 - j0.1069	-2.551 - j1.473
13	0.823 - j0.1083	-2.620 - j1.513
14	0.833 - j0.1097	-2.686 - j1.551
15	0.843 - j0.1109	-2.748 - j1.586
20	0.884 - j0.1164	-3.024 - j1.746
25	0.917 - j0.1208	-3.258 - j1.881
30	0.946 - j0.1245	-3.462 - j1.999
35	0.971 - j0.1278	-3.645 - j2.104
40	0.992 - j0.1307	-3.811 - j2.200
45	1.012 - j0.1332	-3.963 - j2.288
50	1.030 - j0.1356	-4.105 - j2.370

Table C-2 D and γ for perpendicular polarization

ka	D	γ/radian
5	0.207 + j1.5765	-0.830 - j0.479
6	0.214 + j1.6251	-0.882 - j0.509
7	0.219 + j1.6674	-0.929 - j0.536
8	0.224 + j1.7049	-0.971 - j0.561
9	0.229 + j1.7387	-1.009 - j0.583
10	0.233 + j1.7695	-1.046 - j0.604
11	0.236 + j1.7979	-1.079 - j0.623
12	0.240 + j1.8241	-1.111 - j0.642
13	0.243 + j1.8486	-1.114 - j0.659
14	0.246 + j1.8716	-1.170 - j0.676
15	0.249 + j1.8932	-1.197 - j0.691
20	0.2615 + j1.9862	-1.317 - j0.761
25	0.2714 + j2.061	-1.419 - j0.819
30	0.2798 + j2.125	-1.509 - j0.871
35	0.2871 + j2.180	-1.572 - j0.912
40	0.2935 + j2.229	-1.660 - j0.958
45	0.2993 + j2.273	-1.727 - j0.997
50	0.3046 + j2.314	-1.789 - j1.033

APPENDIX D

THE TRANSFORMATION MATRIX METHOD

Consider an N-sided regular polygonal cylinder whose complex surface impedance is denoted by Z. Maxwell's equations relating the time harmonic electric and magnetic fields may be expressed by the relations

$$\nabla \times \vec{F} = jk\vec{E} \tag{D-1a}$$

$$\nabla \times \vec{E} = -jk\vec{F} \tag{D-1b}$$

where the $e^{j\omega t}$ time dependence has been suppressed, and $\vec{F} = \eta_o \vec{H}$, $k = \frac{2\pi}{\lambda}$, $\eta_o = \sqrt{\frac{\mu_o}{\varepsilon_o}} = 120\pi$, μ_o and ε_o are the permeability and permittivity of free space, respectively.

For the cylindrical coordinate system (ρ,ϕ,z) with the metric coefficients $h_\rho = h(\rho,\phi)$, $h_\phi = h(\rho,\phi)$ and $h_z = 1$, we determine $h(\rho,\phi)$ such that the cross section of the cylinder is mapped into a circle of radius ρ_o in the transform space. Expanding (D-1) in cylindrical coordinates and combining the transverse field components E_t and F_t with the metric coefficient $h(\rho,\phi)$, to ensure that they are nonsingular, we obtain

$$E_t = h\, E_t \quad , \quad E_z = E_z \tag{D-2a}$$

$$F_t = h\, F_t \quad , \quad F_z = F_z \tag{D-2b}$$

where E_t, F_t and E_z, F_z are the transverse and longitudinal components of the electric and magnetic fields in the transform space, respectively. The resulting elliptically polarized fields may be expressed in terms of their circularly polarized components as

$$E_{\pm} = \frac{1}{\sqrt{2}} (E_\phi + j\delta E_z) \tag{D-3a}$$

$$F_{\pm} = \frac{1}{\sqrt{2}} (F_\phi + j\delta F_z) \tag{D-3b}$$

where $\delta = \pm 1$. Since (D.1) is valid in the transform space, for a normally incident plane wave, the fields $E_{\pm}$ and $F_{\pm}$ in the transform space, in general may be given by the modal expansions

$$E_{\pm} = \sum_{n=-\infty}^{\infty} A_{\pm}^{n}(\rho) e^{jn\phi} \tag{D-4a}$$

$$F_{\pm} = \sum_{n=-\infty}^{\infty} B_{\pm}^{n}(\rho) e^{jn\phi} \tag{D-4b}$$

where $A_{\pm}^{n}$ and $B_{\pm}^{n}$ are unknown radial functions yet to be determined, and which include the mode coefficients. Substitution of $E_{\pm}$ and $F_{\pm}$ into (D-1) and using the orthogonality condition of ϕ results in two differential equations for $A_{\pm}^{n}$ and $B_{\pm}^{n}$. These may be used to obtain the incoming $(I_{\pm}^{n})$ and outgoing $(O_{\pm}^{n})$ waves at large distances in the form

$$I_{\pm}^{n} = A_{\pm}^{n} + j\delta\, B_{\pm}^{n} \tag{D-5a}$$

$$O_{\pm}^{n} = A_{\pm}^{n} - j\delta\, B_{\pm}^{n} \tag{D-5b}$$

From this, one can find a transformation matrix relating the far field at the radial distance ρ to the field on the surface of the cylinder $(\rho = \rho_o)$ in the form

$$\begin{bmatrix} I_+(\rho) \\ O_-(\rho) \end{bmatrix} = \begin{bmatrix} S(\rho,\rho_o) \end{bmatrix} \begin{bmatrix} I_+(\rho_o) \\ O_-(\rho_o) \end{bmatrix} \tag{D-6a}$$

$$\begin{bmatrix} I_-(\rho) \\ 0_+(\rho) \end{bmatrix} = \begin{bmatrix} P(\rho,\rho_o) \end{bmatrix} \begin{bmatrix} I_-(\rho_o) \\ 0_+(\rho_o) \end{bmatrix} \tag{D-6b}$$

Since the incident field corresponds to the known incoming wave $I^n_{\pm}$, the outgoing waves $0^n_{\pm}$ may be evaluated, from (D-6) and the boundary conditions, so that the total fields $E_{\pm}$ and $F_{\pm}$ may be obtained. To show this we write down the Leontovich impedance boundary condition which must be satisfied at the surface of the cylinder, i.e.

$$\vec{E} - (\vec{E} \cdot \hat{i}_r)\hat{i}_r = Z(\hat{i}_r \times \vec{H}) \tag{D-7}$$

where $\hat{i}_r$ is the outward unit vector with respect to the surfaces. This equations reduces to

$$\left.\begin{aligned} E_\phi &= - ZH_z \\ E_z &= ZH_\phi \end{aligned}\right| \quad \text{at} \quad \rho = \rho_o \tag{D-8}$$

In terms of $I^n_{\pm}$ and $0^n_{\pm}$, (D-8) may be rewritten in the form

$$(1 - \eta)(I^n_- - I^n_+) = (0^n_+ - 0^n_-)(1 + \eta) \tag{D-9a}$$

$$(1 - \eta)(I^n_+ + I^n_-) = - (0^n_+ + 0^n_-)(1 + \eta) \tag{D-9b}$$

respectively, where η is the normalized surface impedance given by

$$\eta = \frac{Z}{\eta_o} = |\eta| e^{i\psi} \tag{D-10}$$

For parallel polarization (TM case), we have the additional relations

$$I^n_{\pm} = I^n_{\mp} \quad , \quad 0^n_{\pm} = 0^n_{\mp} \tag{D-11}$$

and hence

$$I^n_+(\rho_o) = - \left(\frac{1 + \eta}{1 - \eta}\right) 0^n_+(\rho_o) \tag{D-12}$$

while for perpendicular polarization (TE case), we have the relations

$$I^n_{+-} = - I^n_{-+} \quad , \quad 0^n_{+-} = - 0^n_{-+} \tag{D-13}$$

and hence

$$I^n_+(\rho_o) = \left(\frac{1 + \eta}{1 - \eta}\right) 0^n_+(\rho_o) \tag{D-14}$$

APPENDIX E

DERIVATION OF EQUATIONS (4.12) AND (4.13)

From the equations (4.10) and (4.11) for V^n and U^n, the matrix for the incoming and outgoing waves, $I_{\pm}^n$ and $O_{\pm}^n$, can be written in the form

$$\begin{bmatrix} I_{\pm}^n \\ O_{\mp}^n \end{bmatrix} = \begin{bmatrix} H_n^{(1)}(k\rho) - jH_n^{(1)'}(k\rho) & H_n^{(2)}(k\rho) - jH_n^{(2)'}(k\rho) \\ H_n^{(1)}(k\rho) + jH_n^{(1)'}(k\rho) & H_n^{(1)}(k\rho) + jH_n^{(2)'}(k\rho) \end{bmatrix} \begin{bmatrix} c_1 \\ c_2 \end{bmatrix} \tag{E-1}$$

$$= \begin{bmatrix} M(\rho) \end{bmatrix} \begin{bmatrix} c_1 \\ c_2 \end{bmatrix} \tag{E-2}$$

Inverting the matrix equation gives an expression for the constants

$$\begin{bmatrix} c_1 \\ c_2 \end{bmatrix} = \begin{bmatrix} M(\rho) \end{bmatrix}^{-1} \begin{bmatrix} I_{\pm}^n \\ O_{\mp}^n \end{bmatrix} \tag{E-3}$$

Evaluating (E-3) at $\rho = a$ and substituting into (E-2), we obtain

$$\begin{bmatrix} I_{\pm}^n(\rho) \\ O_{\mp}^n(\rho) \end{bmatrix} = \begin{bmatrix} M(\rho) \end{bmatrix} \begin{bmatrix} M(a) \end{bmatrix}^{-1} \begin{bmatrix} I_{\pm}^n(a) \\ O_{\mp}^n(a) \end{bmatrix} \tag{E-4}$$

where in the far field

$$\begin{bmatrix} M(\rho) \end{bmatrix} = \begin{bmatrix} H_n^{(1)}(k\rho) & 0 \\ 0 & H_n^{(2)}(k\rho) \end{bmatrix}, \quad \rho \to \infty \tag{E-5}$$

$$\begin{bmatrix} I_{\pm}^{n}(\rho) \\ 0_{\mp}^{n}(\rho) \end{bmatrix} = - (j)^{-n} \begin{bmatrix} H_n^{(1)}(k\rho) \\ H_n^{(2)}(k\rho) \end{bmatrix} , \quad \rho \to \infty \tag{E-6}$$

and the far components are hence

$$\begin{bmatrix} I_{\pm}^{n}(\rho) \\ 0_{\mp}^{n}(\rho) \end{bmatrix} = \frac{\pi ka}{2} \begin{bmatrix} M(\rho) \end{bmatrix} \begin{bmatrix} M(a) \end{bmatrix}^{-1} \begin{bmatrix} I_{\pm}^{n}(a) \\ 0_{\mp}^{n}(a) \end{bmatrix} \tag{E-7}$$

Using (D-12) in (E-7) and eliminating $I_{\pm}^{n}(\rho)$ from (E-6) and (E-7) we obtain the expressions

$$I_{\pm}^{n}(a) = - \frac{(j)^{-n}(1 + \eta)}{ka[H_n^{(2)}(ka) + j\eta\, H_n^{(2)'}(ka)]} \tag{E-8}$$

$$0_{\mp}^{n}(a) = - \frac{(j)^{-n} H_n^{(2)}(k\rho)[H_n^{(1)}(ka) + j\eta\, H_n^{(1)'}(ka)]}{H_n^{(2)}(ka) + j\eta\, H_n^{(2)'}(ka)} \tag{E-9}$$

Since the incident field is decomposed into $I_{\pm}^{n}(\rho)$ and $0_{\mp}^{n}(\rho)$, the scattered component of the outgoing wave is hence given by

$$0_{\mp}^{n}(\rho) = - \frac{2(j)^{-n}[J_n(ka) + j\eta\, J_n'(ka)]H_n^{(2)}(k\rho)}{H_n^{(2)}(k\rho) + j\eta\, H_n^{(2)'}(ka)} \tag{E-10}$$

and the scattered electric field is obtained from (D-4a) as

$$E_{\pm s} = - \sum_{n=-\infty}^{\infty} (j)^{-n} \frac{J_n(ka) + j\eta\, J_n'(ka)}{H_n^{(2)}(ka) + j\eta\, H_n^{(2)'}(ka)} H_n^{(2)}(k\rho) e^{jn\phi} \tag{E-11}$$

The resulting scattering width for the E polarization is given by

$$\frac{\sigma_e}{\pi a} = \frac{4}{\pi ka} \left| \sum_{n=0}^{\infty} \varepsilon_n \frac{J_n(ka) + j\eta\, J_n'(ka)}{H_n^{(2)}(ka) + j\eta\, H_n^{(2)'}(ka)} \cos(n\phi) \right|^2 \tag{E-12}$$

The corresponding result for the H polarization may be shown to be

$$\frac{\sigma_h}{\pi a} = \frac{4}{\pi ka} \left| \sum_{n=0}^{\infty} \varepsilon_n \frac{J_n'(ka) - j\eta\, J_n(ka)}{H_n^{(2)'}(ka) - j\eta\, H_n^{(2)}(ka)} \cos(n\phi) \right|^2 \qquad \text{(E-13)}$$

where

$$\varepsilon_n = \begin{cases} 1, & n = 0 \\ 2, & n > 0 \end{cases}$$

APPENDIX F

DERIVATION OF EQUATIONS (4.15) AND (4.16)

For the transformation

$$\frac{dz'}{dt} = M(\cos\frac{Nt}{2})^{2/N} \tag{F-1}$$

from the $z'(x + jy)$ to the $t(\theta + j\beta)$ plane, the metric coefficients h_θ and h_β are given by

$$h_\theta^2 = h_\beta^2 = (\frac{a}{2L})^2 \, e^{N\beta/2}\left[1 + 2\cos(N\theta)e^{-N\beta} + e^{-2N\beta}\right]^{\frac{1}{2}} \tag{F-2}$$

In the (ρ,ϕ,z) coordinate system, this corresponds to

$$h_\rho^2 = h_\phi^2 = \left[1 + e^{-2s} + 2e^{-s}\cos(N\phi)\right]^{\frac{1}{2}} \; ; \; s = e^{\beta} \tag{F-3}$$

which may be expressed as a cosine series of the form

$$h_\rho^2 = h_\phi^2 = f(s) + g(s)\cos(N\phi) + h(s)\cos(2N\phi) + \ldots \tag{F-4}$$

where

$$f(s) = 1 + \frac{s^{-2N}}{4} + \frac{s^{-4N}}{64} + \frac{s^{-6N}}{256} + \ldots \tag{F-5}$$

$$g(s) = s^{-N} - \frac{s^{-3N}}{8} + \ldots \tag{F-6}$$

$$h(s) = -\frac{s^{-2N}}{4} + \frac{s^{-4N}}{16} + \ldots \tag{F-7}$$

These coefficients, together with equations (D-1) and (D-5) lead to the coupled differential equations for $I_{\pm}^n$ and $O_{\pm}^n$ of the form

$$\frac{dI_{\pm}^n}{d\rho} = \frac{j}{2\rho}\left\{\left[k\rho - \frac{n^2}{k\rho} + j + k\rho f(s)\right]I_{\pm}^n + \left[-k\rho + \frac{n^2}{k\rho} - j + k\rho f(s)\right]O_{\pm}^n + \left[\frac{k\rho g(s)}{2}\right]\left[\sum_L I_{\pm}^{n+L} + O_{\pm}^{n+L}\right]_{L=\pm N} + \ldots\right\} \tag{F-8}$$

and

$$\frac{dO_{\mp}^{n}}{d\rho} = \frac{j}{2\rho}\left\{\left[k\rho + \frac{n^2}{k\rho} - j - k\rho f(s)\right]O_{\mp}^{n} + \left[-k\rho + \frac{n^2}{k\rho} + j - k\rho f(s)\right]O_{\mp}^{n} - \left[\frac{k\rho g(s)}{2}\right]\left[\sum_{L} I_{\mp}^{n+L} + O_{\mp}^{n+L}\right]_{L=\mp N} + \cdots\right\} \qquad \text{(F-9)}$$

APPENDIX G

THE SCATTERING PHASE SHIFT METHOD

The differential equation satisifed by the scalar wave function ψ for an inhomogeneous isotropic cylindrical scatterer, is given by

$$(\nabla^2 + k^2)\psi = L\psi \tag{G-1}$$

where L is an operator dependent on polarization and the properties of the scatterer. For a cylindrically symmetric scatter

$$L = \frac{1}{\mu}\frac{\partial\mu}{\partial\rho}\frac{\partial}{\partial\rho} + k^2[1 - \mu\varepsilon] \tag{G-2}$$

for the TM case and the operator for the TE case is obtained by interchanging μ and ε.

A solution of (G-1) is given by

$$\psi = \sum_{n=0}^{\infty} \varepsilon_n (j)^{-n} T_n(\rho)\cos(n\phi) \tag{G-3}$$

where T_n satisfies a Sturm-Liouville equation of the form

$$\left\{\rho\frac{\partial}{\partial\rho}\left(\rho\frac{\partial}{\partial\rho}\right) + \left[(k\rho)^2 - n^2\right]\right\} T_n(\rho) = \rho^2 L T_n(\rho) \tag{G-4}$$

and has a general solution of the form

$$T_n(\rho) = C_1^n J_n(k\rho) + C_2^n Y_n(k\rho) + \frac{\pi k}{2}\int^{\rho} LT_n(\rho')\rho' d\rho'$$

$$\cdot \left[J_n(k\rho')Y_n(k\rho) - J_n(k\rho)Y_n(k\rho')\right] \tag{G-5}$$

The asymptotic form of the wave function ψ may be shown to be

$$\psi = \psi^i + \sqrt{\frac{2}{\pi k\rho}}\, f(\phi)e^{-jk\rho} \tag{G-6}$$

where ψ^i the incident field may be assumed to be

$$\psi^i = e^{-jkx} = \sum_{n=0}^{\infty} \varepsilon_n (j)^{-n} \cos(n\phi) J_n(k\rho) \tag{G-7}$$

and the second part of (G.5) represents the scattered part of the wave function. Using the phase shift concept of Morse and Feshbach [106], the wave function can be written in terms of a phase function δ_n and an amplitude function A_n in the form

$$\psi = \sum_{\substack{n=0 \\ \rho\to\infty}}^{\infty} \varepsilon_n (j)^{-n} \cos(n\phi) \sqrt{\frac{2}{\pi k\rho}}\, A_n \cos\left(k\rho - \frac{n\pi}{2} + \frac{\pi}{4} - \delta_n\right) \tag{G-8}$$

where A_n and $f(\phi)$ are given by

$$A_n = e^{j\delta n} \tag{G-9}$$

$$f(\phi) = -\frac{j}{2} - e^{j\,\pi/4} \sum_{n=0}^{\infty} \varepsilon_n \cos n\phi\; e^{j\delta n} \sin(\delta_n) \tag{G-10}$$

Thus $f(\phi)$ is determined completely from the phase function δ_n and hence a knowledge of the phase function determines entirely the scattered field and cross section.

An accurate solution for the phase function may be obtained from the solution of a first order differential equation. Following Brysk and Buchanan [101] we define $\delta_n(\rho)$ by the equation

$$\tan(\delta_n) = \frac{N_n(\rho)}{D_n(\rho)} \tag{G-11}$$

where

$$D_n(\rho) = 1 - \frac{\pi k}{2} \int^{\rho} \left[LT_n(\rho')\right] Y_n(k\rho')\rho' d\rho' \tag{G-12}$$

$$N_n(\rho) = B_n - \frac{\pi k}{2}\int^{\rho}\left[LT_n(\rho')\right]J_n(k\rho')\rho' d\rho' \qquad \text{(G-13)}$$

and

$$B_n = \frac{C_2^n}{C_1^n}$$

Using (G-11) and (G-12), the expression for T_n reduces to the form

$$T_n(\rho) = C_1^n D_n(\rho)\left[J_n(k\rho) + \tan\delta_n(\rho)Y_n(k\rho)\right] \qquad \text{(G-14)}$$

or alternatively, since (G-13) is singular at $\delta_n = \pi/2$,

$$T_n(\rho) = A_n(\rho)\left[J_n(k\rho)\cos\delta_n(\rho) + Y_n(k\rho)\sin\delta_n(\rho)\right] \qquad \text{(G-15)}$$

where

$$A_n(\rho) = C_1^n \frac{D_n(\rho)}{\cos\delta_n(\rho)} \qquad \text{(G-16)}$$

Substitution of (G-15) into (G-4) results in the reduction of the second order differential equation for $T_n(\rho)$ to two first order equations for the phase and amplitude functions respectively, of the form

$$\delta_n'(\rho) = -\frac{\pi k\rho}{2}\frac{(LT_n)T_n}{A_n^2(\rho)} \qquad \text{(G-17)}$$

and

$$A_n'(\rho) = -\frac{\pi k\rho}{2}(LT_n)\left[J_n(k\rho)\sin\delta_n(\rho) - Y_n(k\rho)\cos\delta_n(\rho)\right] \qquad \text{(G-18)}$$

Examination of equations (G-15) and (G-17) shows that the differential equation for the phase function is independent of the amplitude functions and may be solved numerically to any desired degree of accuracy and hence using (G-10), the scattered field is readily obtained.

For a radially inhomogeneous dielectric,

$$L = \begin{cases} k^2[1 - \varepsilon(\rho)] & \text{for TM modes} \quad \text{(G-19)} \\ k^2[1 - \varepsilon(\rho)] + \frac{1}{\varepsilon(\rho)} \frac{\partial \varepsilon(\rho)}{\partial \rho} \frac{\partial}{\partial \rho} & \text{for TE modes} \quad \text{(G-20)} \end{cases}$$

and the differential equations for the phase and amplitude functions reduce to

$$\delta_n'(\rho) = - \frac{\pi k \rho}{2} k^2 \left[1 - \varepsilon(\rho)\right] \left[J_n(k\rho)\cos\delta_n(\rho) + Y_n(k\rho)\sin\delta_n(\rho)\right]^2 \quad \text{(G-21)}$$

$$A_n'(\rho) = - \frac{\pi k \rho}{2} k^2 \left[1 - \varepsilon(\rho)\right] \left[J_n(k\rho)\cos\delta_n(\rho) + Y_n(k\rho)\sin\delta_n(\rho)\right] \cdot A_n(\rho) \left[J_n(k\rho)\sin\delta_n(\rho) - Y_n(k\rho)\cos\delta_n(\rho)\right] \quad \text{(G-22)}$$

for the TM case. The corresponding equations for the TE case are given by

$$\delta_n'(\rho) = - \frac{\pi k \rho}{2} \left\{ \left[J_n'(k\rho)\cos\delta_n(\rho) + Y_n'(k\rho)\sin\delta_n(\rho)\right] \frac{1}{\varepsilon(\rho)} \frac{\partial \varepsilon(\rho)}{\partial \rho} + k^2 \left[1 - \varepsilon(\rho)\right] \times \left[J_n(k\rho)\cos\delta_n(\rho) + Y_n(k\rho)\sin\delta_n(\rho)\right] \right\} \cdot \left[J_n(k\rho)\cos\delta_n(\rho) + Y_n(k\rho)\sin\delta_n(\rho)\right] \quad \text{(G-23)}$$

$$A_n'(\rho) = - \frac{\pi k \rho}{2} \left[J_n(k\rho)\sin\delta_n(\rho) - Y_n(k\rho)\cos\delta_n(\rho)\right] A_n(\rho) \times \left\{ \left[J_n'(k\rho)\cos\delta_n(\rho) + Y_n'(k\rho)\sin\delta_n(\rho)\right] \frac{1}{\varepsilon(\rho)} \frac{\partial \varepsilon(\rho)}{\partial \rho} + k^2 \left[1 - \varepsilon(\rho)\right] \times \left[J_n(k\rho)\cos\delta_n(\rho) + Y_n(k\rho)\sin\delta_n(\rho)\right] \right\} \quad \text{(G-24)}$$

APPENDIX H

PERTURBATION SOLUTION FOR AN IMPERFECTLY CONDUCTING RECTANGULAR CAVITY

Consider a rectangular cavity of height b, width a, and length d and let the surface impedances of the walls be Z_{xo}, Z_{xl}, Z_{yo}, Z_{yl}, Z_{zo}, Z_{zl} as shown in Fig. H-1. For the cavity with perfectly conducting walls, the free space propagation constant k_o is related to the lateral and axial constants $k_{\ell o}$ and β_o, respectively, in the cavity by

$$k_o^2 = k_{\ell o}^2 + \beta_o^2 \tag{H-1}$$

for both TM or TE waves.

Treating the new lateral and axial field constants as perturbation of the values when the walls are perfectly conducting, we can write

$$k_\ell = k_{\ell o} + \Delta k_\ell \tag{H-2a}$$

and

$$\beta_\ell = \beta_o + \Delta\beta \tag{H-2b}$$

Thus in presence of imperfectly conducting walls,

$$k^2 = k_\ell^2 + \beta_\ell^2 \tag{H-3}$$

where the new propagation constant k can be treated as a perturbation of the old value k_o and

$$k = k_o + \Delta k \tag{H-4}$$

Thus

$$\Delta k = \frac{k_{\ell o}}{k_o} \Delta k_\ell + \frac{\beta_o}{k_o} \Delta\beta \tag{H-5a}$$

and using the relations

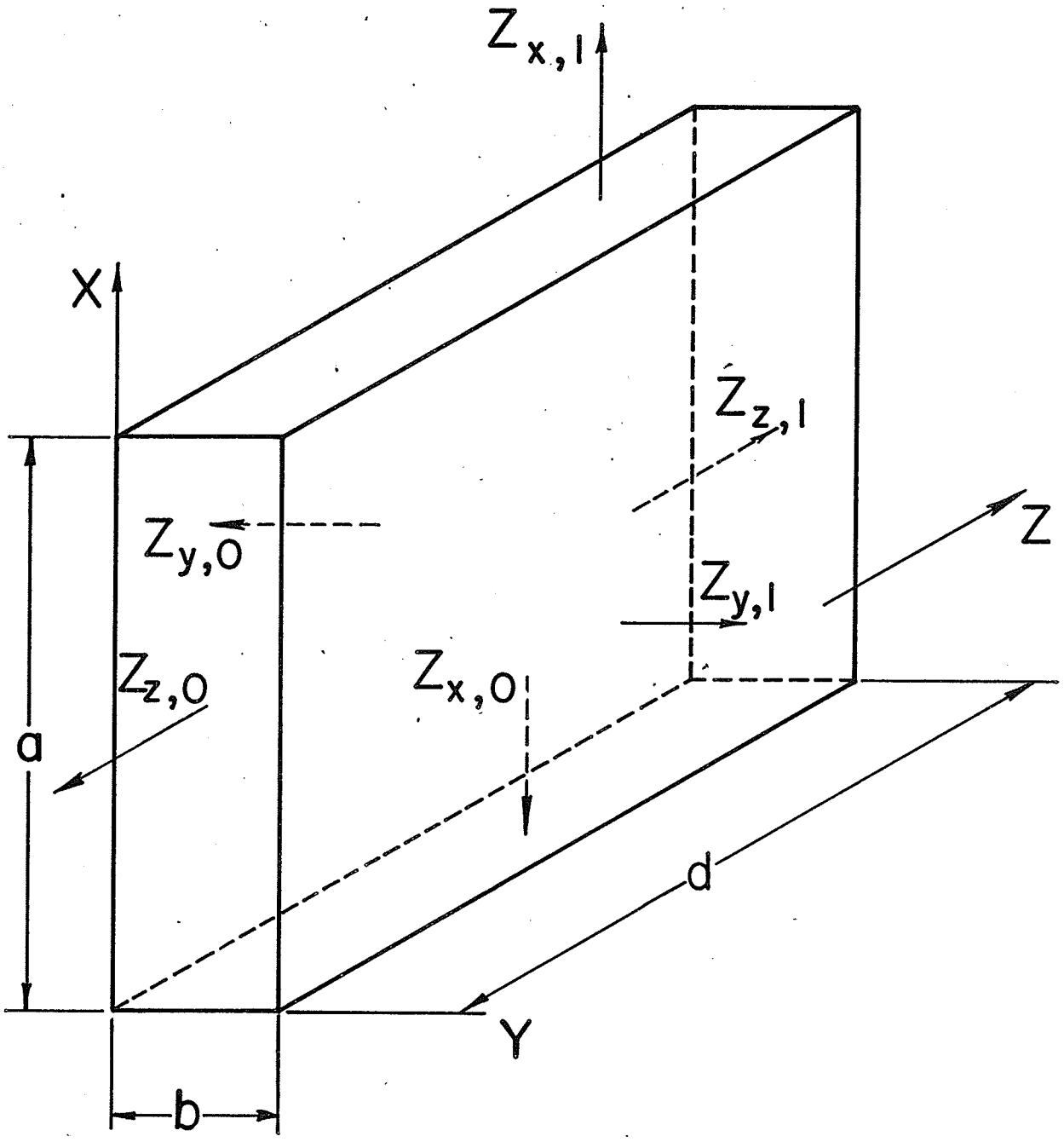

FIG. H.1 RECTANGULAR-BOX RESONATOR

$$k_o = \omega_o \sqrt{\mu_o \varepsilon_o} \tag{H-5b}$$

$$k = \omega \sqrt{\mu_o \varepsilon_o} = (\omega_o + \Delta\omega) \sqrt{\mu_o \varepsilon_o} \tag{H-5c}$$

we obtain

$$\frac{\Delta\omega}{\omega_o} = \frac{\beta_o}{k_o} \frac{\Delta\beta}{k_o} + \frac{k_{\ell o}}{k_o} \frac{\Delta k_\ell}{k_o} = \delta_1 + j\delta_2 \tag{H-6}$$

Hence if $\Delta\beta$ and Δk_ℓ are evaluated, the real shift in the resonant frequency from its unperturbed value ω_o can be readily calculated, together with the bandwidth and the cavity Q, since the resonant frequency, in terms of the Q is given by

$$\omega = \omega_o \left[1 - \left(\frac{1}{2Q}\right)^2\right]^{\frac{1}{2}} + j \frac{\omega_o}{2Q} \tag{H-7}$$

where ω_o is the resonant frequency in the absence of losses. Thus for large values of Q, this reduces approximately to

$$\omega = \omega_o + j \frac{\omega_o}{2Q} \tag{H-8}$$

and since the bandwidth is reciprocal of the Q, we have on comparison of (H-6) and (H-8)

$$Q = \frac{1}{2\delta_2} = \frac{1}{\text{Bandwidth}} \tag{H-9}$$

Further, since

$$k_\ell^2 = k_x^2 + k_y^2 \tag{H-10}$$

for the TE_{0mm} mode types we can write (H-6) in the form

$$\frac{\Delta\omega}{\omega_o} = \frac{k_{\ell o}}{k_o} \left(\frac{\Delta k_x}{k_o}\right) + \frac{\Delta^2 k_y}{2k_o} + \frac{\beta_o}{k_o} \frac{\Delta\beta}{k_o} \tag{H-11}$$

where Δk_x, Δk_y and $\Delta\beta$ have been evaluated previously by Karbowiak [17]

and hence substituting, we obtain

$$(\delta_1 + j\delta_2) = \frac{j}{2}\left[\frac{2}{ak_o}\left(\frac{k_{\ell o}^2}{k_o}\right)^2 (Z_{xo} + Z_{x1}) + \frac{1}{k_o b}(Z_{yo} + Z_{y1}) + \frac{2}{dk_o}\left(\frac{\beta_o}{k_o}\right)^2 (Z_{zo} + Z_{z1})\right] \qquad \text{(H-12)}$$

The real part of equation (H-12) gives the shift in resonant frequency and twice the imaginary part gives the bandwidth. From the above equation, it is evident that the reactive part of the impedance gives rise to the shift in resonant frequency, while the real part, the bandwidth. Further, it can be seen that an inductive wall would result in a decrease in resonant frequency, while a capacitive wall would increase the resonant frequency.

APPENDIX I

EIGENVALUE SOLUTION FOR AN IMPERFECTLY CONDUCTING SPHERICAL CAVITY

Consider a spherical cavity resonator of radius a with a surface impedance z and enclosing a homogeneous dielectric material of permeability μ and permittivity ε. The impedance boundary condition to be satisfied at the inner wall is given by equation (3.5), i.e.

$$\bar{E} - (\bar{E} \cdot \hat{i}_r)\hat{i}_r = Z(\hat{i}_r \times \bar{H}) \qquad \text{(I-1)}$$

where in contrast to equation (3.5), here $\hat{i}_r$ represents the inward radial unit vector. For TM modes, the impedance boundary condition leads to the relation

$$E_\theta = ZH_\phi\Big|_{r=a} \qquad \text{(I-2a)}$$

$$H_\theta = -E_\phi/Z\Big|_{r=a} \qquad \text{(I-2b)}$$

For TE modes, the corresponding relations are

$$H_\theta = -YE_\phi\Big|_{r=a} \qquad \text{(I-3a)}$$

$$E_\theta = H_\phi/Y\Big|_{r=a} \qquad \text{(I-3b)}$$

where $Y = 1/Z$.

The electric and magnetic field components in the spherical coordinate system (r,θ,ϕ) are given in Appendix A, in terms of the electric and magnetic vector potentials A and F. Due to the boundary condition [I-1], the wave functions for these potentials must be of the form

$$\sum_m \sum_n \hat{J}_n(kr)P_n^m(\cos\theta)e^{jm\phi} \qquad \text{(I-4)}$$

where $\hat{J}_n(kr)$ are spherical Bessel functions used by Schelkunoff [107].

For TM modes, the resulting transcendental equation for the eigenvalues k is given by

$$\hat{J}_n'(ka) = - j\omega\varepsilon_o Z\hat{J}_n(ka) \tag{I-5}$$

where the prime denotes differentiation with respect to the argument. Normalizing the impedance Z, with respect to the intrinsic impedance of free space in the form

$$Z = j\xi\eta_o \quad \text{where} \quad \eta_o = 120\pi \tag{I-6}$$

and writing the spherical Bessel function in terms of cylindrical Bessel functions, we obtain

$$uJ'_{n+\frac{1}{2}}(u) + 0.5J_{n+\frac{1}{2}}(u) - u\xi J_{n+\frac{1}{2}}(u) = 0 \tag{I-7}$$

where $u = ka$. The corresponding expression for the TE case is given by

$$uJ_{n+\frac{1}{2}}(u) + \xi[uJ'_{n+\frac{1}{2}}(u) + 0.5J_{n+\frac{1}{2}}(u)] = 0 \tag{I-8}$$

The solutions of (I-7) and (I-8) give the eigenvalues u'_{np} and u_{np} for the TM and TE cases, while the eigenfrequencies are evaluated from the relations

$$(f_r)^{TE}_{mnp} = \frac{u_{np}}{2\pi a(\mu\varepsilon)^{\frac{1}{2}}} \tag{I-9}$$

and

$$(f_r)^{TM}_{mnp} = \frac{u'_{np}}{2\pi a(\mu\varepsilon)^{\frac{1}{2}}} \tag{I-10}$$

The cavity Q and the bandwidth may be calculated by either the method of Appendix H or following the procedure in Harrington [94]. It is to be noted that degenerate modes are also present as in the case of a perfectly conducting cavity.

Typical results for the eigenvalues u_{np} and u'_{np} $(p = 1,2,3\ldots)$

based on (I-7) and (I-8), respectively, are shown in Figs. 4.16 and 4.17, where $0 < \xi \leq 1$ corresponds to the inductive case and $-1 \leq \xi < 0$ corresponds to the capacitive case while $\xi = 0$ to the perfectly conducting case. The results indicate, in general, that an inductive surface lowers the resonance frequencies of all modes, while a capacitive surface impedance raises them. For the case of a complex impedance, an attenuation in the cavity fields results from the complex eigenvalues obtained, although no specific results are shown.

Examination of Fig. 4.17 shows that the first eigenvalue is a perturbation to the zero value of the zero frequency static mode [94] in a perfectly conducting cavity. As an example, $u_{11} = .9143$ for $\xi = -.5$ in the TE case. Thus, unlike the case of a perfectly conducting sphere where the TM mode is the fundamental one, it is found that for the case of a capacitive impedance wall, the TE mode is the new fundamental mode. This may also be explained from the equivalent circuit of the cavity resonator.

BIBLIOGRAPHY

[1] SENIOR, T.B.A., 'Impedance boundary conditions for imperfectly conducting surfaces', Appl. Sci. Res., Sec. B, Vol. 8, pp. 418-436, 1961.

[2] SENIOR, T.B.A., 'A note on impedance boundary conditions', Can. J. Phys., Vol. 40, pp. 663-665, 1962.

[3] BERNARDI, P., 'Studio della propagazione in una guida rettangolare delimitata da una parete di impedenza', Alta Frequenza, Vol. 34, pp. 490-497, July 1965.

[4] BERNARDI, P., 'Elementi per il propetto di guide d'onda rettangolari con parete di impedenza', Alta Frequenza, Vol. 35, No. 12, pp. 960-964.

[5] BERNARDI, P., 'Electromagnetic waves guided by the most general anisotropic impedance walls', Il Nuovo Cimento, Vol. 43, Series X, pp. 338-346, 1966.

[6] BERNARDI, P., 'The impedance wall concept applied to dielectrically loaded waveguide problems', I.E.E.E. Trans. on M.T.T., MTT-16, 2, pp. 126-127, Feb. 1968.

[7] BERNARDI, P., and VALDONI, F., 'Validity range of the impedance wall description for an actual microwave structure', Alta Frequenza, Vol. 36, pp. 377-379, May 1967 (English Issue No. 2, pp. 148E-149E).

[8] KARBOWIAK, A.E., 'Propagation coefficient in a waveguide of finite conductivity', J. Appl. Phys., Vol. 27, pp. 421-422, 1956.

[9] UNGER, H.G., 'Waveguides with anisotropic impedance walls', Proc. Symposium on Electromagnetic Theory and Antennas, Copenhagen, Guigno, 1962 (editor E.C. JORDAN).

[10] KERNS, D.M. and HEDBERG, R.W., 'Propagation constant in rectangular waveguide of finite conductivity', J. Appl. Phys., Vol. 25, pp. 1550, 1954.

[11] BAHAR, E., 'Propagation in a microwave model waveguide of variable surface impedance: theory and experiment', I.E.E.E. Trans. on M.T.T., MTT-14, No. 11, pp. 572-578, 1966.

[12] GALLAWA, R.L., 'Propagation in nonuniform waveguides with impedance walls', Radio Sci. J. Res., N.B.S. 68D, No. 11, pp. 1201-1213, 1964.

[13] MOHSEN, A. and HAMID, M.A.K., 'Wave propagation in a circular waveguide with an absorbing wall', J. Appl. Phys., Vol. 41, No. 1, pp. 433-434, Jan. 1970.

[14] ISAYENKO, Yu.M., MALIN, V.V. and MALINA, Z.A., 'Analysis of a system of waves in a circular waveguide with impedance boundary conditions at the wall', Radio technika i electronika, Vol. 7, pp. 1039-1047, 1962.

[15] BERRETT, P.O. and JOHNSON, C.C., 'Waves in a circular plasma column with general impedance boundary conditions', I.E.E.E. Trans. on Nuc. Sci., NS-11, pp. 34-40, Jan. 1964.

[16] BAHAR, E., 'Generalized scattering matrix equations for waveguide structures of varying surface impedance boundaries', Radio Sci., Vol. 2, (new series), No. 3, pp. 287-297, March 1967.

[17] KARBOWIAK, A.E., 'Theory of imperfect waveguides: The effect of wall impedance', Proc. I.E.E., B102, pp. 698-708, 1955.

[18] SHEVCHENKO, V.V., 'A waveguide with wall impedance as a surface compensator', Radio technika i electronika, Vol. 7, pp. 1034-1039, 1962.

[19] FELSEN, L.B., 'Electromagnetic properties of wedge and cone surfaces with a linearly varying surface impedance', I.E.E.E. Trans. on AP, AP-7, pp. S231-S243, 1959.

[20] SENIOR, T.B.A., 'Diffraction by an imperfectly conducting wedge', Commun. Pure Appl. Maths., Vol. 12, pp. 337-372, 1959.

[21] SENIOR, T.B.A., 'Diffraction by an imperfectly conducting wedge', Studies in Radar Cross Section, Vol. XXV, Engr. Res. Inst., Univ. of Mich., Ann Arbor, Oct. 1957.

[22] KARP, S.N. and KARAL, F.C., 'A new method for the determination of far fields with applications to the problem of radiation of a line source at the tip of an absorbing wedge', I.E.E.E. Trans. on AP, AP-7, S91-S102, 1959.

[23] KARAL, F.C. and KARP, S.N., 'Diffraction of a skew plane electromagnetic wave by an absorbing right angled wedge', Res. Rept. EM-111, Electromagnetic Res. Div., Inst. of Math. Sci., N.Y. Univ., Feb. 1958.

[24] KARAL, F.C. and KARP, S.N., 'Diffraction of a plane wave by a right angled wedge which sustains surface waves on one face', Res. Rept. EM-123, Electromagnetic Res. Div., Inst. of Math. Sci., N.Y. Univ., Jan. 1959.

[25] KARP, S.N., 'Two dimensional Green's function for a right angled wedge under an impedance boundary condition', Res. Rept. EM-129, Electromagnetic Res. Div., Inst. of Math. Sci., N.Y. Univ., March 1959.

[26] SHMOYS, J., 'Diffraction by a half plane with a special impedance variation', I.E.E.E. Trans. on AP, AP-7, pp. 588-590, 1959.

[27] SENIOR, T.B.A., 'Diffraction by a semi-infinite metallic sheet', Proc. Roy. Soc. Lon., Series A, Vol. 213, pp. 436-458, 1952.

[28] SENIOR, T.B.A., 'Diffraction by an imperfectly conducting half plane at oblique incidence', Sci. Rept. 2778-2-T, Rad. Labs., Elect. Eng. Dept., Univ. of Mich., Feb. 1959.

[29] FRIEDMAN, B., 'Surface waves over a lossy conductor', I.E.E.E. Trans. on AP, AP-7, pp. S227-S230, Dec. 1959.

[30] KRITIKOS, H.N., 'Boundary waves along an impedance plane with a linearly varying impedance', I.E.E.E. Trans. on AP, AP-13, pp. 557-583, July 1965.

[31] MILLER, M.A., 'Propagation of electromagnetic waves over a plane surface with anisotropic homogeneous boundary conditions', Dolklady, AN SSSR, Vol. 87, No. 4, p. 571, 1952.

[32] TALANOV, V.I., 'On surface electromagnetic wave systems with non-uniform impedance', Izvestia, Vuz MVO, Radiofizika, Vol. 2, No. 1, pp. 132-133, 1959.

[33] FELSEN, L.B., 'Some aspects of diffraction by variable impedance and anisotropic structures', Microwave Res. Inst., Poltech. Inst. of Brooklyn, N.Y., Rept. R-685-58, PIB-613, Sec. IIIA, Sept. 1958.

[34] WAIT, J.R. and JACKSON, C.M., 'Calculations of the bistatic scattering cross section of a sphere with an impedance boundary condition', Radio Sci., J. of Res., NBS, Vol. 69D, No. 2, pp. 299-315, Feb. 1965.

[35] GARBACZ, R.J., 'Bistatic scattering from a class of lossy dielectric spheres with surface impedance boundary conditions', Phys. Rev., Vol. 133, pp. A14-A16, Jan. 1964.

[36] DEIRMENDJIAN, D., CLASEN, R. and VIEZEE, W., 'Mie scattering with complex index of refraction', J. Opt. Soc. Am., Vol. 51, pp. 620-633, June 1961.

[37] WAIT, J.R., 'Electromagnetic scattering from a radially inhomogeneous sphere', Appl. Sci. Res., Sec. B., Vol. 10, pp. 441-450, 1963.

[38] WESTON, V.H. and HEMENGER, R., 'High frequency scattering from a coated sphere', J. Res. Nat. Bur. Stds., Vol. 66D, pp. 613-619, 1962.

[39] HIATT, R.E., SENIOR, T.B.A. and WESTON, V.H., 'A study of surface roughness and its effects on the backscattering cross section of spheres', Proc. I.R.E., Vol. 48, No. 12, pp. 2008-2016, 1960.

[40] USLENGHI, P.L.E., 'High frequency backscattering from a coated sphere', Alta Frequenza, Vol. 34, No. 11, pp. 189-192, 1965.

[41] MEYER, E. and SEVERIN, H., 'Absorption sanordnugen fur Electromagnetische Zentimeterwellen und ihre akustische Analogien', Angew Phys., Vol. 8, pp. 105-114, March 1956.

[42] MULLER, V., 'Absorption and transmission of electromagnetic waves, Phase G: absorbent coating on metal cylinders', Rome air Development Center, Tech. Rept. TDR-62-21, Astia Doc. No. AD271-790, 1960.

[43] USLENGHI, P.L.E., 'High frequency scattering from a coated cylinder', Can. J. Phys., Vol. 44, pp. 2121-2128, 1964.

[44] ANDREASEN, M.G., 'Scattering from cylinders with arbitrary surface impedance', Proc. I.E.E.E., Vol. 53, pp. 812-817, 1965.

[45] KELLER, J.B., 'A geometrical theory of diffraction', Symposium on the Calculus of Variations and its Applications, Symposia Appl. Maths., Vol. 8, McGraw Hill, N.Y., (1958), p. 27-52 and discussion at end of Chapter IX.

[46] KELLER, J.B., 'Geometrical theory of diffraction', J. Opt. Soc. Am., Vol. 52, p. 116, 1962.

[47] MEVEL, J., 'E'tude sur L'interaction de deuz spheres voisines places dans un champ electromagnetique', Ann. Telecomm., (France), Vol. 12, No. 6, pp. 186-188, 1957.

[48] LIANG, C. and LO. Y.T., 'Scattering by two spheres', Radio Sci., Vol. 2 (new series), pp. 1481-1495, 1967.

[49] STREIFER, W., 'Creeping wave propagation constants for impedance boundary conditions', I.E.E.E. Trans. on AP, AP-12, pp. 764-765, 1964.

[50] BHARTIA, P., ROSS, R.A. and HAMID, M.A.K., 'Ray optical scattering by two spheres', Archiv der Elect. Ubertragung, Vol. 24, No. 5, pp. 215-222, 1970.

[51] BHARTIA, P. and HAMID, M.A.K., 'Eigenvalues for a spherical cavity with an impedance wall', I.E.E.E. Trans. ON MTT, MTT-19, No. 1, Jan. 1971.

[52] BHARTIA, P. and HAMID, M.A.K., 'Ray optical scattering by an imperfectly conducting sphere', accepted for publication in Archiv der Electrichen Ubertragung, 1971.

[53] BHARTIA, P., SHAFAI, L. and HAMID, M.A.K., 'Scattering by imperfectly conducting cylinders', accepted for publication in International Journal of Electronics, 1971.

[54] BHARTIA, P., SHAFAI, L. and HAMID, M.A.K., 'Scattering from an imperfectly conducting cylinder coated with an inhomogeneous dielectric', accepted for publication in International Journal of Electronics, 1971.

[55] LUNEBERG, R.K., 'Mathematical Theory of Optics', Standord Univ. Press, Stanford, California, 1965.

[56] KLINE, M., 'An asymptotic solution of Maxwell's equations', In 'The Theory of Electromagnetic Waves', J. Wiley and Sons, Interscience Div., N.Y., p. 225, 1951.

[57] KLINE, M., 'Electromagnetic Theory and Geometrical Optics', In 'Electromagnetic Waves', Langer, R.E., Univ. of Wisconsin Press, Madison, Wisconsin, p. 3-31, 1962.

[58] KELLER, J.B., 'Diffraction by an aperture', J. Appl. Phys., Vol. 28, pp. 426-444, 1957.

[59] KELLER, J.B., LEWIS, R.M. and SECKLER, B.D., 'Diffraction by an aperture II', J. Appl. Phys., Vol. 28, pp. 570-579, 1957.

[60] FELSEN, L.D., 'Plane wave scattering by small cones', I.R.E. Trans. on AP, AP-5, p. 211- , 1957.

[61] KELLER, J.B., 'Diffraction by a convex cylinder', I.R.E. Trans. on AP, AP-4, pp. 312-321, 1956.

[62] LEVY, B.R. and KELLER, J.B., 'Diffraction by a smooth object'. Commun. Pure and Appl. Maths., Vol. 12, pp. 159-209, 1959.

[63] AHLUWALIA, D, LEWIS, R.M. and BOERSMA, J., 'Uniform asymptotic theory of diffraction by a plane wave', Conference Digest, URSI Fall Meeting, Univ. of Michigan, 1967.

[64] BUCHAL, R.M. and KELLER, J.B., 'Boundary layer problems in diffraction theory', Commun. Pure. Appl. Maths., Vol. 13, pp. 85-114, 1960.

[65] KRAVTOS, Yu.A., 'Asymptotic solution of the Maxwell equations near the caustic surface', IZV, VUZ, Radiofizika, Vol. 7, p. 1049, 1964.

[66] LUDWIG, D., 'Uniform asymptotic expansions at a caustic', Commun. Pure Appl. Maths., Vol. 19, pp. 215- , 1966.

[67] HAMID, M.A.K., 'Near field transmission between horn antennas', Res. Rept. 43, Antenna Lab., Dept. of Elect. Engg., Univ. of Toronto, Toronto, 1966.

[68] FELSEN, L.B. and YEE, H.Y., 'Ray optical techniques for waveguide discontinuities', I.E.E.E. Trans. on AP, pp. 268-269, 1968.

[69] RUDDUCK, R.C., 'Application of wedge diffraction to antenna theory', Res. Rept. 1691-13, Antenna Lab., Dept. of Elect. Engg., Ohio State Univ., 1965.

[70] RUSSO, P.M., RUDDUCK, R.C. and PETERS, L.Jr., 'A method for computing E plane patterns of horn antennas', I.E.E.E. Trans. on AP, AP-13, pp. 219-224, 1965.

[71] SENIOR, T.B.A. and GOODRICH, R.F., 'Scattering by a sphere', Proc. I.E.E., Vol. 111, pp. 907-916, May 1964.

[72] STRATTON, J.A., 'Electromagnetic theory', McGraw-Hill Book Co., Inc., New York, N.Y., 1941.

[73] YERUKHIMOVICH, Y.A. and PIMENOV, Y.V., 'Diffraction of a plane electromagnetic wave by a perfectly conducting sphere of large diameter', Radio Technika i Electronika, Vol. 8, No. 3, pp. 345-350, 1963.

[74] ERUKHIMOVICH, Y.A., 'Solution of the problem of the diffraction of a plane electromagnetic wave by a sphere of large diameter using an approximate method', Radio Technika i Electronika, Vol. 10, No. 1, pp. 16-42, Jan. 1965.

[75] FEDEROV, A.A., 'Asymptotic solution of the problem of diffraction of plane electromagnetic waves on ideally conducting spheres', Radio Technika i Electronika, Vol. 3, No. 12, pp. 1451-1462, 1958.

[76] TRINKS, W., 'Fur vielfachstreuungan kleinen kugeln', Ann Phys., Dtsch 22, pp. 561-590, 1935.

[77] GERMOGENOVA, O.A., 'The scattering of a plane electromagnetic wave by two spheres', Akad. Nauk. SSSR, Izevestia, Ser. Geofrz, No. 4, pp. 648-653, 1963.

[78] BONKOWSKI, R.R., LUBITZ, C.R. and SCHENSTED, C.E., 'Studies in radar cross section II: Cross sections of corner reflectors and other multiple scatterers at microwave frequencies', Rept. No. UMM-106, E.R.I., Univ. of Mich., Ann Arbor, Michigan, Oct. 1953.

[79] ZITRON, N. and KARP, S., 'Higher order approximations in multiple scattering, I., Two dimensional scalar case', J. Math. Phys., 2, No. 3, pp. 394-402, 1961.

[80] ZITRON, N. and KARP, S., 'Higher order approximations in multiple scattering, II., Three dimensional scalar case', J. Math. Phys., 2. No. 3, pp. 402- 406, 1961.

[81] TWERSKY, V., 'Multiple scattering of electromagnetic waves by arbitrary configuration', J. Math. Phys., Vol. 8, No. 3, pp. 589-610, 1967.

[82] ANGELAKOS, D.J. and KUMAGAI, K., 'High frequency scattering by multiple spheres', I.E.E.E. Trans. on AP, AP-12, No. 1, pp. 105-109, 1964.

[83] CRUZAN, O.R., 'Translational addition theorems for spherical vector wave functions', Quart. Appl. Math., 20, No. 1, pp. 33-40, 1962.

[84] BRUNING, J.H. and LO, Y.T., 'Electromagnetic scattering by two spheres', Proc. I.E.E.E., Vol. 57, No. 5, pp. 119-120, Jan. 1968.

[85] HAMID, M.A.K., 'Diffraction by a conical horn', I.E.E.E. Trans. on AP, AP-16, No. 2, pp. 520-528, Sept. 1968.

[86] TWERSKY, V., 'Multiple scattering of radiation by an arbitrary planar configuration of parallel cylinders and by two parallel cylinders', J. Appl. Phys., 23, 404, 1952.

[87] ROSS, R.A. and BHARTIA, P., 'Scattering coefficients for the bistatic scattering of electromagnetic waves from perfectly conducting spheres', Rept. No. 69-TR-1, University of Manitoba, Winnipeg, 1969.

[88] FOCK, V.A., 'Electromagnetic diffraction and propagation problems', Pergamon Press, 1965.

[89] LOGAN, N.A., 'General research in diffraction theory - Vol. I', Lockheed Missiles and Space Division, Technical Rept. LMSD-288087, 1959.

[90] WATSON, G.N., 'A treatise on the theory of Bessel functions', Cambridge Univ. Press, 1948.

[91] WESTON, V.H., 'Theory of absorbers in scattering', I.E.E.E. Trans. on AP, AP-11, pp. 578-584, 1963.

[92] MIDGLEY, D., 'A theory of receiving aerials applied to the reradiation of an electromagnetic horn', Proc. I.E.E., Vol. 108, pp. 645-650, 1961.

[93] EINARSSON, O., KLEINMAN, R.E., LAURIN, P. and USLENGHI, P.L.E., 'Studies in radar cross sections L-diffraction and scattering by regular bodies IV: The circular cylinder', Sci. Rept. 3, Project 5635, Rad. Lab., Elect. Engg. Dept., Univ. of Michigan, Ann Arbor, Feb. 1966.

[94] HARRINGTON, R.F., 'Time Harmonic Electromagnetic Fields', McGraw-Hill Book Co., N.Y., 1961.

[95] OCZKOWSKI, G., 'Locating zeros and poles of a complex valued function', Res. Rept. 69-TR-3, NAG-002, Elect. Engg. Dept., Univ. of Manitoba, Winnipeg, Jan. 1969.

[96] SHAFAI, L., 'Application of coordinate transformation to two-dimensional scattering and diffraction problems', Can. J. of Phys., Vol. 47, pp. 745-804, 1969.

[97] SHAFAI, L., 'Electromagnetic fields in the presence of cylindrical objects of arbitrary physical properties and cross sections', Can. J. of Phys., Vol. 48, pp. 1789-1798, 1970.

[98] SHAFAI, L. and TSE, S.H., 'Scattering from a particular class of conducting corrugated cylinders', Can. J. of Phys., Vol. 49, pp. 66-75, 1971.

[99] BICKLEY, W.G., 'Two dimensional potential problems concerning a single closed boundary', Phil. Trans. Roy. Soc. Lon., Ser. A., Vol. 228, pp. 235-274, 1929.

[100] MORSE, B.J., 'Diffraction by polygonal cylinders', J. Math. Phys., Vol. 5, No. 2, pp. 199-214, Feb. 1964.

[101] BRYSK, H. and BUCHANAN, M.L., 'Scattering by a cylindrical gaussian potential, exact solution', Can. J. Phys., Vol. 43, pp. 28-37, 1965.

[102] SHAFAI, L., 'Scattering by cylindrically symmetrical objects, method of phase and amplitude functions', to be published in Int. J. of Electronics.

[103] HILDERBRAND, F.B., 'Introduction to Numerical Analysis', McGraw-Hill Book Co., N.Y., 1956.

[104] MAURER, S.J. and FELSEN, L.B., 'Ray-optical techniques for guided waves', Proc. I.E.E.E., Vol. 55, No. 10, pp. 1718-1729, 1967.

[105] 'High Performance Shielded Antennas', Catalog 25, Andrew Corporation, Montreal, 1967.

[106] MORSE, P.M. and FESHBACH, H., 'Methods of Theoretical Physics', Vol. 2, McGraw-Hill Book Co., N.Y., 1953.

[107] SCHELKUNOFF, S.A., 'Electromagnetic waves', Princeton, N.J., Van Nostrand, 1943.